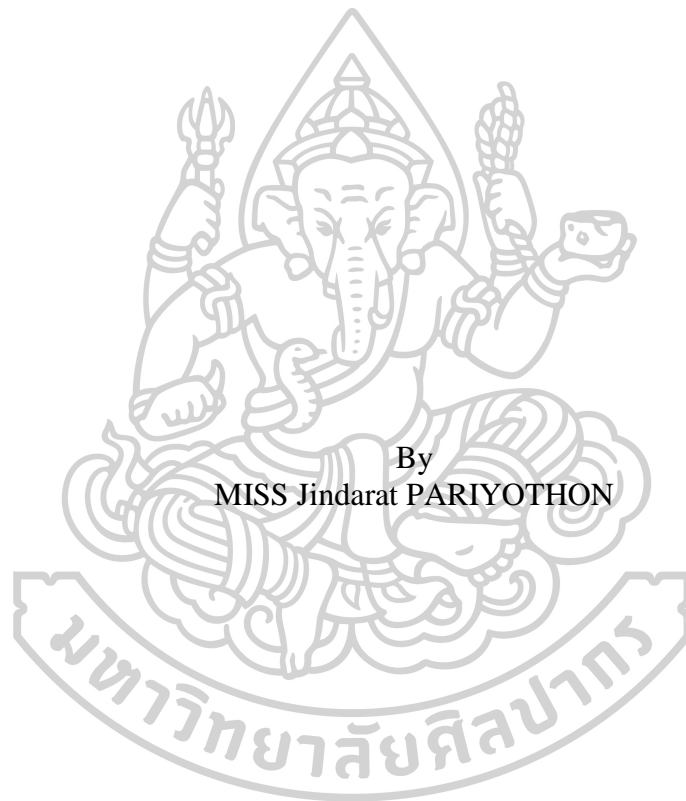




INVESTIGATION OF ATMOSPHERIC WATER VAPOUR IN THAILAND



By
MISS Jindarat PARIYOTHON

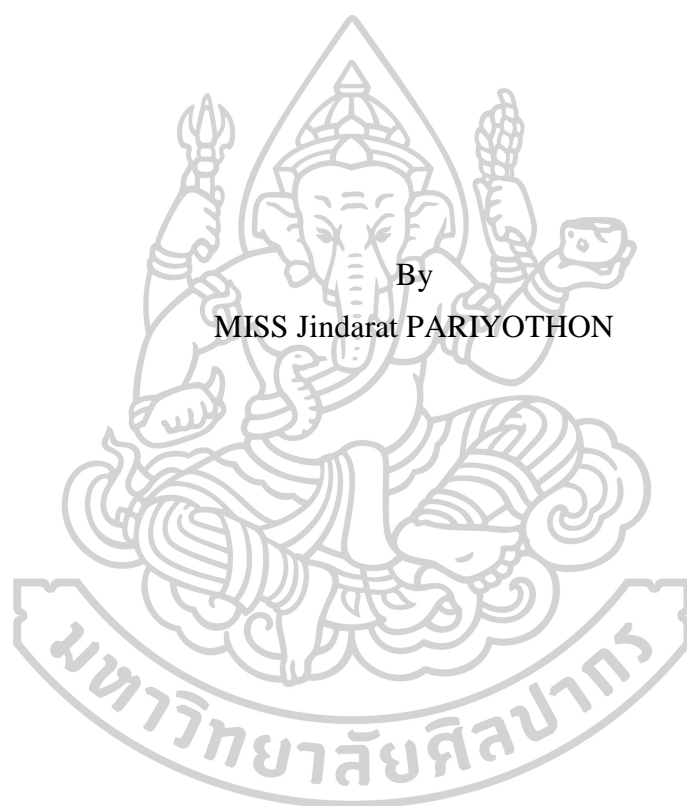
A Thesis Submitted in Partial Fulfillment of the Requirements
for Doctor of Philosophy (PHYSICS)
Department of PHYSICS
Graduate School, Silpakorn University
Academic Year 2020
Copyright of Graduate School, Silpakorn University

การศึกษาปริมาณไอน้ำในบรรยากาศในประเทศไทย



วิทยานิพนธ์นี้เป็นส่วนหนึ่งของการศึกษาตามหลักสูตรปรัชญาดุษฎีบัณฑิต
สาขาวิชาฟิสิกส์ แบบ 1.1 ปรัชญาดุษฎีบัณฑิต
ภาควิชาฟิสิกส์
บัณฑิตวิทยาลัย มหาวิทยาลัยศิลปากร
ปีการศึกษา 2563
ลิขสิทธิ์ของบัณฑิตวิทยาลัย มหาวิทยาลัยศิลปากร

INVESTIGATION OF ATMOSPHERIC WATER VAPOUR IN
THAILAND



By
MISS Jindarat PARIYOTHON

A Thesis Submitted in Partial Fulfillment of the Requirements
for Doctor of Philosophy (PHYSICS)
Department of PHYSICS
Graduate School, Silpakorn University
Academic Year 2020
Copyright of Graduate School, Silpakorn University

Title INVESTIGATION OF ATMOSPHERIC WATER VAPOUR IN
 THAILAND
By Jindarat PARIYOTHON
Field of Study (PHYSICS)
Advisor Professor Serm Janjai , Ph.D.

Graduate School Silpakorn University in Partial Fulfillment of the
Requirements for the Doctor of Philosophy

..... Dean of graduate school

(Associate Professor Jurairat Nunthanid, Ph.D.)

Approved by

..... Chair person

(Assistant Professor Itsara Masiri , Ph.D.)

..... Advisor

(Professor Serm Janjai , Ph.D.)

..... External Examiner

(Assistant Professor Keerati Kirdsiri , Ph.D.)



60306801 : Major (PHYSICS)

Keyword : Water vapour, Precipitable water, Model, Artificial Neural Network, Satellite, Spatial distribution, ERA reanalysis, Radiosonde

MISS JINDARAT PARIYOTHON : INVESTIGATION OF ATMOSPHERIC WATER VAPOUR IN THAILAND THESIS ADVISOR : PROFESSOR SERM JANJAI, Ph.D.

This study aims to investigate the nature of water vapour in Thailand. The study comprises five parts. The first part is to develop a simple empirical model to estimate the precipitable water (PWV). In developing the model, the upper air data from four meteorological stations situated in the main regions of Thailand namely Chiang Mai (18.78°N, 98.98°E), Ubon Ratchathani (15.25°N, 104.87°E), Bangkok (13.67°N, 100.60°E) and Songkhla (7.2°N, 100.6°E) were used to estimate the precipitable water (PWV). Then the PWV was correlated to surface relative humidity (RH), ambient air temperature (T_a) and saturated water vapour pressure (p_{vs}) at these stations to obtain the model. This model performs reasonably when tested against an independent data set. The second part of the study use the Artificial Neural Network (ANN) as an alternative method to estimate monthly average PWV. The input layer of this ANN comprises RH, T_a , p_{vs} and month (m), and the output layer consists of only one parameter namely PWV. These data were collected from Chiang Mai, Ubon Ratchathani, Songkhla and Bangkok. A five-year period (2009-2013) of the input and output data were used to train the ANN and another two-year period (2014-2015) of the input and output data were used to evaluate the performance of the trained ANN. It is found that PWV derived from the ANN agrees well with those obtained from sunphotometers. The third part of this study deals with the investigation of spatial distribution of water vapour in the country. To accomplish this, the data from the water vapour channel of MTSAT-1R satellite and PWV data from sunphotometers at the four stations, were collected and processed. Then a model relating the satellite-derived brightness temperature to the PWV was created. After the validation, the model was used to calculate PWV over the country and the results were displayed as monthly and yearly PWV maps. The maps reveal that PWV varies strongly with the seasons and the geographical regions of the country. The fourth part of this work examines spatial and temporal changes in monthly PWV over Thailand using 37 years of monthly ERA-Interim re-analysis data (1981-2017). PWV from the ERA-Interim were compared with that derived from radiosonde observations at the four stations namely Bangkok (13.67°N; 100.61°E), Singapore (1.37°N; 103.98°E), Kuala Lumpur (2.72°N; 101.70°E) and Danang (16.07°N; 108.35°E) and it was shown to have an average RMSE and MBE of 0.264 cm and -0.137 cm, respectively. Then, PWV from ERA data was used to estimate spatial patterns of monthly average PWV for the winter (Nov, Dec, Jan), summer (Feb, Mar, Apr, May) and rainy (Jun, Jul, Aug, Sep, Oct) seasons as well as the yearly averages. Significant increasing trend in PWV are found in the rainy season. Significant increasing trend is also found over the southern half of Thailand during the winter season. The final part of the study concerns the investigation of vertical variation of water vapour in the upper atmosphere. It was found that the water vapour in the upper troposphere varies with the seasons and the systematic variation in the lower stratosphere was not observed.



ACKNOWLEDGEMENTS

A thesis entitled “Investigation of atmospheric water vapour in Thailand” is submitted in partial fulfillment of the requirement for the Degree of Doctor of Philosophy (Physics), Graduate School, Silpakorn University.

The authors would like to thank the Thailand Research Fund (TRF, RDG59300001) for financially supporting this research work.

I would like to express my sincere thanks to Professor Dr. Serm Janjai, my academic advisor for their patient helpful guidance, enthusiastic encouragement and support throughout this research work.

Besides my advisor, I would like to thank the rest of my thesis committee: Asst. Prof. Dr. Itsara Masiri and Assoc. Prof. Dr. Keerati Kirdsiri for their insightful comments.

I am grateful to the Thai Meteorological Department for providing meteorological data and taking care of the instruments installed at its regional offices.

I would like to thank Mr. Kriengchai Chotana the director of the Upper Air Observation station in Bangkok, Ms. Samrit Suthiprapa the director of the ozone and radiation analysis department, Ms. Kesarin Gooseprasert of meteorologist the expert section of the research and academic cooperation, the Meteorological Department provides advice on radio emission and helps with the information needed in the research.

I am also grateful to Solar Energy Research Laboratory of Silpakorn University for funding my Ph.D. research.

I would like to thank all researchers in Solar Energy Research Laboratory of Silpakorn University, that help and support especially to Asst. Prof. Dr. Sumaman Buntoung for helps throughout the study.

Finally, I wish to thank my family and friends for their encouragement and friendship throughout my life.

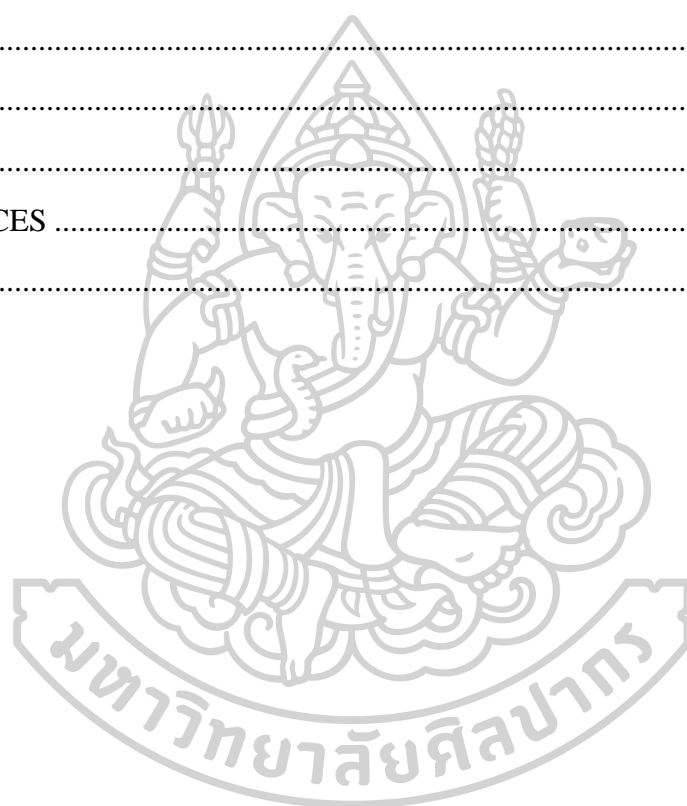
Jindarat PARIYOTHON

TABLE OF CONTENTS

	Page
ABSTRACT.....	D
ACKNOWLEDGEMENTS.....	F
TABLE OF CONTENTS.....	G
LIST OF TABLES.....	J
LIST OF FIGURE.....	K
Chapter 1.....	1
Introduction.....	1
1.1 Rationale of this work.....	1
1.2 Objectives.....	1
1.3 Organization of the thesis.....	2
Chapter 2.....	3
Literature review.....	3
Chapter 3.....	5
Development of an empirical model for calculation of precipitable water in the atmosphere using surface meteorological data.....	5
3.1 Methodology and Data.....	5
3.1.1 Ground-based measurements.....	5
3.1.2 Upper air observation.....	15
3.2 Relation between the PWV and ground-based measurement.....	20
3.2.1 Modeling.....	20
3.2.2 Model validation.....	22
3.3 Conclusion.....	29
Chapter 4.....	30
Estimation of Atmospheric Precipitable Water in Thailand using an Artificial Neural Network.....	30

4.1 Artificial Neural Network.....	30
4.2 Data and Methodology	31
4.2.1 Collection of input and output data for ANN.....	31
4.2.2 Artificial neural network (ANN) modeling.....	32
4.2.3 Training the ANN model.....	33
4.2.4 Testing the ANN model	33
4.3 Conclusion	35
Chapter 5.....	36
Distribution of precipitable water vapour over Thailand using MTSAT-1R satellite data.....	36
5.1 Introduction.....	36
5.2 Data acquisition	37
5.2.1 Satellite data	38
5.3 Ground-based data	45
5.4 Modeling and validation.....	45
5.5 Mapping of PWV.....	49
5.6 Conclusion	52
Chapter 6.....	53
Spatial and Temporal Changes of Precipitable Water Vapour in Thailand.....	53
6.1 Introduction.....	53
6.2 Methodology.....	54
6.2.1 Data sets	54
6.2.2 Comparison PWV from ERA with PWV derived from radiosonde and MODIS	57
6.3 Results.....	61
6.3.1 Seasonal and yearly average PWV.....	61
6.3.2 Long-term yearly trends	63
6.3.3 PWV changes and its relationship to changes in air temperature	66
6.3.4 PWV trends and relevant teleconnections.....	72
6.4 Discussion and Conclusion.....	75

Chapter 7.....	77
Investigation of water vapour in the upper atmosphere.....	77
7.1 Introduction.....	77
7.2 Measurement and Data	77
7.3 Analysis.....	95
7.4 Conclusion	106
Chapter 8.....	107
Conclusion	107
Appendix 1.....	109
Publication	109
REFERENCES	119
VITA.....	120



LIST OF TABLES

	Page
Table 5.1 Spectral band width and spatial resolution of the MTSAT-1R (Takeuchi et al., 2008).	39
Table 5.2 Period of the data from MTSAT-1R for modeling and validation.	39
Table 5.3 Period of monthly average PWV from sunphotometer at the four stations for modeling and validation.	45
Table 5.4 The coefficient values of Equation (5.1) and statistic values. (R^2 is coefficient of determination and N is number of data)	47
Table 5.5 Comparison between the monthly averaged PWV from measurement and those monthly averaged PWV from model.	49
Table 6.1 Details of the data sets used in the analysis.	55
Table 6.2 Comparison of ERA-Interim vs IGRA and ERA-Interim vs MODIS	58
Table 6.3 Statistics describing change in Preipitable water (PWV), as obtained from direct measurements of PWV (third column), change in saturation vapour pressure (e_s) (fourth column), and change in relative humidity (RH) (fifth column). The last three rows describe the combined effect of e_s and RH in estimating PWV. Notice the overlap between measured and combines estimates (in bold).	72
Table 7.1 Summary of the radiosonde observations at the Thai Meteorological Department station, Bang Na, Bangkok in 2017.	85

LIST OF FIGURE

	Page
Figure 3.1 Thermometer screen cabinet of the Thai Meteorological Department at Bangna, Bangkok (TMD).	6
Figure 3.2 Psychrometer completed with wet-dry thermometers of the Thai Meteorological Department at Bangna, Bangkok.....	8
Figure 3.3 A map of Thailand showing the locations of the four meteorological stations used to measure air temperature, relative humidity and surface pressure.	9
Figure 3.4 Example of the variation of daily average air temperature and relative humidity at Chiang Mai in 2009.	11
Figure 3.5 Example of the variation of daily average saturated water vapour pressure at Chiang Mai in 2009.....	11
Figure 3.6 Example of the variation of daily average air temperature and relative humidity at Ubon Ratchathani in 2009.	12
Figure 3.7 Example of the variation of daily average saturated water vapour pressure at Ubon Ratchathani in 2009.....	12
Figure 3.8 Example of the variation of daily average air temperature and relative humidity at Bangna, Bangkok in 2009.	13
Figure 3.9 Example of the variation of daily average saturated water vapour pressure at Bangna, Bangkok in 2009.....	13
Figure 3.10 Example of the variation of daily average air temperature and relative humidity at Songkhla in 2006.	14
Figure 3.11 Example of the variation of daily average saturated water vapour pressure at Songkhla in 2006.	14
Figure 3.12 The release of a balloon with radiosonde equipment to measure the upper air and radiosonde signal transmission system.	15
Figure 3.13 The precipitable water at 7:00 am from radiosonde at the Northern Meteorological Center in Chiang Mai, 2009.	18
Figure 3.14 The precipitable water at 7:00 am from radiosonde at the Northeastern Meteorological Center in Ubon Ratchathani, 2009.	18

Figure 3.15 The precipitable water at 7:00 am from radiosonde at the Thai Meteorological Department, Bang Na in Bangkok, 2009.....	19
Figure 3.16 The precipitable water at 7:00 am from radiosonde at the Southern Eastern Meteorological Center in Songkhla, 2006.	19
Figure 3.17 The relation between the normalized PWV obtained from the radiosonde and the normalized surface data (when RH is the relative humidity, p_{vs} is the saturated water vapour pressure and T_a is the air temperature).....	21
Figure 3.18 Installations feature of sunphotometer instruments at the four sites in Thailand.	22
Figure 3.19 Monthly average precipitable water in the atmosphere in 2008 at Chiang Mai station.	24
Figure 3.20 Monthly average precipitable water in the atmosphere in 2011 at Ubon Ratchathani station.....	24
Figure 3.21 Monthly average precipitable water in the atmosphere in 2008 at Nakhon Pathom station.....	25
Figure 3.22 Monthly average precipitable water in the atmosphere in 2008 at Songkhla station.....	25
Figure 3.23 Comparison between the monthly averaged PWV calculated from the model (PWV_{model}) and those measured from the sunphotometer (PWV_{meas}) at the four stations in Thailand.	27
Figure 3.24 Comparison between PWV from the model and that from the sunphotometer at the four stations (Chiang Mai, Ubon Ratchathani, Nakhon Pathom, Songkhla).	28
Figure 4.1 A simplified model of a biological neuron (Kumar, 2009).....	30
Figure 4.2 Artificial Neural Network (ANN) architecture (Sözen et al., 2004).	31
Figure 4.3 Structure of ANN for PWV estimation.	32
Figure 4.4 Comparison between measured and ANN estimated monthly average PWV. (RMSE is root mean square error, MBE is mean bias error and N is the total number of data points).	34
Figure 5.1 Schematic diagram of the method for generating the PWV maps.	37

Figure 5.2 Multifunctional Transport Satellite (MTSAT-1R).....	38
Figure 5.3 MTSAT-1R spectral response functions: full spectral range from the visible to the thermal infrared (Renzullo et al., 2006).	39
Figure 5.4 The satellite image data from MTSAT-1R in the water vapour channel (Janjai et al., 2011).....	40
Figure 5.5 An example of Satellite Projection (Janjai et al., 2011).	41
Figure 5.6 An example of a rectified satellite image (Cylindrical projection).	41
Figure 5.7 The relationship between the gray level with the brightness temperature from the water vapour channel of the MTSAT-1R satellite.	42
Figure 5.8 Example of monthly average brightness temperature in 2008 at Chiang Mai station.	43
Figure 5.9 Example of monthly average brightness temperature in 2008 at Ubon Ratchathani station.	43
Figure 5.10 Example of monthly average brightness temperature in 2008 at Nakhon Pathom station.....	44
Figure 5.11 Example of monthly average brightness temperature in 2008 at Songkhla station.....	44
Figure 5.12 The relation between the normalized monthly precipitable water from the sunphotometers and the normalized monthly brightness temperature from MTSAT-1R.....	46
Figure 5.13 Comparison between the monthly average PWV calculated from the empirical model (PWV_{model}) and those measured from the ground-based sunphotometer (PWV_{meas}) at the four stations in Thailand.....	48
Figure 5.14 The comparison between the monthly averaged PWV from the semi-empirical model and that obtained from sunphotometer. The diagonal line represents the reference where the PWV from the upper air is equal to the PWV obtained from the latitudes model.	48
Figure 5.15 Monthly average precipitable water over Thailand.....	50
Figure 5.16 Yearly average precipitable water over Thailand.....	51
Figure 6.1 Station locations (▲).....	56

Figure 6.2 Monthly comparisons of PWV from ERA-Interim (PWV_{ERA}) vs PWV from MODIS (PWV_{MODIS}) radiosonde and from IGRA (PWV_{IGRA}).....	59
Figure 6.3 The monthly average PWV for (A) winter, (B) summer, (C) rainy and (D) yearly average PWV.	62
Figure 6.4 Temporal trends of PWV for (A) winter, (B) summer, (C) rainy and (D) yearly average. The values at the contours indicate the values of the trends. Dark and light shades represent that the trends were statistically significant at 99% and 95% confidence levels, respectively.	65
Figure 6.5 Monthly average rate of change β (km^{-1}). Each monthly statistic is the average of 37 yearly observations.....	67
Figure 6.6 (A) Performance of a simple model for PWV (using surface vapour density divided by rate of change β vs ERA-Interim PWV. Each data point represents year i and month j . (B) As in Figure 6.6(A) but with averages calculated for each of the 37 years.....	69
Figure 6.7 Change in yearly average surface data for Bangkok ($13.67^{\circ}N$; $100.61^{\circ}E$) as determined from ERA-Interim re-analysis: A) Precipitable water vapour (PWV); B) Relative humidity; C) Saturation vapour pressure; D) Characteristic height and E) screen-level air temperature.....	71
Figure 6.8 The patterns of significant correlation between PWV and particular index (A) PWV and WP in rainy season, (B) PWV and SOI in rainy season, (C) PWV and SOI in summer season, and (D) PWV and SOI in winter season. The 95% confidence interval is marked in gray.	74
Figure 7.1 Location of the upper air weather station of the Thai Meteorological Department (TMD), Bang Na, Bangkok in Thailand.	78
Figure 7.2 Internet iMet-1 radiosonde with temperature and humidity sensors.....	79
Figure 7.3 The system of the upper air monitoring.	80
Figure 7.4 Attaching a balloon to a helium pipe.....	81
Figure 7.5 Filling helium in a balloon.	81
Figure 7.6 The balloon lifts Pendulum weight of 2 kg.	82
Figure 7.7 Parachute preparation.	82

Figure 7.8 Preparing to release a balloon.....	83
Figure 7.9 Balloon and radiosonde released into the atmosphere.	83
Figure 7.10 Antenna adjustment receive radio signals from the radiosonde.	84
Figure 7.11 Ground receiver.	84
Figure 7.12 Altitude profiles of air temperature; T_a (A) and relative humidity; RH (B) in the upper troposphere and lower stratosphere (UTLS) obtained from radiosonde (i-Met 1) over Bangkok, Thailand on 24 February 2017.....	86
Figure 7.13 Altitude profiles of air temperature; T_a (C) and relative humidity; RH (D) in the upper troposphere and lower stratosphere (UTLS) obtained from radiosonde (i-Met 1) over Bangkok, Thailand on 30 March 2017.....	87
Figure 7.14 Altitude profiles of air temperature; T_a (E) and relative humidity; RH (F) in the upper troposphere and lower stratosphere (UTLS) obtained from radiosonde (i-Met 1) over Bangkok, Thailand on 27 April 2017.....	88
Figure 7.15 Altitude profiles of air temperature; T_a (G) and relative humidity; RH (H) in the upper troposphere and lower stratosphere (UTLS) obtained from radiosonde (i-Met 1) over Bangkok, Thailand on 8 June 2017.....	89
Figure 7.16 Altitude profiles of air temperature; T_a (I) and relative humidity; RH (J) in the upper troposphere and lower stratosphere (UTLS) obtained from radiosonde (i-Met 1) over Bangkok, Thailand on 28 June 2017.....	90
Figure 7.17 Altitude profiles of air temperature; T_a (K) and relative humidity; RH (L) in the upper troposphere and lower stratosphere (UTLS) obtained from radiosonde (i-Met 1) over Bangkok, Thailand on 28 August 2017.	91
Figure 7.18 Altitude profiles of air temperature; T_a (M) and relative humidity; RH (N) in the upper troposphere and lower stratosphere (UTLS) obtained from radiosonde (i-Met 1) over Bangkok, Thailand on 28 September 2017.....	92
Figure 7.19 Altitude profiles of air temperature; T_a (O) and relative humidity; RH (P) in the upper troposphere and lower stratosphere (UTLS) obtained from radiosonde (i-Met 1) over Bangkok, Thailand on 30 November 2017.	93
Figure 7.20 Altitude profiles of air temperature; T_a (Q) and relative humidity; RH (R) in the upper troposphere and lower stratosphere (UTLS) obtained from radiosonde (i-Met 1) over Bangkok, Thailand on 22 December 2017.....	94

Figure 7.21 Vertical distributions of water vapour mixing ratio obtained from the iMet-1 Radiosonde over Bangkok, Thailand on 24 February 2017 (during controlled descent at 39.9 km).	96
Figure 7.22 Vertical distributions of water vapour mixing ratio obtained from the iMet-1 Radiosonde over Bangkok, Thailand on 30 March 2017 (during controlled descent at 37.4 km).	97
Figure 7.23 Vertical distributions of water vapour mixing ratio obtained from the iMet-1 Radiosonde over Bangkok, Thailand on 27 April 2017 (during controlled descent at 34.0 km).	98
Figure 7.24 Vertical distributions of water vapour mixing ratio obtained from the iMet-1 Radiosonde over Bangkok, Thailand on 8 June 2017 (during controlled descent at 37.9 km).	99
Figure 7.25 Vertical distributions of water vapour mixing ratio obtained from the iMet-1 Radiosonde over Bangkok, Thailand on 28 June 2017 (during controlled descent at 39.0 km).	100
Figure 7.26 Vertical distributions of water vapour mixing ratio obtained from the iMet-1 Radiosonde over Bangkok, Thailand on 28 August 2017 (during controlled descent at 40.0 km).	101
Figure 7.27 Vertical distributions of water vapour mixing ratio obtained from the iMet-1 Radiosonde over Bangkok, Thailand on 28 September 2017 (during controlled descent at 38.6 km).	102
Figure 7.28 Vertical distributions of water vapour mixing ratio obtained from the iMet-1 Radiosonde over Bangkok, Thailand on 30 November 2017 (during controlled descent at 39.5 km).	103
Figure 7.29 Vertical distributions of water vapour mixing ratio obtained from the iMet-1 Radiosonde over Bangkok, Thailand on 22 December 2017 (during controlled descent at 38.5 km).	104
Figure 7.30 Vertical distributions of volume mixing ratio (ppmv) in the UTLS region obtained from the iMet-1 Radiosonde over (13.67°N, 100.60°E) Bangkok, Thailand from February through December in 2017.	105

Chapter 1

Introduction

1.1 Rationale of this work

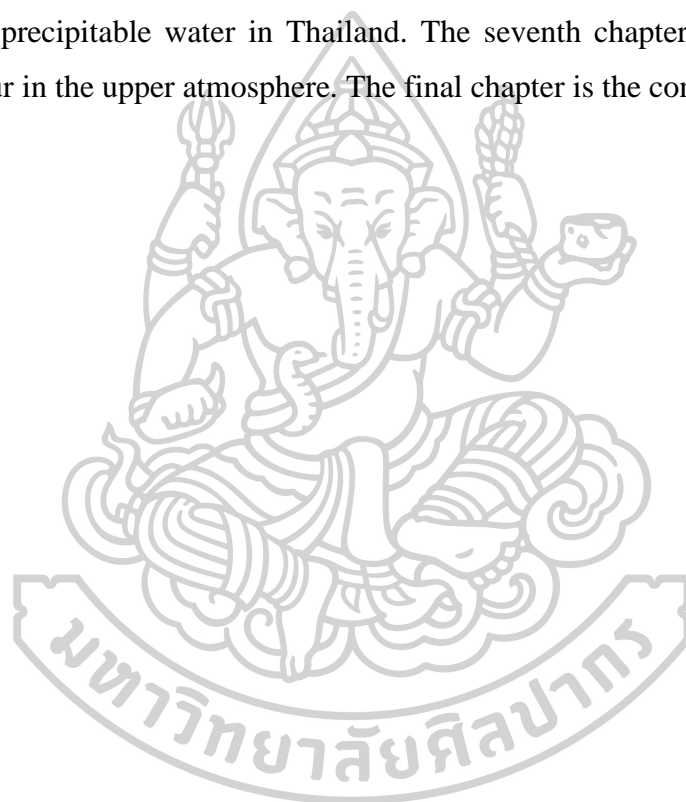
Generally, water (H₂O) in the atmosphere can be divided into three states that are gas, liquid and solid. The water in gas state is water vapour. The water vapour is a meteorological parameter that has an important role in atmospheric chemical and physical processes. Water vapour in the troposphere influences the optical properties of aerosols and hence clouds and rain (Kämpfer, 2012). It also has an impact on visibility (Iqbal, 1983). Moreover, water vapour can absorb atmospheric radiation and is the most active natural greenhouse gas in the atmosphere. More than 60% of the natural greenhouse effect is contributed by water vapour (Taylor, 2005). This is because the water vapour in the atmosphere allows most of ultraviolet and visible radiation passing to the earth's surface but absorbs a large fraction of infrared radiation emitted by the earth's surface (Iqbal, 1983; Nunez, 1993). In order to study the intensity of the radiation at the earth's surface and the energy balance of the earth's atmosphere as well as the changes in atmospheric conditions, it is necessary to know the amount of water vapour in the atmosphere. Although the upper atmosphere contains very small amount of water vapour, it plays an important role in atmospheric circulation and stability (Kämpfer, 2012). In summary, water vapour significantly influences the surface and atmospheric energy balance and warrants detailed studies of its behaviour and distribution.

1.2 Objectives

1. To develop an empirical model for calculation of precipitable water in the atmosphere using surface meteorological data.
2. To estimate precipitable water in the atmosphere in Thailand using an artificial neural network.
3. To investigate the distribution of precipitable water over Thailand using MTSAT-1R satellite data.
4. To study the spatial and temporal changes of precipitable water in Thailand.
5. To investigate water vapour in the upper atmosphere in Thailand.

1.3 Organization of the thesis

The thesis consists of eight chapters. The first chapter is an introduction on water vapour in the atmosphere. The second chapter presents the literature review. The third chapter presents the development of an empirical model for estimating precipitable water by using radiosonde and surface meteorological data. The fourth chapter describes the method for calculating precipitable water from ANN model. The fifth chapter explains a technique for mapping monthly average precipitable water by using the satellite imagery data. The sixth chapter describes spatial and temporal changes of precipitable water in Thailand. The seventh chapter presents a study of water vapour in the upper atmosphere. The final chapter is the conclusion.



Chapter 2

Literature review

The amount of water vapour is popularly determined in the form of precipitable water (PWV), which is the depth of the water in a column of the atmosphere precipitated. The units of PWV is in term of mm or cm. In general, PWV can be measured using ground-based instruments, e.g. microwave radiometer and sunphotometer, and also upper air radiosonde (Cuomo et al., 1997). However, the number of these instruments are limited due to their high price.

There are several alternative solutions to this problem. Hay et al. (1971) used a classical modeling approach to determine the atmospheric PWV from temperature and relative humidity data in Canada. The above studies displayed the amount of PWV in the form of a contour maps covering the entire country.

Reitan et al. (1960) calculated the water vapour in the atmosphere in the United States from the data of air temperature and relative humidity at meteorological stations over the country. The water vapour is displayed as a contour map covering the whole country. The map shows changes in the amount of water vapour in the area and seasonally throughout the United States.

Revuelta et al. (1985) created a statistical model showing the relationship between water vapour, dew point temperature and saturated vapour pressure in Salamanca, Spain. The result has been compared with the values obtained from the radiosonde device which provides a consistent value.

In some previous studies, Artificial Neural Network (ANN) has been used successfully in atmospheric science, climate change and Land surface temperature (LST) studies (Pasini and Ameli, 2003 ; Sahin, 2012).

In Turkey, Senkal et al. (2012) use Artificial neural network (ANN) method was applied for modeling and prediction of mean precipitable water and solar radiation in a given location and given date (month), given altitude, temperature, pressure and humidity in Turkey (26–458E and 36–428N) during the period of 2000–2002. The results for Turkey also revealed that correlation values indicate a relatively

good agreement between the observed values and the ANN-calculated precipitable water and solar radiation values.

Another solution is to use satellite data to estimate the PWV at regional and global scales (Takeuchi et al., 2016). Larsen and Stamnes (2005) developed a technique for calculating the amount of water vapour in atmospheric haze cases using radiation reflected from the ground and retrieved by satellite sensors.

Lee and Park (2007) conducted a study and tested a model for determining the amount of water vapour in the East Asian region using brightness temperature at wavelengths 11 and 12 μm , which are sensitive to water vapour. These data were obtained from GOES-9 and MTSAT-1R satellites. The technique was able to retrieve PWV to a satisfactory level of uncertainty with the root mean square difference of about 0.58 cm. Similarly, Akatsuka et al. (2010) also used the brightness temperature data from the MTSAT satellite to calculate PWV in East and Southeast Asia and the western Pacific. Model and measured data agreed to within root mean difference of 11.08%.

In addition, Soden and Bretherton (1993) used relative humidity and air temperature vertical profiles and the values of surface atmospheric pressure as deduced from the daily radiosonde measurements of the Wyoming University database for Çukurova region in Turkey, they estimated the daily and monthly mean values of precipitable water at various layers from the surface for the period of time between 1990 and 2006.

From previous studies, most of them were investigate the atmospheric water vapour in Europe and North America. However, the investigation of PWV in Thailand, located in the tropics and exhibits large seasonal changes in PWV, is very limited (Exell, 1978). Therefore, in this work, we have proposed an empirical model to investigate atmospheric water vapour in Thailand in order to gain knowledge about the atmospheric water vapour of the country.

Chapter 3

Development of an empirical model for calculation of precipitable water in the atmosphere using surface meteorological data

In this work, we aim to develop an empirical model to estimate the water vapour in term of precipitable water using commonly available surface meteorological data. The details of the work are presented as follows.

3.1 Methodology and Data

3.1.1 Ground-based measurements

Because the amount of water vapour in the atmosphere relates to temperature, relative humidity and atmospheric pressure, in this research work, such data are obtained from four regions of Thailand for determining monthly average PWV. The instruments and data used in this part are described as follows:

- Thermometer

The surface air temperature used in this work is measured by a thermometer installed inside a double-sided screen cabinet of the Thai Meteorological Department (Figure 3.1). This screen cabinet is used to shield the thermometers from direct sunlight, rainfall and other elements. It allows for the free circulation of air around the thermometer thus creating a uniform temperature in the screen cabinet. The base of the screen is positioned at about 1.25 – 2 m above the ground on a metal stand.



Figure 3.1 Thermometer screen cabinet of the Thai Meteorological Department at Bangna, Bangkok (TMD).

- Psychrometer

Humidity is the amount of water vapour in the atmosphere caused by condensation and evaporation. It can be measured as absolute humidity (the amount of water vapor in a unit volume of air) or a relative humidity (the ratio of moisture in the atmosphere to the maximum moisture the atmosphere can hold).

Wet and dry bulb psychrometers are the most simple and common way of measuring humidity. This type of hygrometer uses two mercury thermometers, It consists of two identical thermometers the wet-bulb thermometer which the bulb is

covered with a jacket of tight-fitting muslin cloth that can be saturated with distilled water, and the dry-bulb thermometer. When the cloth is soaked and the thermometers are properly ventilated, the wet-bulb temperature will be lower than the dry-bulb temperature (actual air temperature) because of cooling due to the evaporation of water from the cloth. The drier air is the greater the evaporation and thus the more the wet-bulb temperature is depressed.

Relative humidity is calculated by comparing the ambient temperature (the temperature given by the dry bulb) to the difference in temperatures between the two thermometers. The relative humidity used in this research is obtained from the hygrometer of the Meteorological Department. The example of the psychrometer is shown in Figure 3.2.

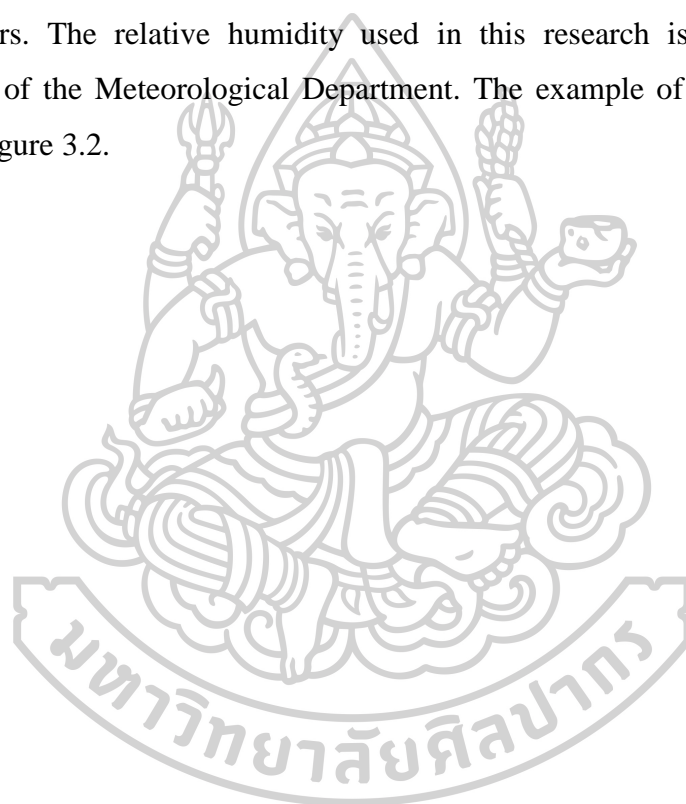




Figure 3.2 Psychrometer completed with wet-dry thermometers of the Thai Meteorological Department at Bangna, Bangkok.

The data of air temperature and relative humidity used in this study are from four meteorological stations in Thailand, namely Chiang Mai (CM; 18.98°N, 98.98°E) in the north, Ubon Ratchathani (UB; 15.25°N, 104.87°E) in the northeast, Bangkok (BKK; 13.67°N, 100.60°E) in the center of the country and Songkhla (SK; 7.20°N, 100.60°E) in the south (Figure 3.3).

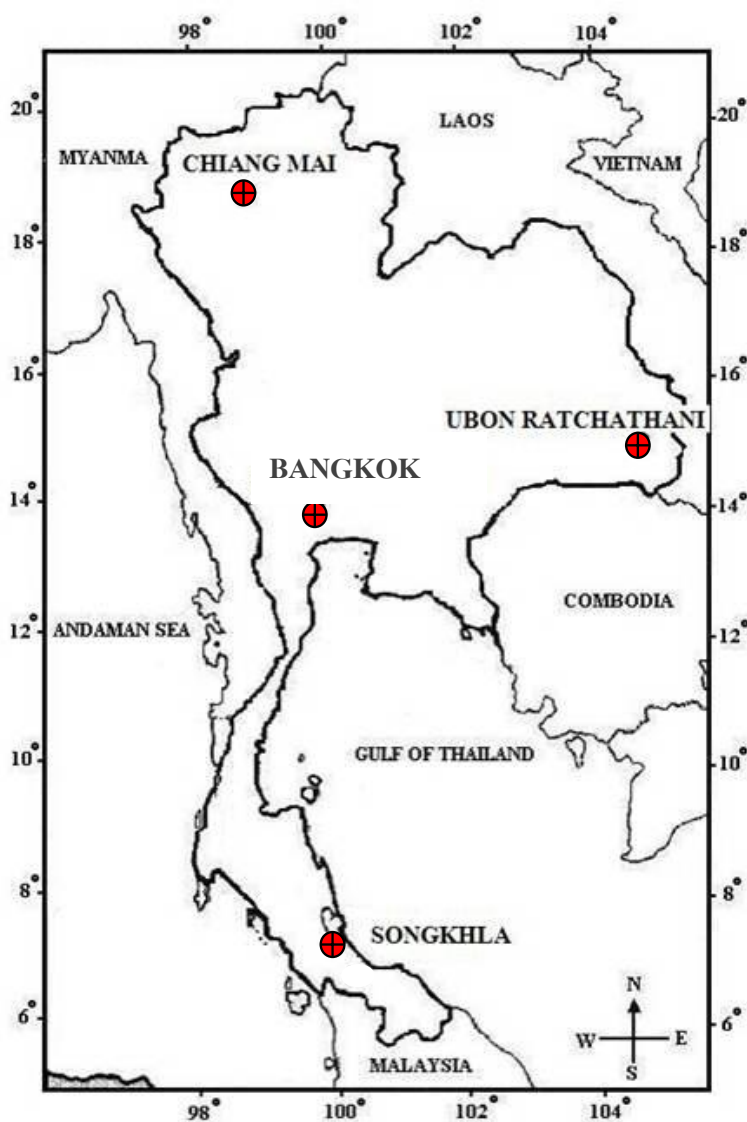


Figure 3.3 A map of Thailand showing the locations of the four meteorological stations used to measure air temperature, relative humidity and surface pressure.

These data were collected for a 16-years period between 1 January, 2000 – 31 December, 2015. The data is in hourly basis at 1:00, 4:00, 7:00, 10:00, 13:00, 16:00, 19:00 and 22:00 h (local time). The data set were then processed to daily average data and then the monthly average data. After that, we have divided the data into two groups. The first group (January 2000 to December 2013) was used for model formulation and the second group (January 2014 to December 2015) was employed for model validation.

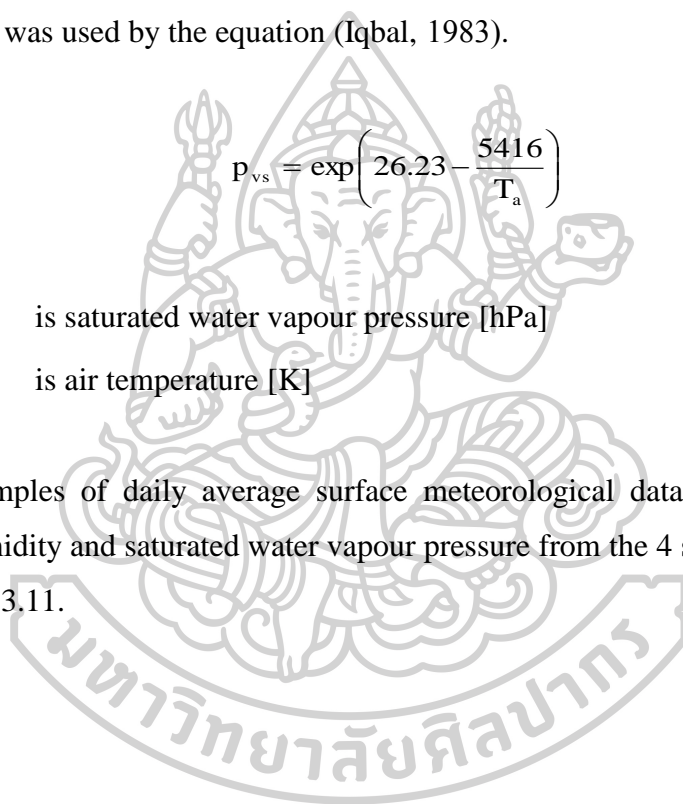
In order to obtain saturated water vapour pressure, the monthly average air temperature was used by the equation (Iqbal, 1983).

$$p_{vs} = \exp\left(26.23 - \frac{5416}{T_a}\right) \quad (3.1)$$

where p_{vs} is saturated water vapour pressure [hPa]

T_a is air temperature [K]

Examples of daily average surface meteorological data of air temperature, relative humidity and saturated water vapour pressure from the 4 stations are shown in Figure 3.4 - 3.11.



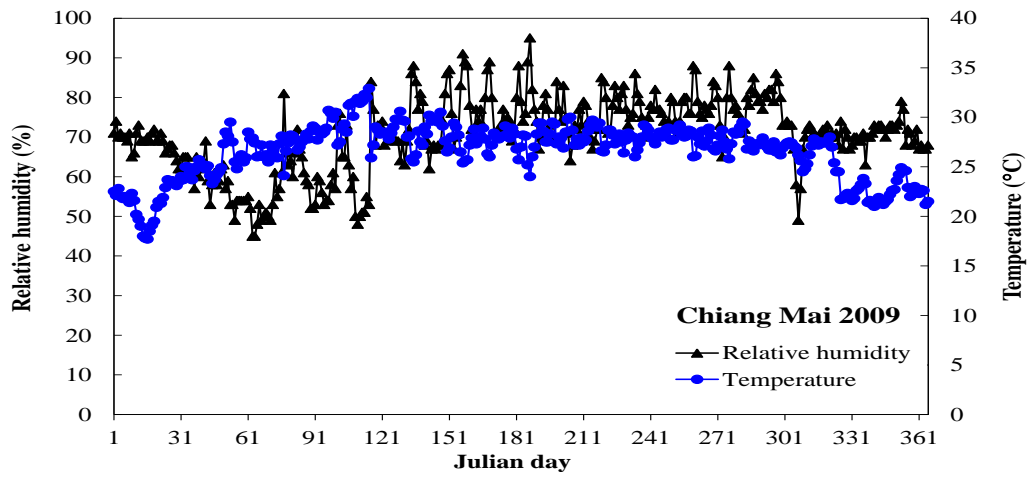


Figure 3.4 Example of the variation of daily average air temperature and relative humidity at Chiang Mai in 2009.

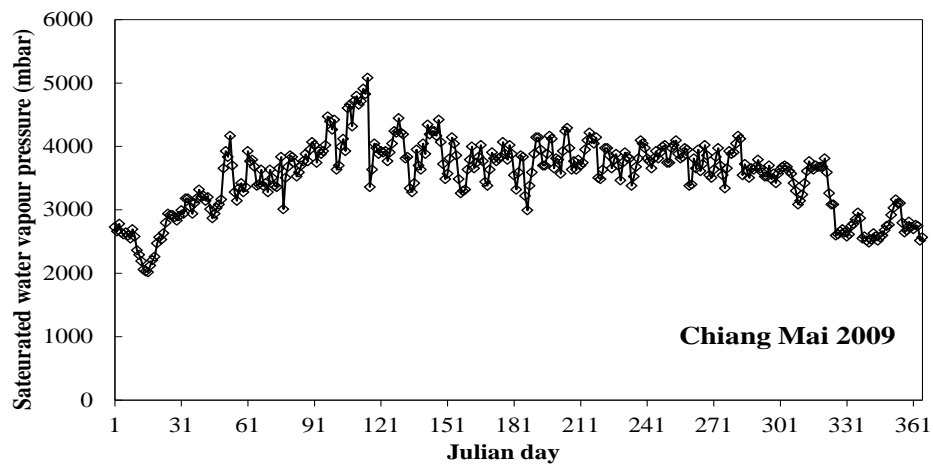


Figure 3.5 Example of the variation of daily average saturated water vapour pressure at Chiang Mai in 2009.

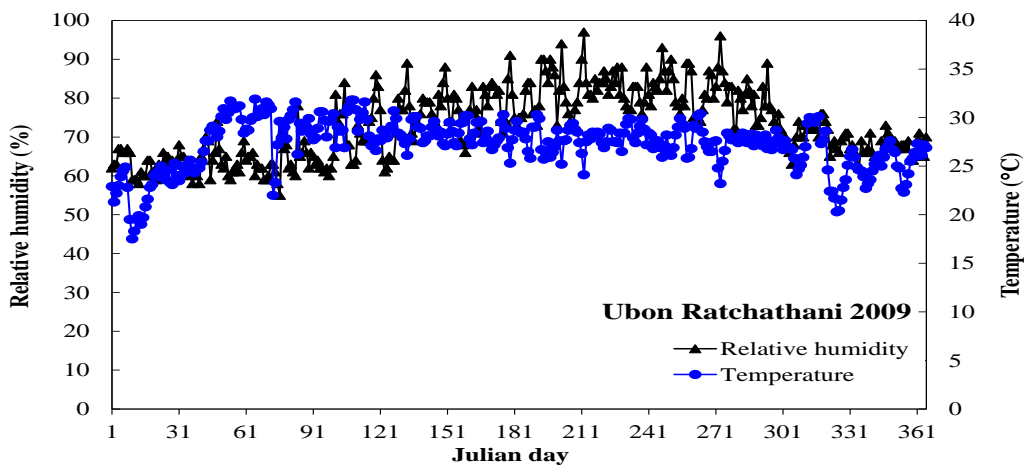


Figure 3.6 Example of the variation of daily average air temperature and relative humidity at Ubon Ratchathani in 2009.

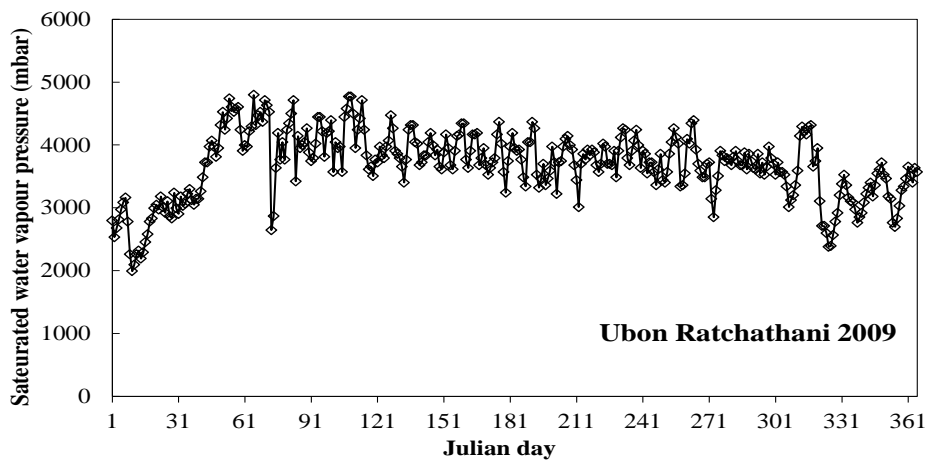


Figure 3.7 Example of the variation of daily average saturated water vapour pressure at Ubon Ratchathani in 2009.

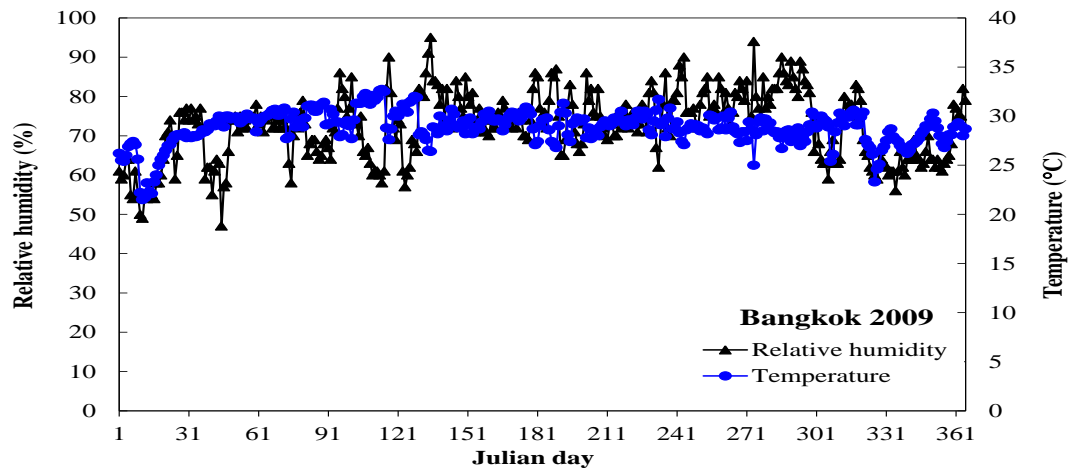


Figure 3.8 Example of the variation of daily average air temperature and relative humidity at Bangna, Bangkok in 2009.

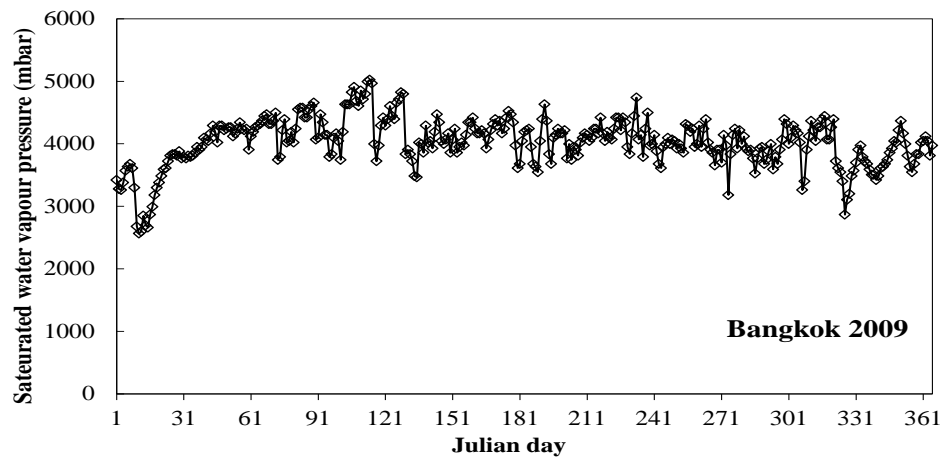


Figure 3.9 Example of the variation of daily average saturated water vapour pressure at Bangna, Bangkok in 2009.

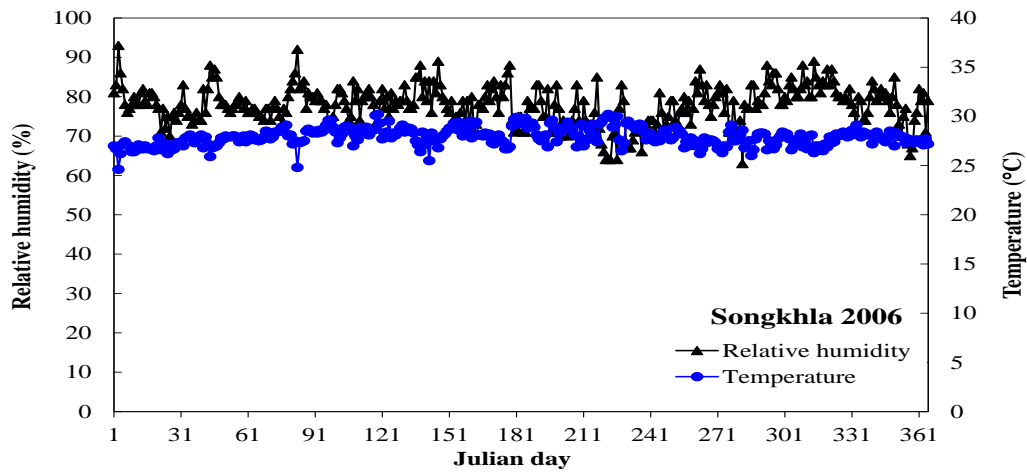


Figure 3.10 Example of the variation of daily average air temperature and relative humidity at Songkhla in 2006.

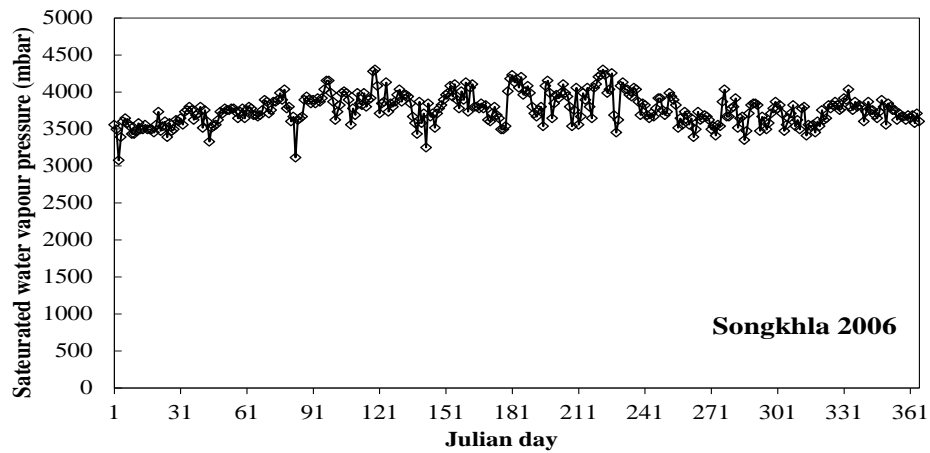


Figure 3.11 Example of the variation of daily average saturated water vapour pressure at Songkhla in 2006.

3.1.2 Upper air observation

In this work, we used radiosonde data obtained from the main Thai Meteorological Department in different regions of the country to calculate the amount of water vapor in the atmosphere. The details of the instrument and data are described as follows.

3.1.2.1 Radiosonde

Measurement of the upper atmosphere above the earth's surface, especially in the troposphere layer, can be done using upper air observation as radiosonde (Figure 3.12). It can measure temperature, air pressure, wind direction and speed and relative humidity at various heights. Generally, upper air observation will be performed every 6 hours at 7:00 am, 13:00 pm, 7:00 pm and 1:00 am (local time). However, since the instrument is expensive and cannot be reused, the Thailand Meteorological Department has measurements only at 7:00 am.

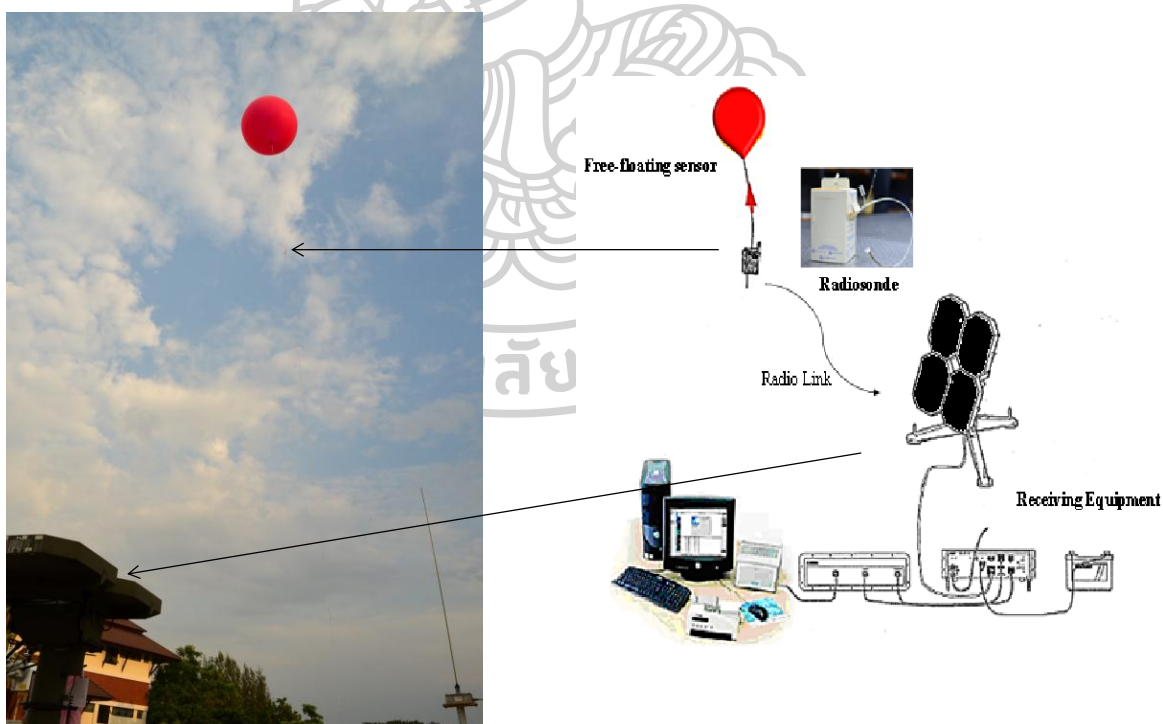


Figure 3.12 The release of a balloon with radiosonde equipment to measure the upper air and radiosonde signal transmission system.

We have collected the data from the upper air observation from the four meteorological stations in Thailand where we have collected the surface meteorological data. The data collected consist of air temperature, relative humidity and air pressure at various altitudes from 1,000 - 5 hPa. This data is collected in the period 1 January, 2000 - 31 December, 2015.

3.1.2.2 Processing radiosonde data

After obtaining the data of the upper air observation, we did quality control for the data of temperature and relative humidity data at various air pressure levels from 1,000 hPa – 5 hPa according to the method of Feng et al. (2004). Following the method, the data at the same level and same stations were averaged in a month. If any individual data is different from the average value greater than $\pm 2SD$, the data will be omitted. Then, the method of Pierrehumbert (1972) was used to calculate daily PWV in the atmosphere from the air temperature and relative humidity obtained from the radiosonde of the Meteorological Department. The amount of water vapour can be estimated from the equation:

$$PWV = \int_{p_0}^0 \left(\frac{M}{g} \right) dp \quad (3.2)$$

where PWV is the precipitable water [cm], g is the acceleration due to gravity [980 cm/s^2], M is the mixing ratio [-], p is the pressure of the air [hPa]. Because the equation (3.2) is in an integral form, it requires continuous data. But the data obtained from the radiosonde are discrete and cannot be used directly. Therefore, the equation (3.2) is converted into the form of algebraic equations as follows:

$$PWV \approx \frac{1}{g} [M_1(p_0 - p_1) + M_2(p_1 - p_2) + \dots + M_n(p_{n-1} - p_n)] \quad (3.3)$$

where p_i is the pressure of the air [hPa] at the level i , i is the order of the data ($i = 1, 2, \dots, n$), p_0 is the surface pressure [hPa], n is total level of the measurement [-].

Mixing ratio of water vapour and dry air at various heights ($i = 1, 2, \dots, n$) can be obtained from the equation (Wallace and Hobbs, 2006).

$$M_i = 0.622 \frac{p_{vi}}{p_i - p_{vi}} \quad (3.4)$$

where p_{vi} is the water vapour pressure [hPa]. For water vapour pressure at various heights, it can be calculated from the relative humidity as the equation:

$$p_{vi} = RH_i \times p_{vsi} \quad (3.5)$$

where RH_i is the relative humidity [-]. p_{vsi} is the saturated water vapour pressure [hPa]. The saturated water vapour pressure can be calculated from the air temperature using the equation (Murray, 1966)

$$p_{vsi} = \begin{cases} 6.106607 \times 10^{(7.5T_i/237.3+T_i)}, & T_i > 0 \\ 6.106607 \times 10^{(9.5T_i/265.5+T_i)}, & T_i < 0 \end{cases} \quad (3.6)$$

where T_i is the air temperature [$^{\circ}\text{C}$]

We have applied the above method to calculate the PWV using radiosonde data from 1 January, 2000 to 31 December, 2015 at 7:00 am of the four measurement stations. Examples of the PWV obtained from the radiosondes are shown in Figure 3.13 - 3.16.

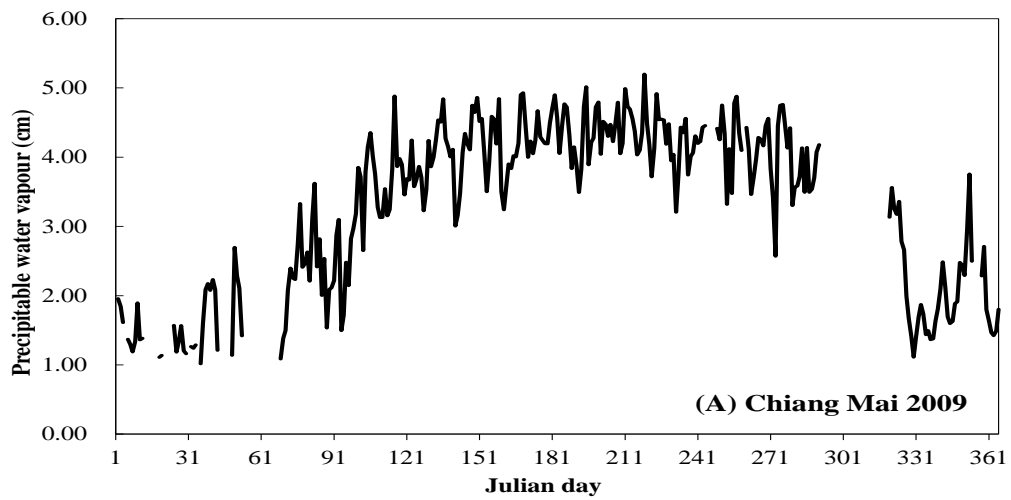


Figure 3.13 The precipitable water at 7:00 am from radiosonde at the Northern Meteorological Center in Chiang Mai, 2009.

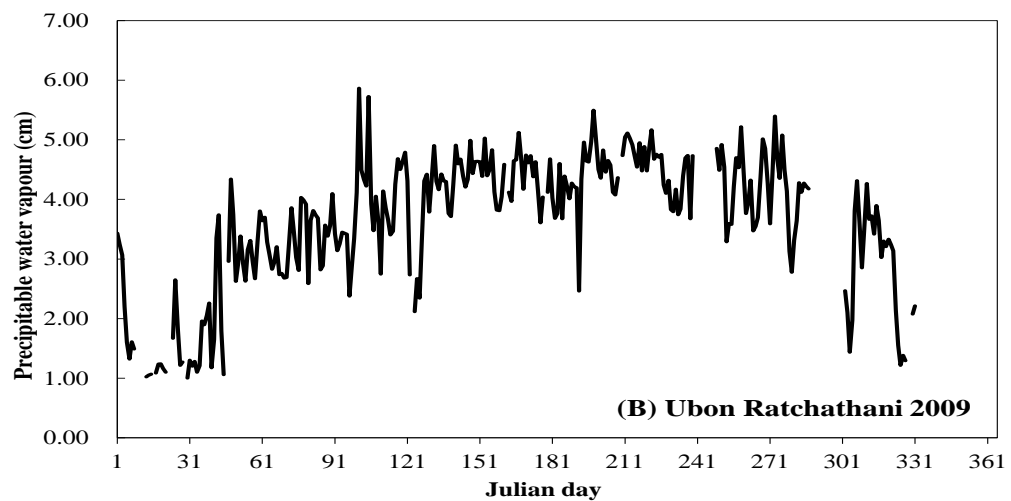


Figure 3.14 The precipitable water at 7:00 am from radiosonde at the Northeastern Meteorological Center in Ubon Ratchathani, 2009.

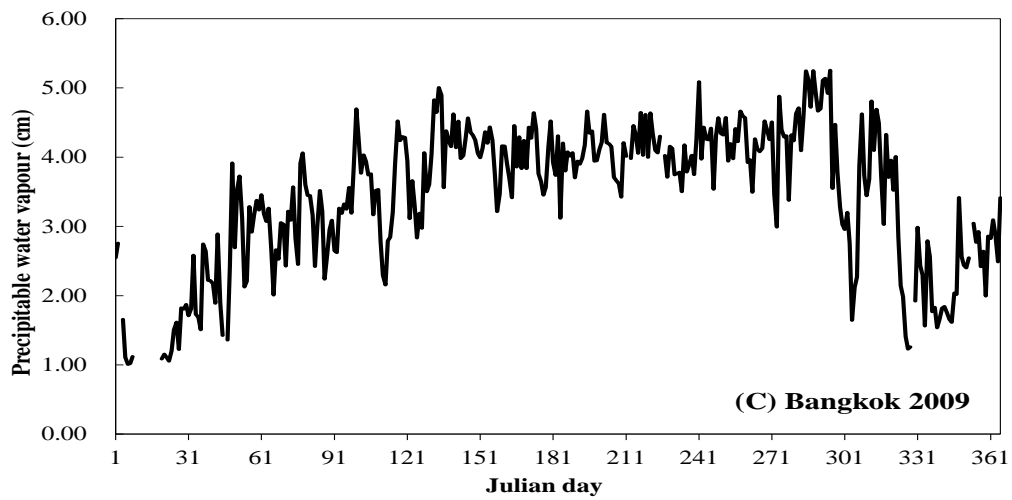


Figure 3.15 The precipitable water at 7:00 am from radiosonde at the Thai Meteorological Department, Bang Na in Bangkok, 2009.

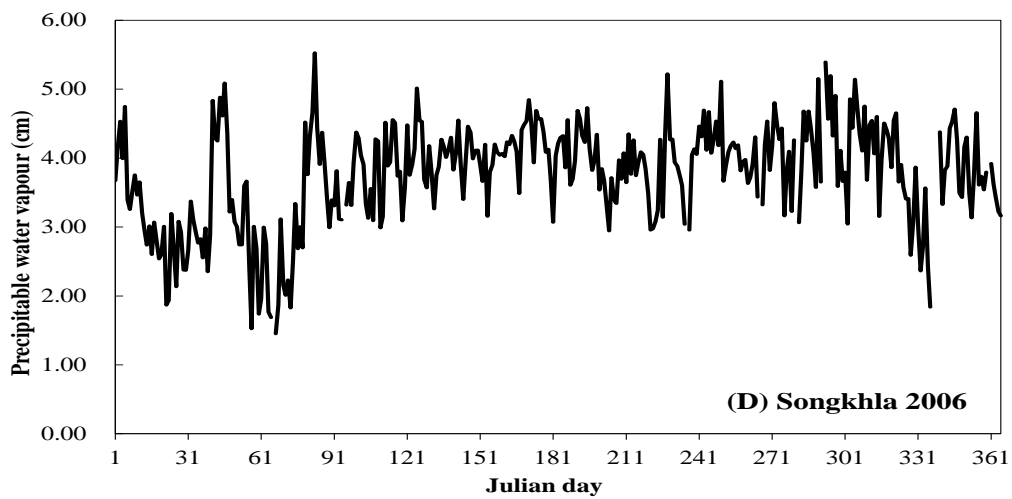


Figure 3.16 The precipitable water at 7:00 am from radiosonde at the Southern Eastern Meteorological Center in Songkhla, 2006.

From Figure 3.13-3.16, it can be seen that the amount of PWV obtained from the radiosonde at the four meteorological stations, namely Chiang Mai, Ubon Ratchathani and Bangkok are similar in seasonal variation, which is high value during the rainy season (May - October) and low value during the dry season (November - April). For Songkhla, there is a high value of PWV in the atmosphere throughout the year.

3.2 Relation between the PWV and ground-based measurement

3.2.1 Modeling

We used monthly average air temperature (T_a), monthly average relative humidity (RH), and monthly average saturated water vapour pressure (p_{vs}) from the surface meteorological data, and the monthly average PWV data obtain from the upper air measurement at the four meteorological stations, namely Chiang Mai, Ubon Ratchathani, Bangkok and Songkhla to generate a model. The data used for the model formulation is between 1 January 2000 - 31 December 2013.

Firstly, the PWV from the radiosonde were normalized by the highest value. Also, the product of air temperature, relative humidity, saturated water vapour pressure ($RH \cdot p_{vs} / T_a$) were normalized by its highest value. After that the normalized PWV was plotted against the normalized $RH \cdot p_{vs} / T_a$ to obtain the relation. The result is shown in Figure 3.17.

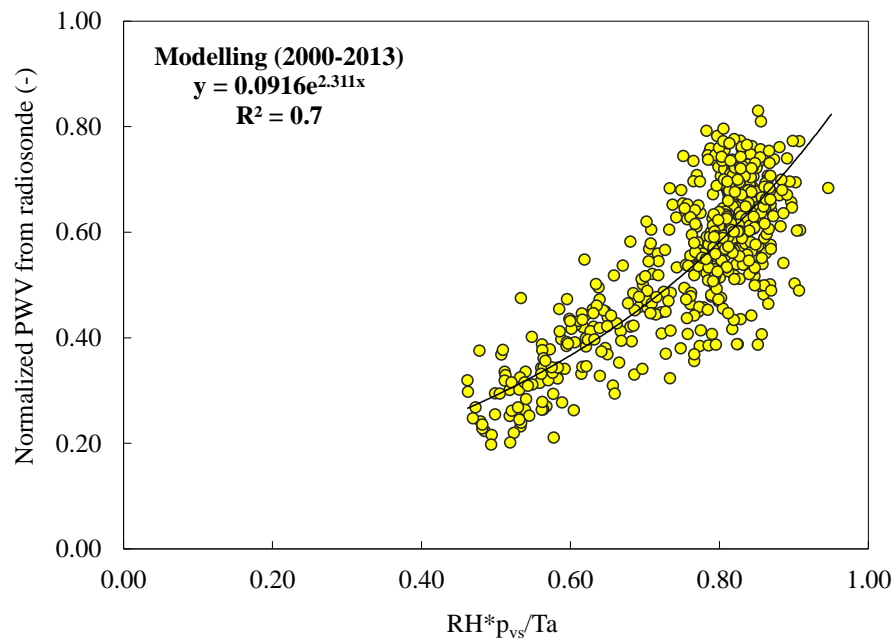


Figure 3.17 The relation between the normalized PWV obtained from the radiosonde and the normalized surface data (when RH is the relative humidity, p_{vs} is the saturated water vapour pressure and T_a is the air temperature).

A non-linear regression technique (Seber and Wild, 1989) was used to fitted the relation and the result is obtained as the following equation:

$$PWV = 0.0916 \exp[2.311RH \cdot p_{vs}/T], \quad R^2 = 0.7 \quad (3.7)$$

where

PWV is the precipitable water [cm]

RH is the relative humidity [-]

T_a is the air temperature [K]

p_{vs} is the saturated water vapour pressure [hPa]

R^2 is coefficient of determination [-]

3.2.2 Model validation

To validate the accuracy of the model, we used the monthly average air temperature, relative humidity and saturated water vapour pressure from four stations, namely Chiang Mai, Ubon Ratchathani, Bangkok and Songkhla during 2014 – 2015 to calculate the monthly average PWV by using the model according to the equation (3.7).

After that, the monthly average PWV calculated from the model were compared with the monthly average PWV obtained from sunphotometers (Cimel CE-318). These instruments are at Chiang Mai (CM), Ubon Ratchathani (UB), Nakhon Pathom (NP, 13.82°N, 100.04°E) and Songkhla (SK) (Figure 3.18).

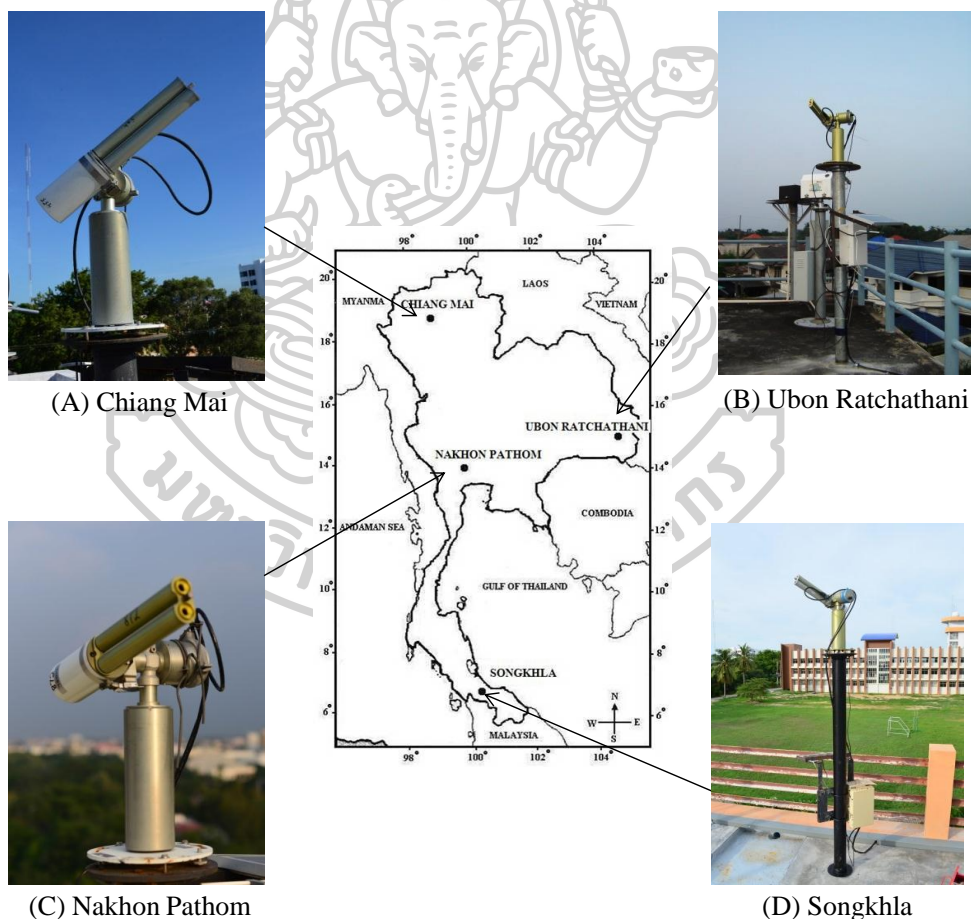
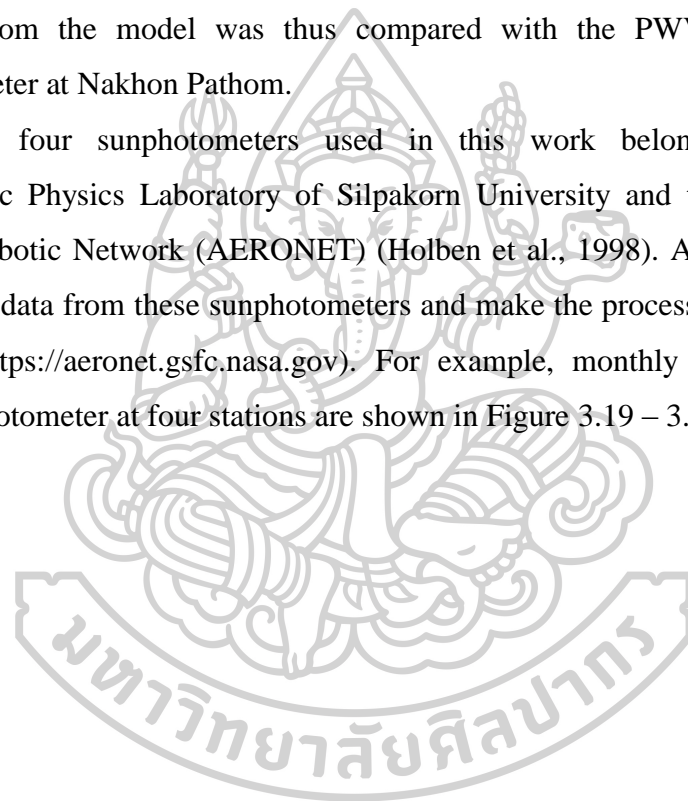


Figure 3.18 Installations feature of sunphotometer instruments at the four sites in Thailand.

The sunphotometer measures the direct irradiance, the almucantar irradiance (i.e., observed along a circle parallel to the horizon at a given elevation angle) and the principal plane irradiance (over an arc of varying elevation angle given a fix azimuth) at the Earth's surface (Cimel, 2001). The instrument has or eight channels: 340, 380, 440, 500, 675, 870, 940 and 1020 nm. The retrieval of the PWV is based on measurements taken at 940 nm (water absorption peak) and 1020 nm (no water absorption) (Reagan et al., 1987; Bruegge et al., 1992).

As in Bangkok there does not have any sunphotometer, the PWV for Bangkok obtained from the model was thus compared with the PWV measured by the sunphotometer at Nakhon Pathom.

The four sunphotometers used in this work belong to the Tropical Atmospheric Physics Laboratory of Silpakorn University and they are member of Aerosol Robotic Network (AERONET) (Holben et al., 1998). AERONET of NASA process the data from these sunphotometers and make the processed data available on internet (<https://aeronet.gsfc.nasa.gov>). For example, monthly average PWV data from sunphotometer at four stations are shown in Figure 3.19 – 3.22.



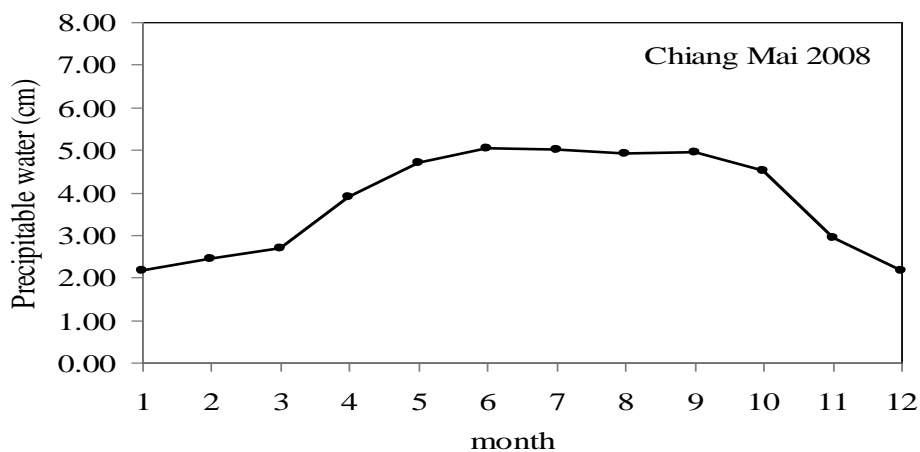


Figure 3.19 Monthly average precipitable water in the atmosphere in 2008 at Chiang Mai station.

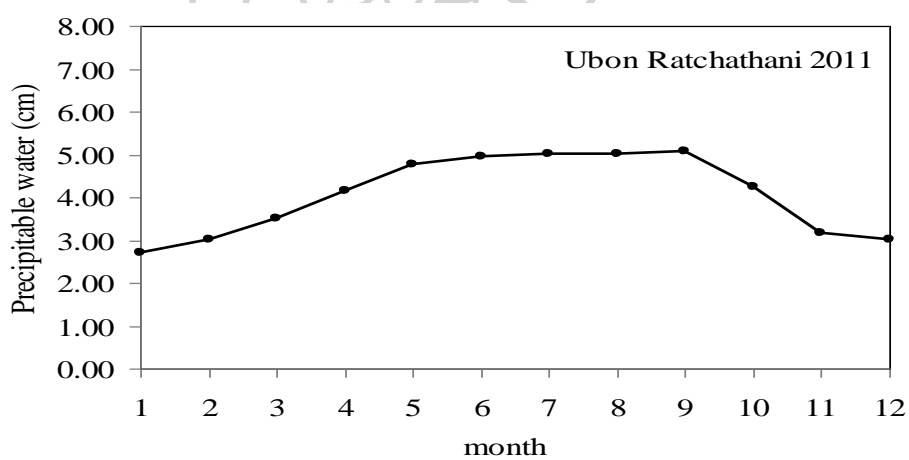


Figure 3.20 Monthly average precipitable water in the atmosphere in 2011 at Ubon Ratchathani station.

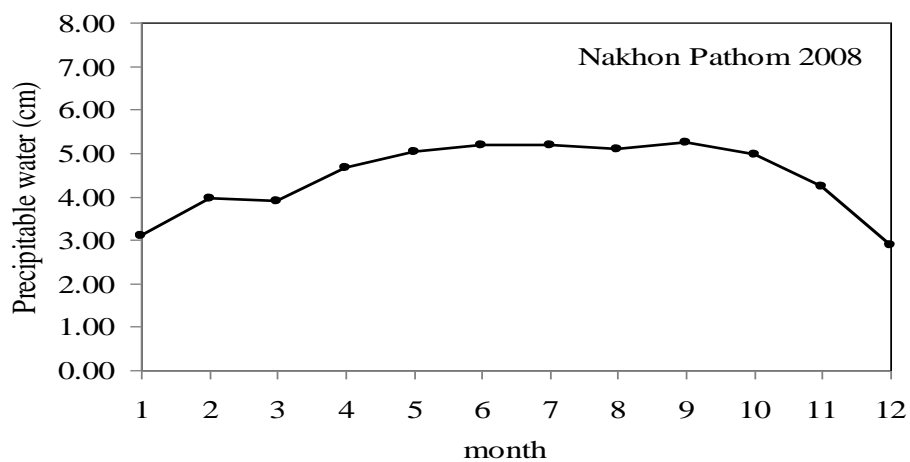


Figure 3.21 Monthly average precipitable water in the atmosphere in 2008 at Nakhon Pathom station.

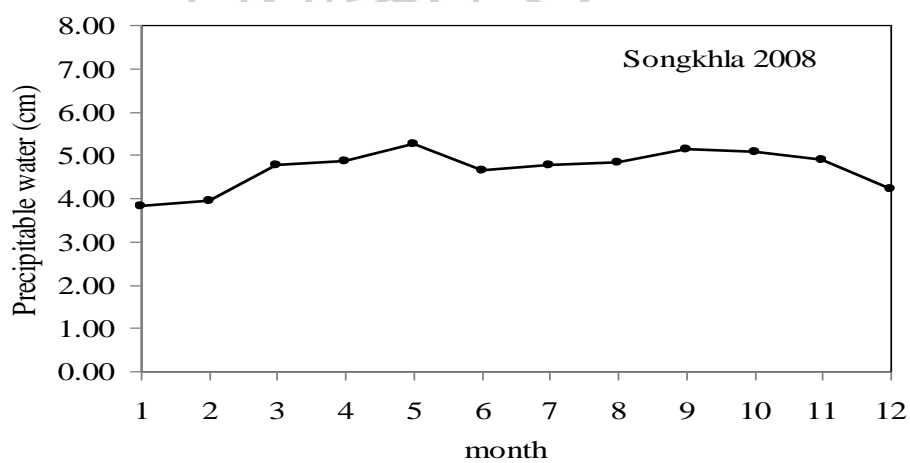


Figure 3.22 Monthly average precipitable water in the atmosphere in 2008 at Songkhla station.

The result of the model validation is shown in Figure 3.23 and Figure 3.24. The difference between these datasets can be presented in term of root mean square error (RMSE) and mean bias error (MBE). RMSE and MBE are defined as follows:

$$\text{RMSE}(\%) = \frac{\sqrt{\frac{1}{N} \sum_{i=1}^N (\text{PWV}_{i,\text{mod}} - \text{PWV}_{i,\text{meas}})^2}}{\frac{\sum_{i=1}^N \text{PWV}_{i,\text{meas}}}{N}} \times 100 \quad (3.8)$$

$$\text{MBE}(\%) = \frac{\frac{1}{N} \sum_{i=1}^N (\text{PWV}_{i,\text{mod}} - \text{PWV}_{i,\text{meas}})}{\frac{\sum_{i=1}^N \text{PWV}_{i,\text{meas}}}{N}} \times 100 \quad (3.9)$$

where $\text{PWV}_{i,\text{mod}}$ is the precipitable water from the empirical model, $\text{PWV}_{i,\text{meas}}$ is the precipitable water from the ground-based sunphotometer, i is the order of the data ($i = 1, 2, \dots, N$) and N is total number of the data.

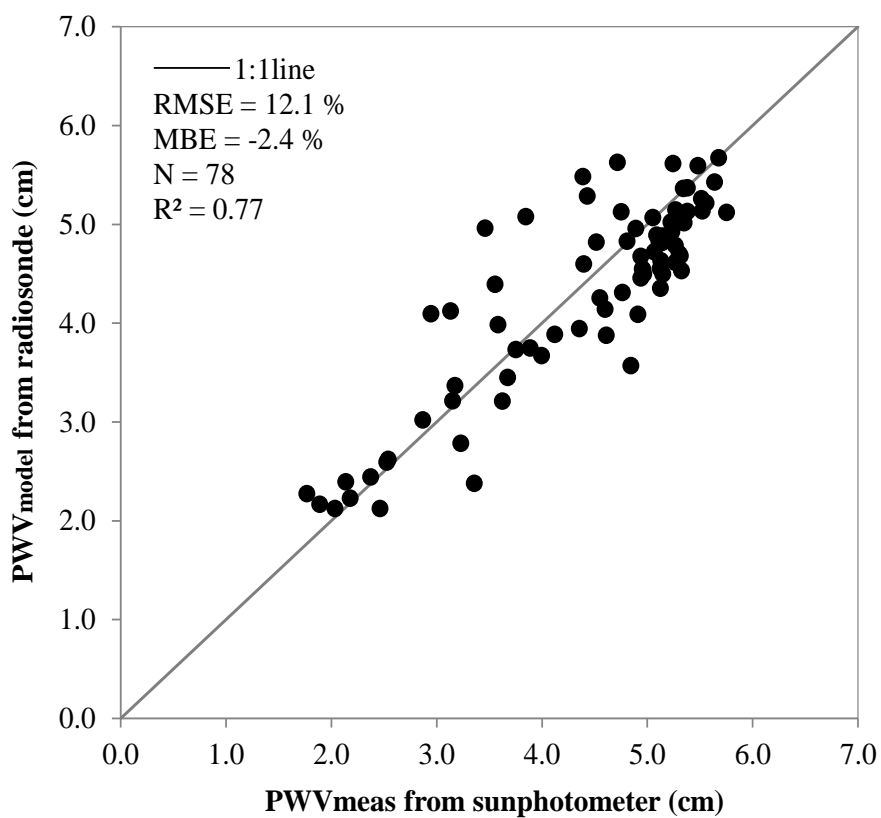
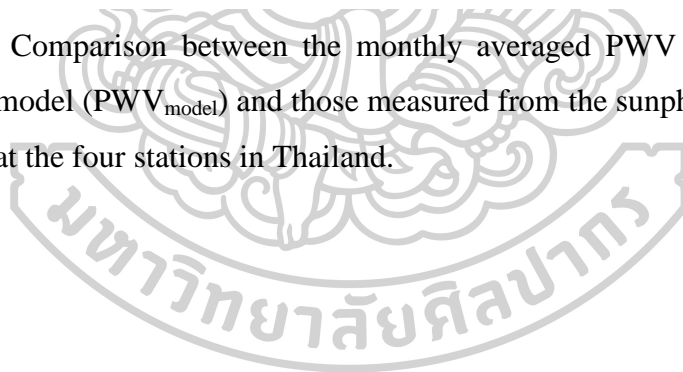


Figure 3.23 Comparison between the monthly averaged PWV calculated from the model (PWV_{model}) and those measured from the sunphotometer (PWV_{meas}) at the four stations in Thailand.



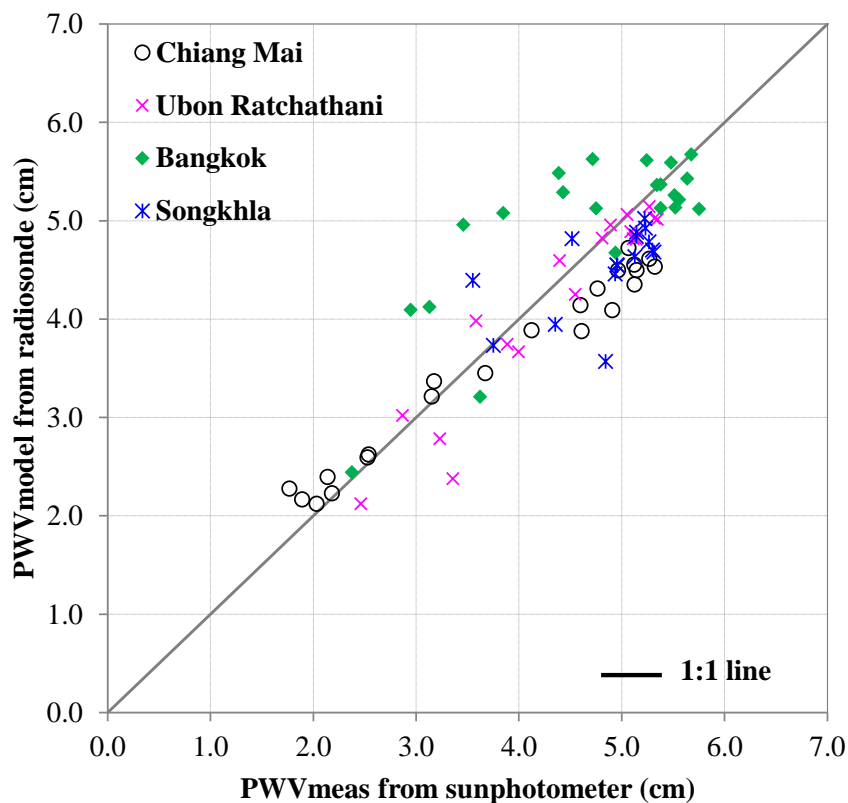
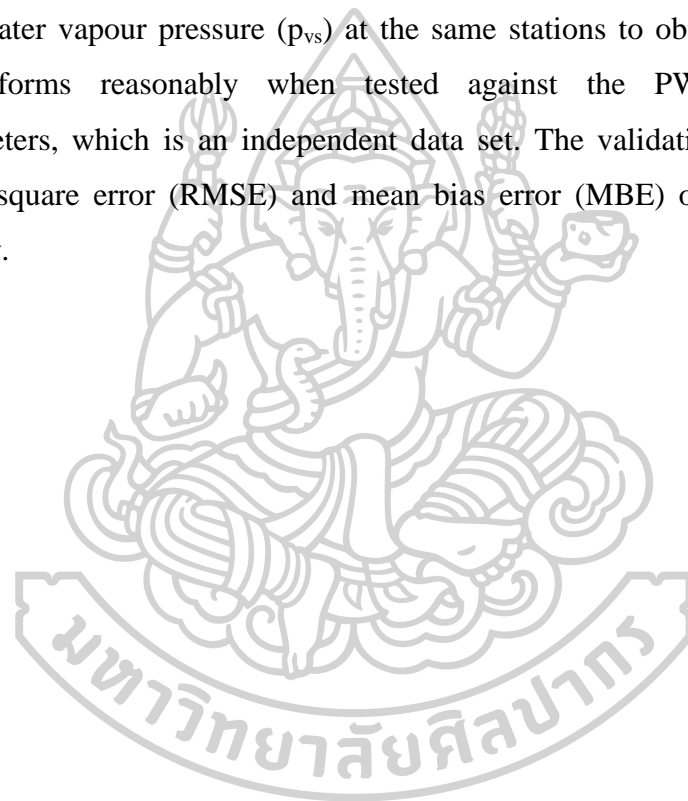


Figure 3.24 Comparison between PWV from the model and that from the sunphotometer at the four stations (Chiang Mai, Ubon Ratchathani, Nakhon Pathom, Songkhla).

From the validation of the model, the results show that the semi-empirical model can be used to estimate monthly average PWV with the root mean square error (RMSE) of 12.1% and mean bias error (MBE) of -2.4%, when compared with the ground-based data. It is to be noted that the data estimated from the model for Bangkok was compared with the data measured at Nakhon Pathom. Thus, the result for this comparison shows large scatter.

3.3 Conclusion

In this work, a simple semi-empirical model to estimate precipitable water using commonly available surface meteorological data, namely relative humidity (RH) and ambient temperature (T_a) was developed. In the model formulation, the upper air data including relative humidity and temperature at each height from the radiosonde at the four meteorological stations situated in the main regions of Thailand namely Chiang Mai, Ubon Ratchathani, Bangkok and Songkhla were collected and used to estimate the PWV. Then, PWV was correlated to the surface RH, T_a and saturated water vapour pressure (p_{vs}) at the same stations to obtain the model. This model performs reasonably when tested against the PWV obtained from sunphotometers, which is an independent data set. The validation result shows the root mean square error (RMSE) and mean bias error (MBE) of 12.1% and -2.4% , respectively.



Chapter 4

Estimation of Atmospheric Precipitable Water in Thailand using an Artificial Neural Network

Due to the importance of the atmospheric water vapour, there are several methods proposed to estimate the amount of water vapour. Apart from the empirical model introduced in Chapter 2, in this chapter, we describe an alternative method using an Artificial Neural Network (ANN) as a tool. The details of this method is explained as follows.

4.1 Artificial Neural Network

The science behind ANN is derived from the biological brain model (Garson, 1998). It consists of neurons which is group of connected cells (Figure 4.1). Impulses from input cells are received by these neurons make some transformation and then output is given to other neurons or output cells. Hence the network is formed with the help of connected layers which gets input from the above layer and output is passed to the next layer of neurons. The model of a neuron is shown in Figure 4.2.

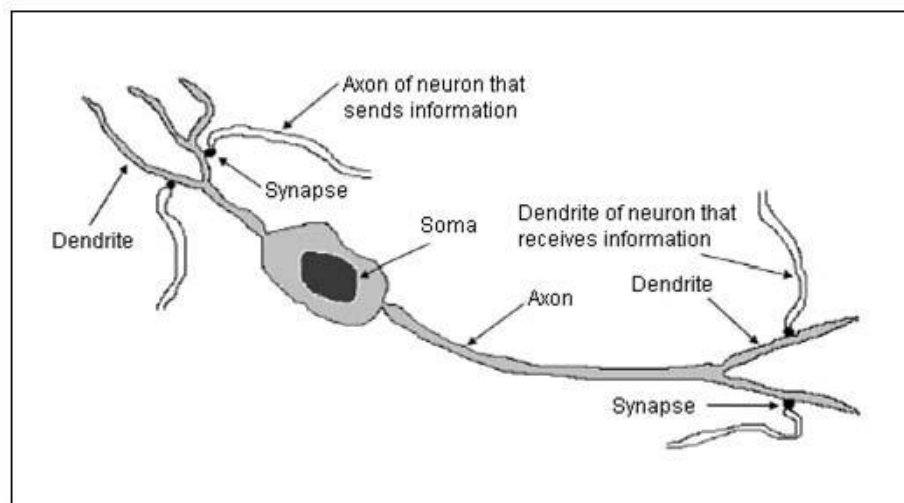


Figure 4.1 A simplified model of a biological neuron (Kumar, 2009).

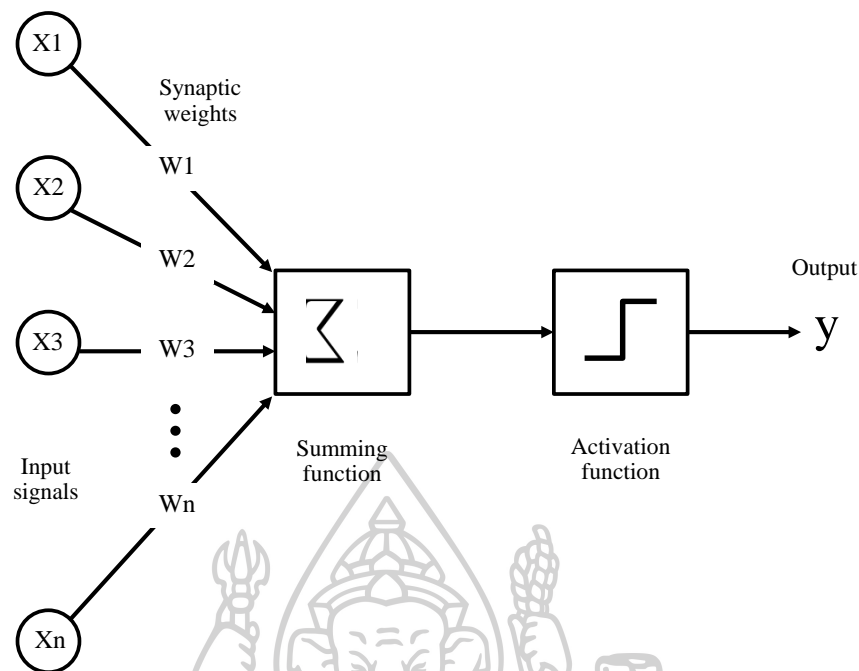


Figure 4.2 Artificial Neural Network (ANN) architecture (Sözen et al., 2004).

ANN method offers an advantage that it does not require the establishment of equations to calculate PWV. Instead, it requires only numerical data of input and output for training ANN. Afterward, the ANN which has been trained are applied to new input data in order to obtain new output, being similar to a function of human brains. Therefore, the objective of this work is to use ANN to obtain PWV in Thailand.

4.2 Data and Methodology

4.2.1 Collection of input and output data for ANN

In this work, the input data selected for ANN are monthly average data of relative humidity, air temperature, saturated water vapour pressure and month (m) obtained from the surface meteorological measurement. To obtain the saturated water vapour pressure, air temperature was used following the method of Iqbal (1983). These data are from the four meteorological stations: Chiang Mai, Ubon Ratchathani, Bangkok and Songkhla, during the period of 2009-2015.

For the output of the ANN, monthly average PWV measured by sunphotometers were used. These data are from the four stations, namely Chiang Mai, Ubon Ratchathani, Nakhon Pathom and Songkhla. The PWV data used in this part are in the same period of the input data.

4.2.2 Artificial neural network (ANN) modeling

The ANN model developed in this work has four-layers: one input layer, two hidden layers and one output layer (Figure. 4.3). The input layer of the model consists of four neurons that correspond to the four input variables. The input variables are: (1) relative humidity; (2) air temperature; (3) saturated water vapour pressure and (4) month. The output layer has one neuron that represents monthly averaged PWV in the model. The data during 2009-2013 were applied to train the ANN model.

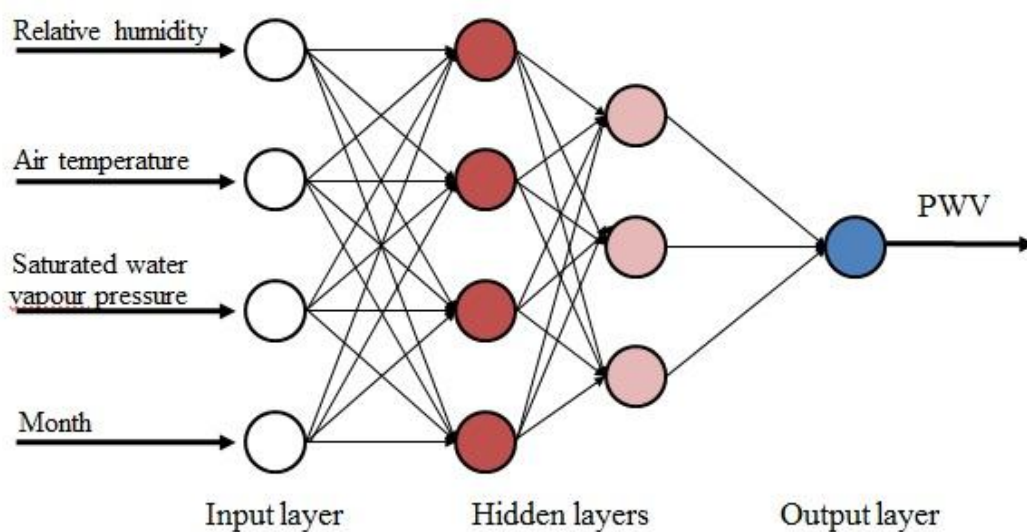


Figure 4.3 Structure of ANN for PWV estimation.

4.2.3 Training the ANN model

ANN can modify their behavior in response to their environment. Unlike a mathematical model, the structure of an ANN model itself cannot represent the system behavior, unless it is properly trained. The objective of training the network is to adjust the weights of the interconnecting neurons of the network so that application of a set of inputs produces the desired set of outputs. Initially, random values were used as weights and it was set to be 1.0. For brevity, one input–output set can be referred to as a vector. Training assumes that each input vector is paired with a target vector representing the desired output; together these are called a training pair.

A wide variety of training algorithms has been developed, each with its own strength and weakness. The PWV ANN models are trained by the backpropagation algorithm so that the application of a set of inputs would produce the desired set of outputs (Hecht-Nielsen, 1992).

The steps of the training procedure are summarized as follows: 1) an input vector is applied; 2) the output of the network is calculated and compared to the corresponding target vector; 3) the difference (error) is fed back through the network; and 4) weights are changed according to an algorithm called the delta rule (Wasserman, 1989) that tends to minimize the error. The vectors of the training set are sequentially applied. This procedure is repeated over the entire training set for as many times as necessary until the error is within some acceptable criteria, or until the outputs did not significantly change anymore. After the end of training, simulations are done with the trained model to check the accuracy of the training achieved.

4.2.4 Testing the ANN model

For validation process, the air temperature, relative humidity, saturated water vapour pressure and month at the four stations during 2014-2015 were used as input to the trained ANN model. The estimated monthly average PWV obtained from the ANN were compared with independent data measured from the sunphotometers. To evaluate the performance of the ANN, root mean square error (RMSE) and mean bias error (MBE) were calculated to indicate the difference between the two datasets. The comparison results are shown in Figure 4.4 The result shows that monthly average PWV obtained from the trained ANN model and that from the measurements for the

four stations were in good agreement with RMSE and MBE of 7.5% and -0.1%, respectively.

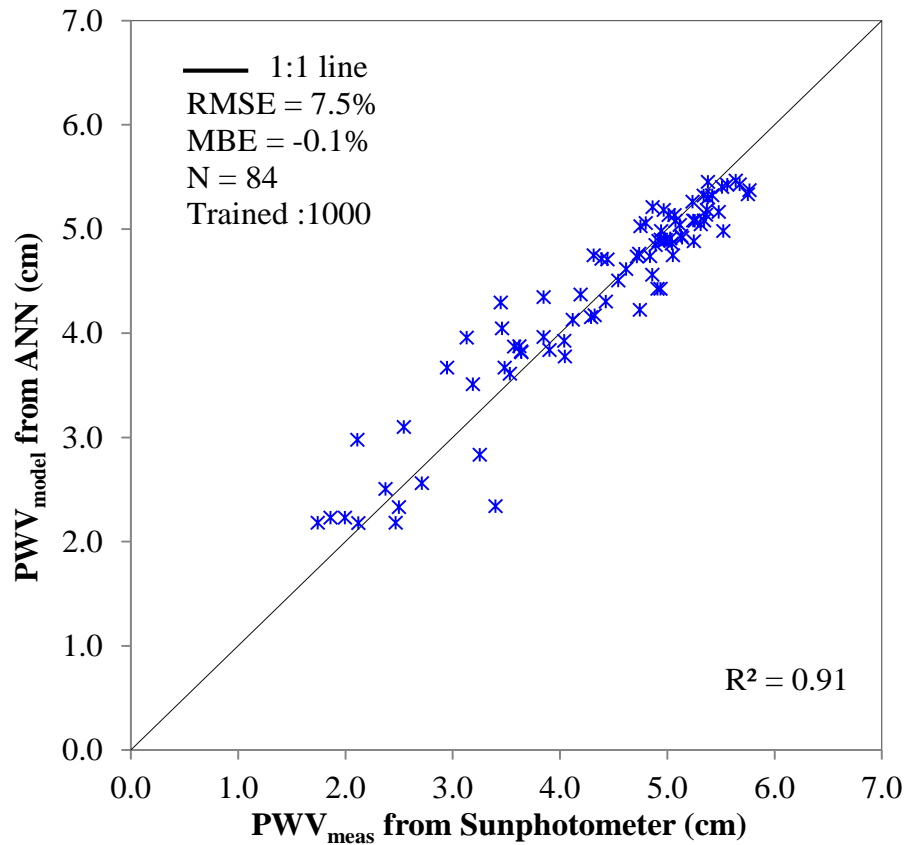
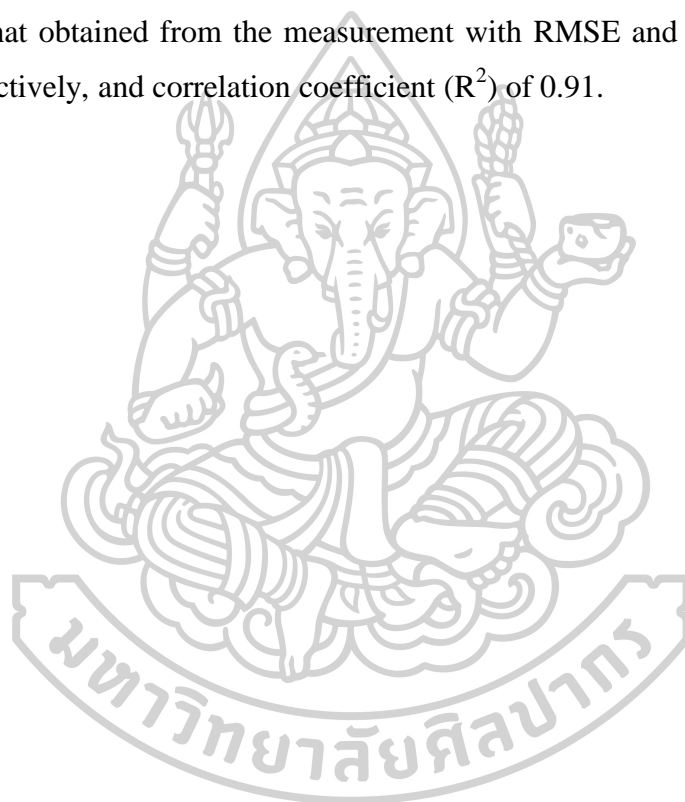


Figure 4.4 Comparison between measured and ANN estimated monthly average PWV. (RMSE is root mean square error, MBE is mean bias error and N is the total number of data points).

4.3 Conclusion

In this work, the artificial neural network (ANN) model was used to estimate monthly average PWV. The input of ANN is surface ambient air relative humidity (RH), surface ambient air temperature (T_a), saturated water vapour pressure (p_{vs}) and month (m). The ANN model was trained using the back propagation algorithm using the data from the four stations during the period: 2009-2013. The PWV from sunphotometers during a two-year period (2014-2015) was used to demonstrate the performance of the ANN. The result shows that PWV estimated from the ANN agrees well with that obtained from the measurement with RMSE and MBE of 7.5% and -0.1%, respectively, and correlation coefficient (R^2) of 0.91.



Chapter 5

Distribution of precipitable water vapour over Thailand using MTSAT-1R satellite data

5.1 Introduction

In general, PWV can be measured using ground-based instruments, e.g. microwave radiometer and sunphotometer, and also upper air radiosonde (Cuomo et al., 1997). However, the number of these instruments are limited due to their high price. An alternative solution to this problem is to use a classical modeling approach (Reitan et al., 1960; Hay et al., 1971) to determine the atmospheric PWV from temperature and relative humidity data. The results of above studies can be displayed the amount of PWV in the form of a contour maps covering the entire country. However, such approach is complicated and needs a number of input data which may not be available. Another solution is to use satellite data to estimate the PWV at regional and global scales (Takeuchi et al., 2010).

Apart from empirical models, satellite approach is another option to estimate water vapor over a large area, for example, over a country or over the globe. Larsen and Stamnes (2005) developed a technique for calculating the amount of water vapour in atmospheric haze cases using radiation reflected from the ground and retrieved by satellite sensors. Lee and Park (2007) conducted a study and tested a model for determining the amount of water vapour in the East Asian region using brightness temperature at wavelengths 11 and 12 μm , which are sensitive to water vapour. These data were obtained from GOES-9 and MTSAT-1R satellites. The technique was able to retrieve PWV to a satisfactory level of uncertainty with the root mean square difference of about 0.58 cm. Similarly, Akatsuka et al. (2010) also used the brightness temperature data from the MTSAT satellite to calculate PWV in East and Southeast Asia and the western Pacific. Model and measured data agreed to within root mean difference of 11.08%.

For this study, the distribution of PWV in the atmosphere over Thailand was investigated. The MTSAT-1R satellite data in the infrared channel that is sensitive to atmospheric water vapour was used to formulate an empirical model. This model was

validated and then used to estimate PWV over Thailand and the results are shown as maps.

5.2 Data acquisition

In order to estimate precipitable water from meteorological satellite data covering Thailand, concurrent with brightness temperature data in the infrared wavelength (6.2-7.3 μm) from MTSAT-1R and precipitable water measured from the ground-based measurement were obtained. Details are described in the following sections (Figure 5.1).

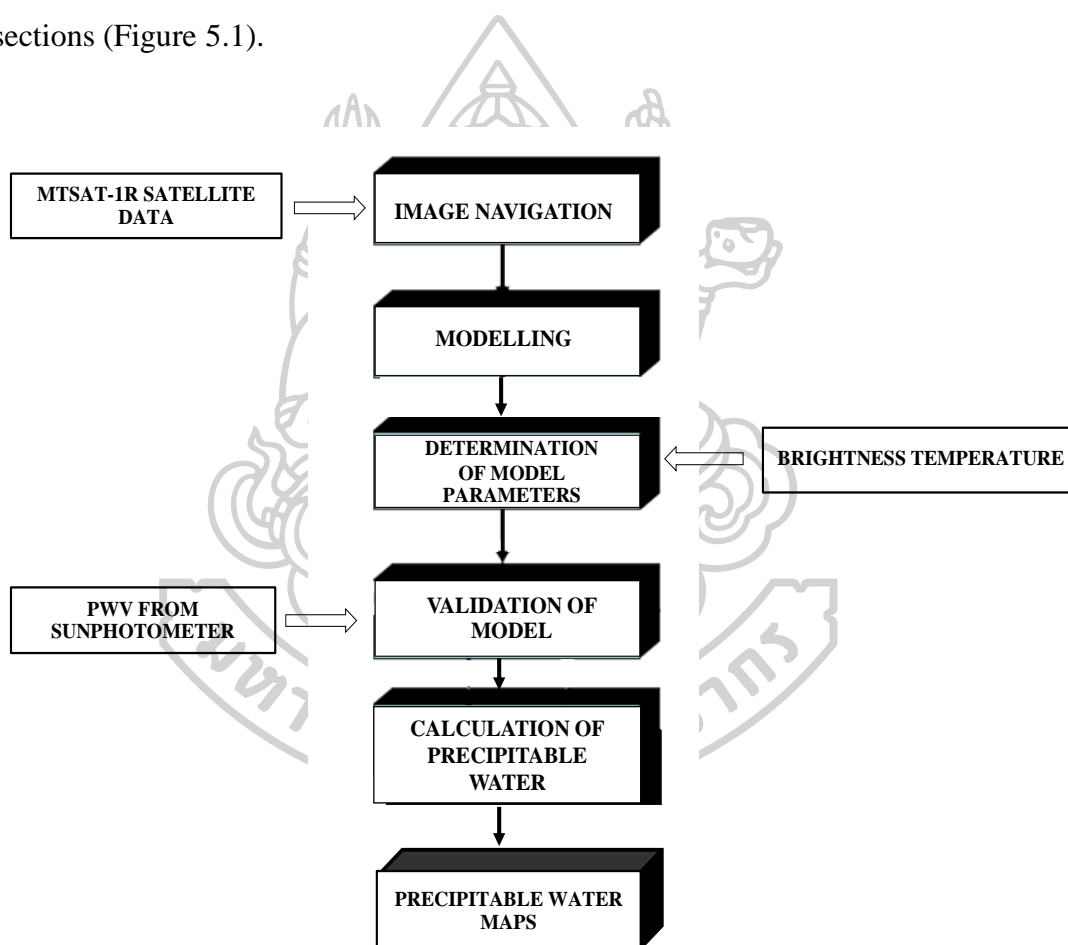


Figure 5.1 Schematic diagram of the method for generating the PWV maps.

5.2.1 Satellite data

5.2.1.1 MTSAT-1R

The Multi-functional Transport Satellite (MTSAT-1R) is Japanese weather satellite for geosynchronous orbit shown in Figure 5.2. That is over 35,786 km above the earth's surface at 140°E longitude. MTSAT-1R covers east and southeast asia and the western pacific region. This satellite provides image data at five channels every hour (Table 5.1) and shown in Figure 5.3. The IR3 images acquired at 0:00 and 24:00 (UTC) every day. This study used nine years (2007-2015) (Table 5.2) of data from the IR3 water vapour channel (6.2-7.3 μm) to examine PWV variability in Thailand region.

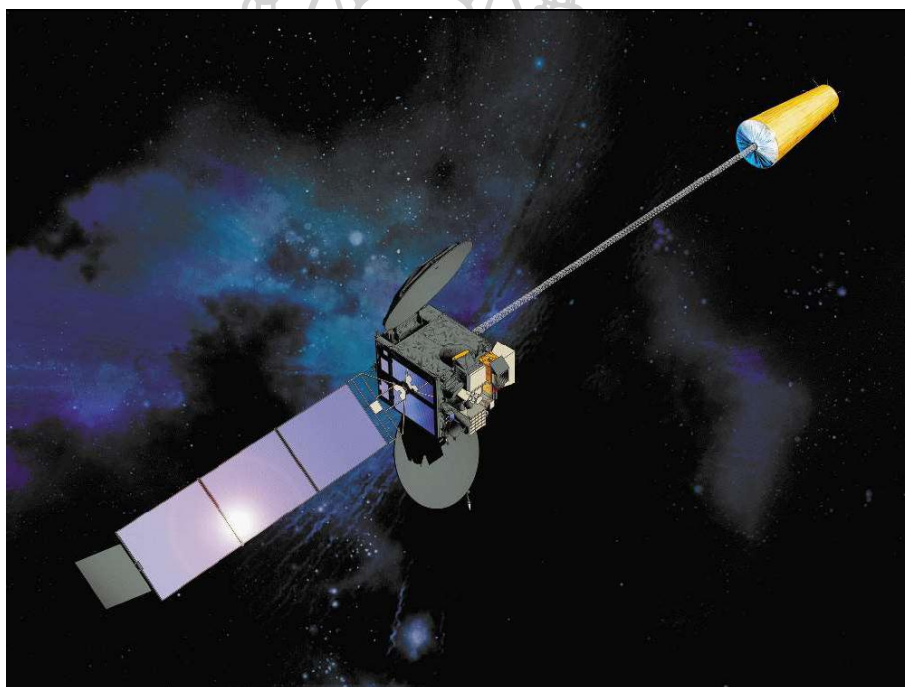


Figure 5.2 Multifunctional Transport Satellite (MTSAT-1R).

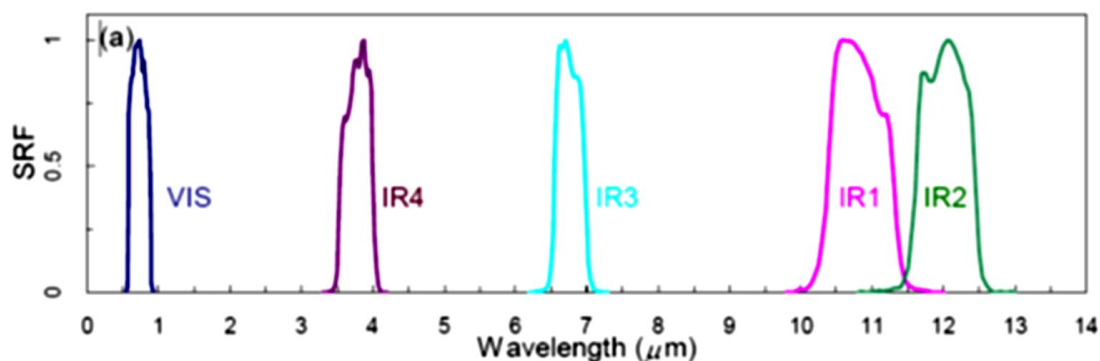


Figure 5.3 MTSAT-1R spectral response functions: full spectral range from the visible to the thermal infrared (Renzullo et al., 2006).

Table 5.1 Spectral band width and spatial resolution of the MTSAT-1R (Takeuchi et al., 2008).

Channel	Wavelength (μm)	Spatial Resolution (km)
VIS	0.55 - 0.90	1
IR1	10.3 - 11.3	4
IR2	11.5 - 12.5	4
IR3	6.2 - 7.3	4
IR4	3.5 - 4.0	4

Table 5.2 Period of the data from MTSAT-1R for modeling and validation.

Channel	Model formulation	Model validation
Water vapour (6.2-7.3 μm)	January, 2007 – December, 2013	January, 2014 – December, 2015

5.2.1.2 Satellite conversion

The retrieved satellite data cover the entire area of Thailand with a spatial resolution of $4 \times 4 \text{ km}^2$. Such information is in a satellite projection, the image is seen as a curve of the Earth's surface (Figure 5.4). Therefore, the satellite images were transformed to the cylindrical map projection (Figure 5.5) using a computer program written in Interactive Data Language (IDL). Then, the satellite map projection data were navigated using coastlines as references and sectorized. Each image covers latitude of 4.9°N - 20.80°N and longitude of 96.0°E - 106.0°E , and consists of 550×850 pixels (Figure 5.6). Each pixel contains a gray level value as digital 8-bit data (0 to 1023) (Janjai et al., 2011).

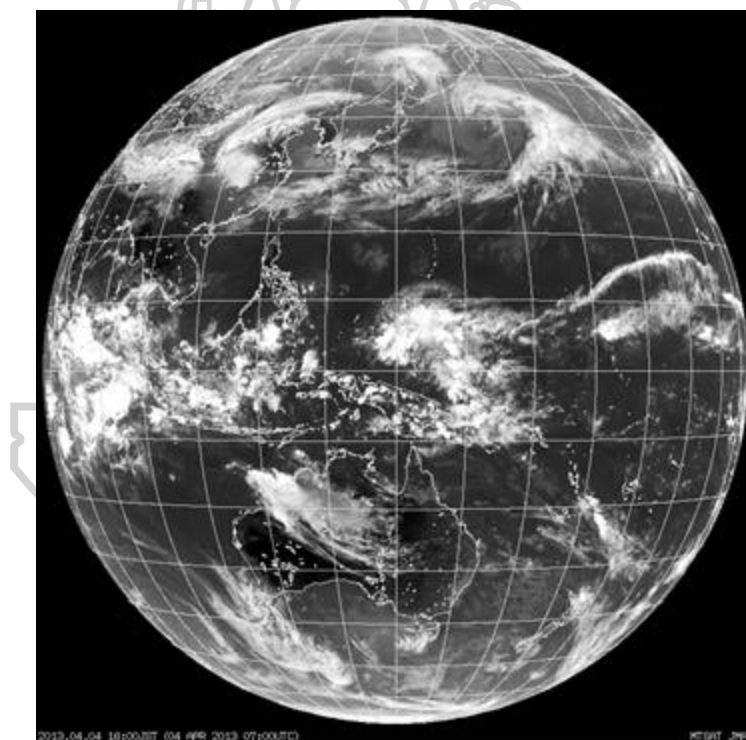


Figure 5.4 The satellite image data from MTSAT-1R in the water vapour channel (Janjai et al., 2011).

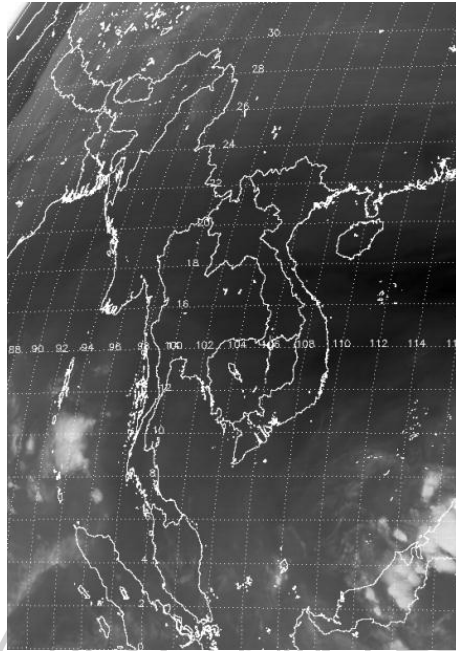


Figure 5.5 An example of Satellite Projection (Janjai et al., 2011).

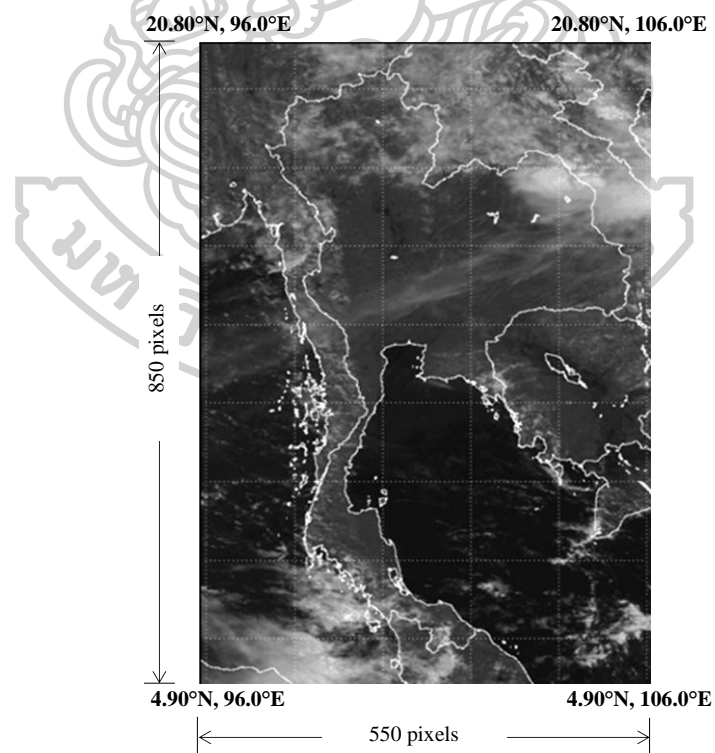


Figure 5.6 An example of a rectified satellite image (cylindrical projection) (Janjai et al., 2011)..

The gray level of each satellite pixel was converted to brightness temperature (T_B) using the conversion table from the satellite data agency as shown in Figure 5.7.

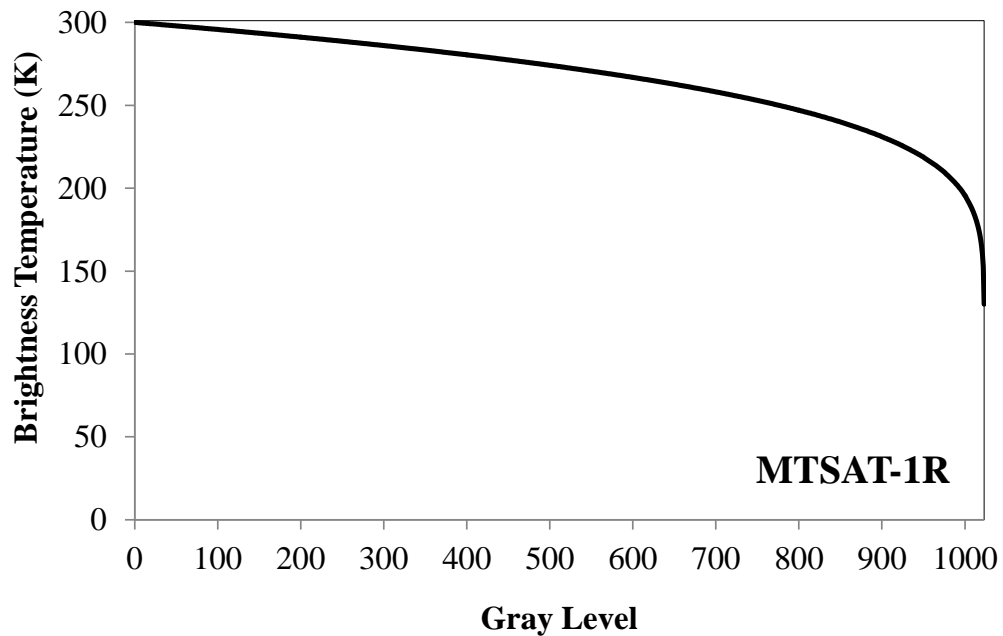


Figure 5.7 The relationship between the gray level with the brightness temperature from the water vapour channel of the MTSAT-1R satellite.

These data were obtained on an hourly basis from January 2007 to December 2015 and then averaged on a monthly basis. The monthly data of brightness temperature were used for modeling and validation, and also mapping of PWV (Figure 5.8 - 5.11).

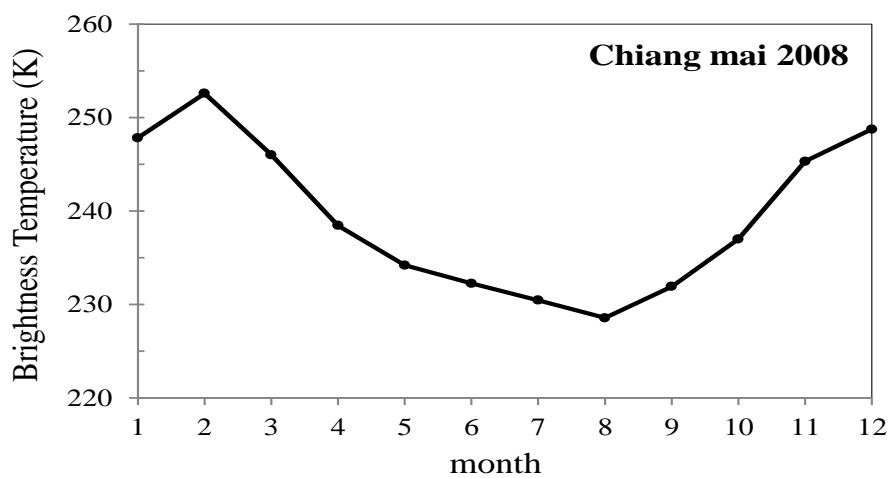


Figure 5.8 Example of monthly average brightness temperature in 2008 at Chiang Mai station.

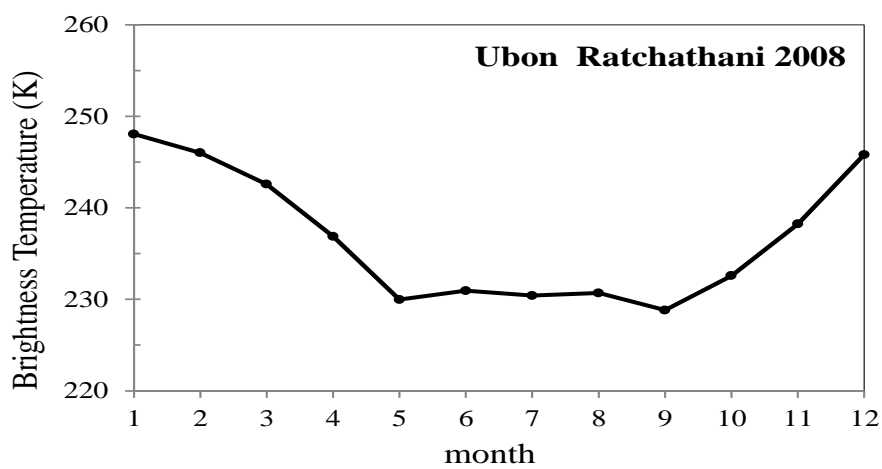


Figure 5.9 Example of monthly average brightness temperature in 2008 at Ubon Ratchathani station.

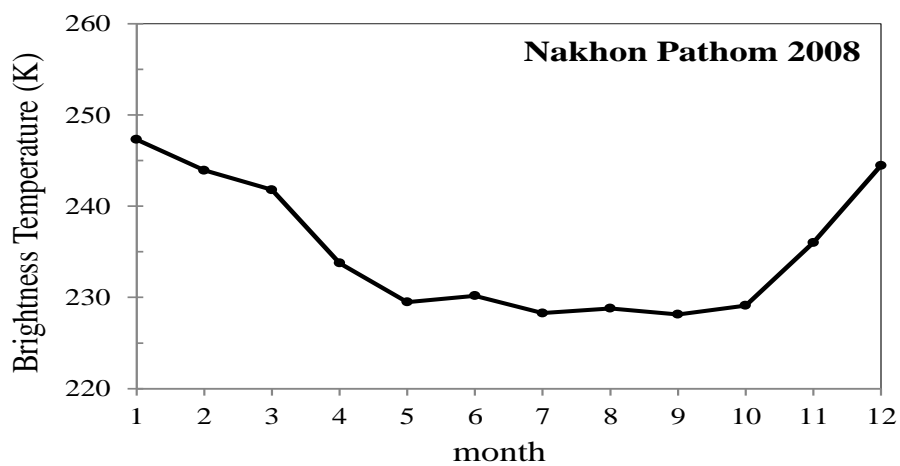


Figure 5.10 Example of monthly average brightness temperature in 2008 at Nakhon Pathom station.

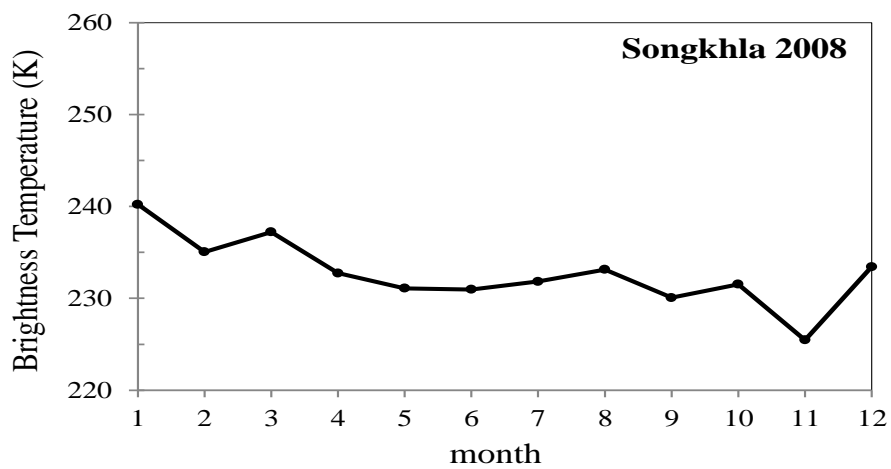


Figure 5.11 Example of monthly average brightness temperature in 2008 at Songkhla station.

5.3 Ground-based data

The PWV measured by sunphotometers were used to create a model for calculating PWV and test the model. These data are from the four meteorological stations, namely Chiang Mai (18.98°N, 98.98°E), Ubon Ratchathani (15.25°N, 104.87°E), Nakhon Pathom (13.82°N, 100.04°E) and Songkhla (7.20°N, 100.60°E) as described in Chapter 3. In this work, the PWV data obtained from these instruments during the period of 2007-2015 were downloaded from the AERONET website (<https://aeronet.gsfc.nasa.gov>) and then processed into monthly average PWV data.

5.4 Modeling and validation

The monthly average PWV data were separated into two groups. The first group was used for model formulation and the second group was used for model validation. The period of the data are shown in Table 5.3.

Table 5.3 Period of monthly average PWV from sunphotometer at the four stations for modeling and validation.

Station	Model formulation	Model validation
Chiang Mai (18.98°N, 98.98°E)	January, 2007– December, 2013	January, 2014– December, 2015
Ubon Ratchathani (15.25°N, 104.87°E)		
Silpakorn University, Nakhon Pathom (13.82°N, 100.04°E)		
Songkhla (7.20°N, 100.60°E)		

For modeling, the monthly average brightness temperature data obtained from the MTSAT-1R satellite at the four stations during January, 2007-December, 2013 were obtained and normalized with its highest value. Similarly, the PWV data obtained from the ground-based measurement were normalized with its highest value. Then the relation between the normalized brightness temperature and the normalized precipitable water was performed. The result is shown in Figure 5.12.

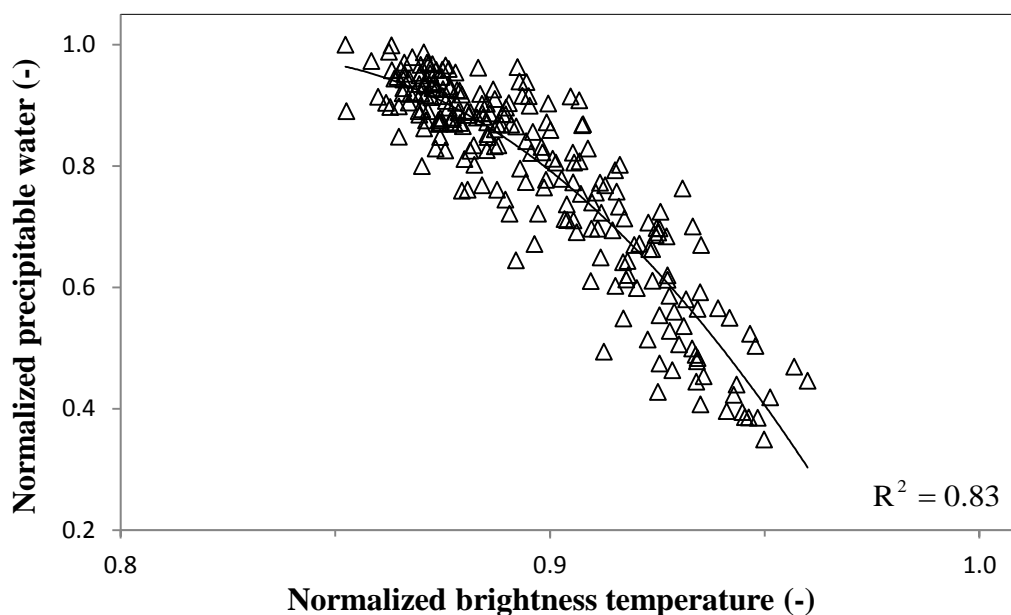


Figure 5.12 The relation between the normalized monthly precipitable water from the sunphotometers and the normalized monthly brightness temperature from MTSAT-1R.

From the result, the best fit by the least-square technique (Bates and Watts, 1988) can be expressed as a quadratic equation:

$$PWV' = a_1 + a_2 T_B' + a_3 T_B'^2 \quad (5.1)$$

where PWV' is the normalized monthly average PWV, T_B' is the normalized monthly average brightness temperature, and a_1 , a_2 and a_3 are regression coefficients. The values of coefficients and associated statistical values are shown in Table 5.4.

Table 5.4 The coefficient values of Equation (5.1) and statistic values. (R^2 is coefficient of determination and N is number of data)

Coefficient	Value of coefficient	t-statistic	p-value	R^2	N
a_1	-31.339	-4.8186	<0.05	0.83	232
a_2	73.960	5.3587	<0.05		
a_3	-42.328	-5.7822	<0.05		

When the Eq. (5.1) is applied to MTSAT-1R data, the monthly average PWV estimation formula using MTSAT data can be written as:

$$PWV' = -31.339 + 73.96T'_B - 42.328T'^2_B \quad (5.2)$$

$$PWV = (PWV') \times 5.754 \quad (5.3)$$

where PWV is monthly average precipitable water (cm), 5.754 is maximum precipitable water value for normalization.

As shown in Table 5.4, all regression coefficients are significant at the 95% level of confidence. Therefore, the empirical model was used for estimating monthly average PWV and validated with independent data from PWV measured at the four stations during 2014-2015. The result of the model validation is shown in Figure 5.13 and Figure 5.14.

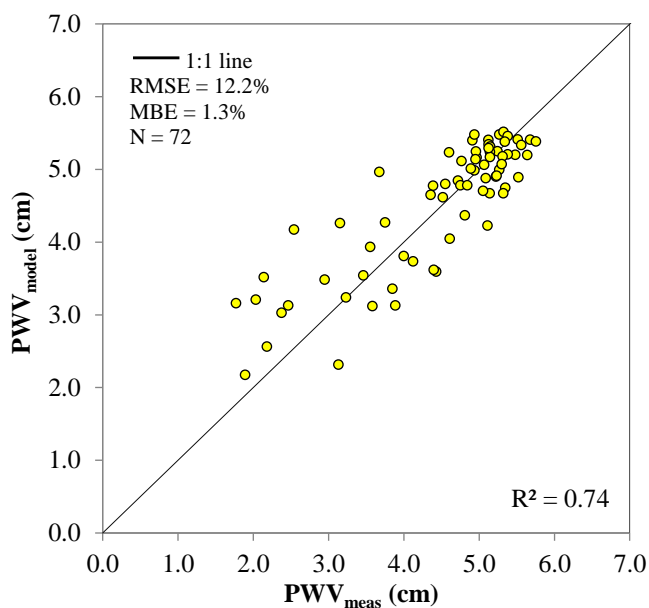


Figure 5.13 Comparison between the monthly average PWV calculated from the empirical model (PWV_{model}) and those measured from the ground-based sunphotometer (PWV_{meas}) at the four stations in Thailand.

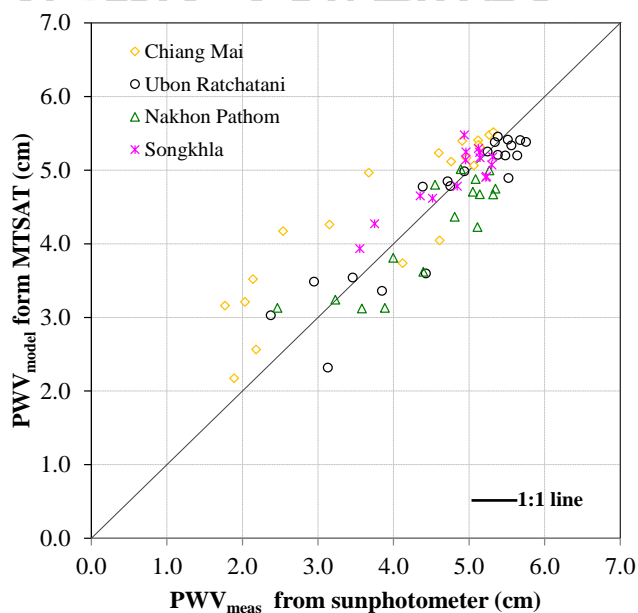


Figure 5.14 The comparison between the monthly averaged PWV from the semi-empirical model and that obtained from sunphotometer. The diagonal line represents the reference where the PWV from the upper air is equal to the PWV obtained from the latitudes model.

In this work, the root mean square error (RMSE) and mean bias error (MBE) were used for an evaluation of the model's performance. The result are shown in Table 5.5.

Table 5.5 Comparison between the monthly averaged PWV from measurement and those monthly averaged PWV from model.

Station	RMSE (%)	MBE (%)
Chiang Mai	20.1	13.3
Ubon Ratchathani	11.3	-7.0
Nakhon Pathom	8.6	-2.7
Songkhla	6.0	2.1
All 4 stations	12.2	1.3

The results show that the empirical model can be used to estimate monthly averaged PWV with the RMSE and MBE of 12.2% and 1.3%, respectively, when compared with the ground-based data. This results can be considered as an acceptable level of work in this field (Wong, 2015). Therefore, the model can be used to calculate the water vapour over the country.

5.5 Mapping of PWV

After validation, the empirical model was used to estimate a climatology of PWV using nine years (2007-2015) of MTSAT-1R data over Thailand. Figure 5.15 and Figure 5.16 provide monthly and yearly PWV maps, respectively.

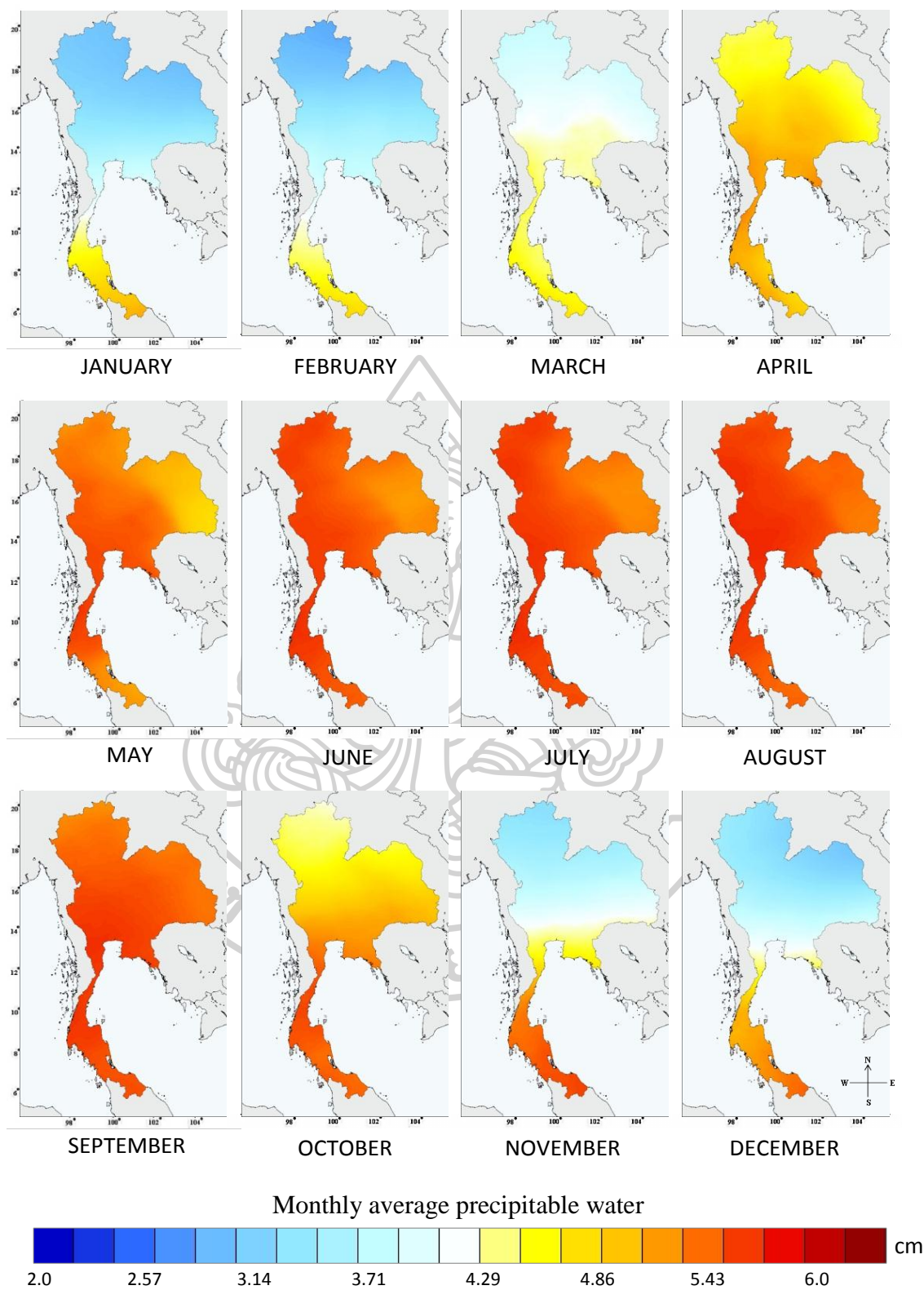
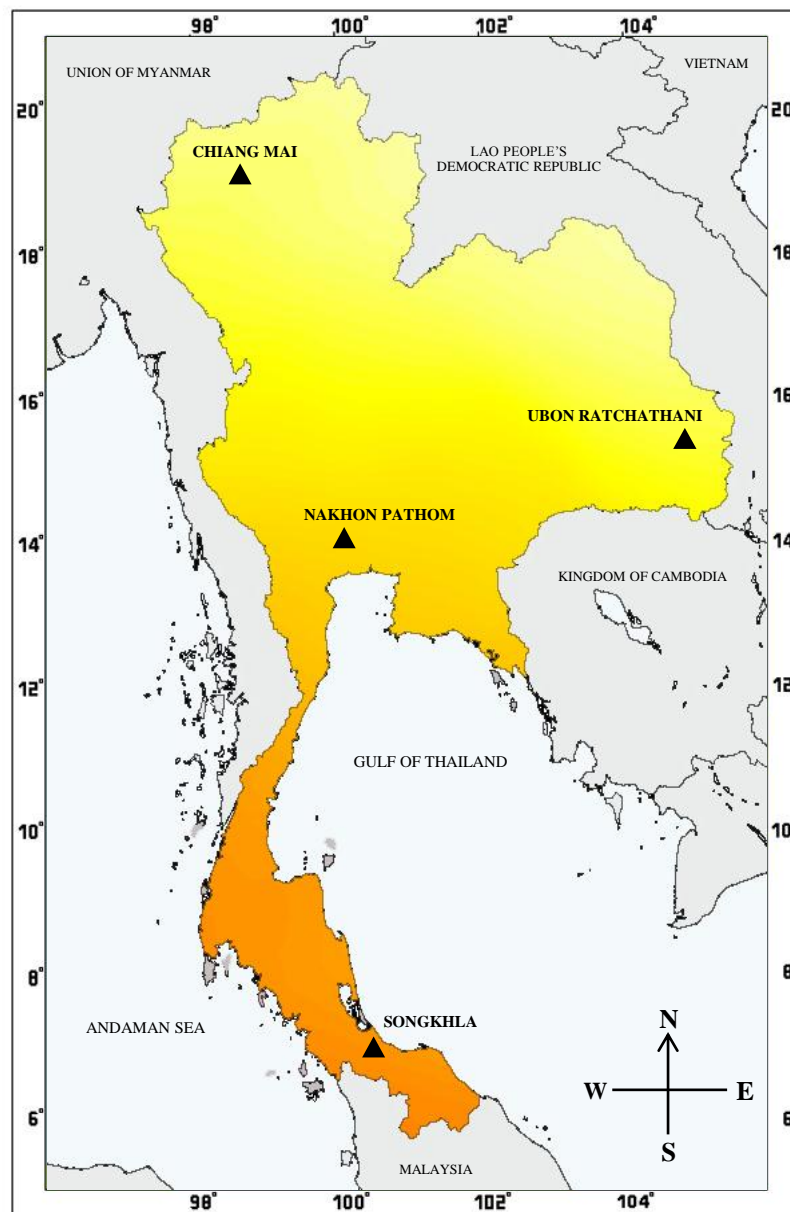
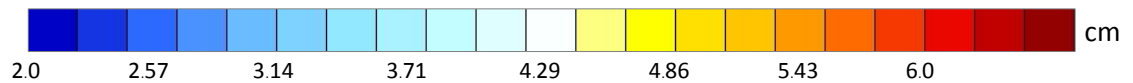


Figure 5.15 Monthly average precipitable water over Thailand.



Yearly average precipitable water



Data Min = 3.987 cm, Max = 5.332 cm

Figure 5.16 Yearly average precipitable water over Thailand.

The results in Figure 5.15 show the distribution of monthly average PWV over Thailand. It is clearly seen that PWV in this region varies strongly at the temporal and spatial scale. The variations depend on the influence of local monsoons. During November to April which is in the period of northeast monsoon, there is less water vapour in the atmosphere in the northern and central parts of the country as dry air is transported from China. However, in the southern part, there is higher amount of the PWV because the monsoon brings rain to this region. For the period of May to October, the area around the country is influenced by the southwest monsoon, transporting the moist air from the Andaman Sea into Thailand and thus resulting in a high amount of PWV. This result is consistent with the distribution of rainfall in Thailand (Janjai et al., 2015).

The map of the long-term yearly PWV is shown in Figure 5.16. It can be seen that the amount of PWV varies with latitude, increasing in the south and gradually decreasing in the north.

5.6 Conclusion

This study has examined the spatial distribution of water vapour over Thailand. Concurrent data from the brightness temperature of MTSAT-1R satellite and the precipitable water from sunphotometers were used to develop an empirical model. Model validation was satisfactory when tested against independent data from four sunphotometer located in Thailand. Results were displayed as monthly and yearly precipitable water maps. The maps reveal that precipitable water varies strongly with the seasons and the geographical regions of the country.

Chapter 6

Spatial and Temporal Changes of Precipitable Water Vapour in Thailand

6.1 Introduction

Water vapour is the most important natural greenhouse gas. It is however, marked by very high spatial and temporal variability, with an average residence time of around 9 days in the atmosphere (Tuinenburg, 2017). Global climate models point to increase water vapour amounts as climate warms (Randall et al., 2007), leading to an enhanced greenhouse warming. These results are supported by measurements across the globe, indicating that global-average column water vapour increases by about 7% for every degree of warming (Wentz and Schabel, 2000; Trenberth et al., 2005; Schneider et al., 2010; Takahashi, 2016). However, these average figures contain considerable regional variability as reported in global analyses of radiosonde data (Trenberth et al., 2005; Mieruch et al., 2008) and there is need to develop regional studies to examine how representative these global changes are. Studies in tropical regions are particularly warranted as column water vapour trends in tropical areas are amongst the highest reported globally (Dai et al., 2011).

There is also a need to examine in more detail changes in water vapour following a warming event. A warming environment relates to an increased capacity by the atmosphere to hold moisture, but this effect may be offset by a lower relative humidity, leading to no increase or a decrease in actual vapour pressure. These changes in specific and relative humidity are important in estimating feedback effects, especially in the tropics where the hydrologic cycle is strongest. A reduced relative humidity may produce a lower vapour pressure compared to what would occur if the relative humidity were to remain constant in a warming world, therefore reducing the feedback effect. There is, however no clear agreement on the possible changes in relative humidity and its spatial variability (Soden et al., 2002; Minschwaner and Dessler, 2004).

This study examines the above issues in the tropical region of Thailand using instrumental records of column water vapour covering a period of several decades. Specifically, we present detailed spatial patterns of water vapour for the Thailand

region and examine long-term trends and their likely causes. Our approach has been conditioned by several factors. Firstly, unlike midlatitude regions of the northern hemisphere, there are few stations recording column water vapour of a long-term duration and with suitable instrumental records (www.tmd.go.th). Secondly Thailand extends from 6°N to 20°N and from 98°E to 106°E with dry winters in the north and humid/tropical conditions in the south all year long (Janjai et al., 2013). Therefore, data from one or two stations would not suffice and it is not possible to conduct detailed studies involving many surface observations, for example similar to that of Alshawaf et al. (2017) over Germany.

Given our objectives, re-analysis data from the European Centre for Medium-range Weather Forecast (ECMWF) i.e. the ERA-Interim data set (Dee et al., 2011) was used in this study as it was considered the most appropriate, having been revised and improved over the years. Furthermore, this data set performed well when compared with ground-based observation (Bock and Nuret, 2009). Also, it is one of the advanced global atmospheric re-analysis data (Zhang et al., 2018). A section of our study focuses on the validation of the re-analysis data with local estimates of PWV using radiosonde soundings and the MODIS satellite data. Detailed analysis of the ERA data for the Thailand region follows after establishing confidence limits on its ability to predict local PWV. The data sets used and subsequent analysis are described in more detail in the next section.

6.2 Methodology

6.2.1 Data sets

Monthly radiosonde data were sourced to a common provider, the Integrated Global Radiosonde Archive (IGRA2) from the National Climatic Data Center (NCDC) available online at www.ncdc.noaa.gov/data-access/weather-balloon/integrated-global-radiosonde-archive (Durre et al., 2006; 2008). The data set encompasses more than 1,500 global stations dating back to the 1960s. The data set records variables such as air temperature, relative humidity, pressure and geopotential height at standard pressure levels, namely 1000, 925, 850, 700, 500, 400, 300, 250, 200, 150, 100, 70, 50, 20, 10, 7, 5, 3, 2 and 1 hPa (Durre et al., 2006). All data at these levels were used in our analysis. There are strict quality control algorithms that check

for inconsistencies such as duplicate levels, outliers, and manual checks on reasonable thresholds, amongst others. A useful metadata on background instrumentation and station history is also available. Monthly radiosonde data encompassing air temperature, geopotential height and mixing ratio were selected for a number of stations covering the years 2009-2015. We used three tropical stations in capital cities and a coastal station in tropical Vietnam with good quality control, complete or near-complete records and a continuous history of instrumentation that were used. They consisted of Bangkok (BK) Bangna Agromet (13.67°N; 100.61°E), Singapore (SP) Changi Airport (1.37°N; 103.98°E), Kuala Lumpur (KL) Airport (2.72°N; 101.70°E) and Danang (DN) (16.07°N; 108.35°E). The information on the data used is summarized in Table 6.1 and the locations of the sites related to the data is shown in Figure 6.1. Monthly data from these stations were used to obtain PWV using Equation (3.2).

Table 6.1 Details of the data sets used in the analysis.

Data set	Location	instrument	Freq.	period	Source
Radiosondes	Bangkok (13.67°N; 100.61°E) Singapore (1.37°N; 103.98°E) Kuala Lumpur (2.72°N; 101.70°E) Danang (16.07°N; 108.35°E)	Vaisala (RS80) Vaisala (RS92) Graw DMF09 Vaisala (RS80)	1 or 2 daily observation (0:00; 12:00 UTC)	2009-2015	IGRA [§]
ERA-Interim	4-22°N; 96-107°E (Resolution 0.25°×0.25°)		6 hourly	1981-2017	ECMWF [#]
MODIS	Bangkok (13.67°N; 100.61°E) Singapore (1.37°N; 103.98°E) Kuala Lumpur (2.72°N; 101.70°E) Danang (16.07°N; 108.35°E) (Resolution 1°×1°)	Terra and Aqua	1 or 2 daily observation	2009-2015	NOAA [*]

[§] *Integrated Global Radiosonde Archive*

[#] *European Centre for Medium Range Weather Forecast*

^{*} *National Oceanographic and Atmospheric Administration (USA)*



Figure 6.1 Station locations (▲).

A second data set used for comparison consisted in monthly average PWV from the MODIS instrument aboard the Terra and Aqua satellites (Platnick et al., 2015). The two products, MOD08_M3 (Terra) and MYD08_M3 (Aqua) rely on an algorithm that estimates absorption of near infrared solar radiation by water vapour during daytime, and thermal infrared absorption at night, both for cloudless conditions. Apparent reflectance in the water vapour channel (0.94 μm) and two window channels (0.865 and 1.24 μm) are estimated and related to a water vapour transmission and total PWV via a look up table (Kaufman and Gao, 1992; King et al.,

1992; Gao and Kaufman, 2003). We used the monthly average product, available at a spatial resolution of about $100 \text{ km} \times 100 \text{ km}$. The monthly gridded data corresponding to the radiosonde locations were selected to compare with the radiosonde and the ERA-Interim data.

By definition, re-analysis data are developed by re-visiting forecasts issued by regional and global climate models. Predictions for a specific time ($T_{i+\Delta t}$) and issued from T_i are compared with measured data from various sources and are then assimilated into the model output at time $T_{i+\Delta t}$. Model parameters are then adjusted so as to give the best possible fit to the measured data at $T_{i+\Delta t}$, therefore providing a range of model variables that best match observations

The ERA re-analysis data (www.ecmwf.int) is a further improvement as it can accept both regular and irregular meteorological data, it provides a better representation of stratospheric circulation, it has a better representation of the hydrologic cycle and a better humidity analysis, and it employs a 4D variable assimilation to minimize errors (Berrisford et al., 2011). It is presently used in a large number of climates and trend analysis studies (Bengtsson et al., 2004; Simmons et al., 2006; Rienecker et al., 2008; Dee et al., 2011). For our study, we selected monthly average PWV output at 0.25-degree data resolution and sectorised the Thailand region bounded by latitudes 4°N - 22°N and longitudes 96°E - 107°E . Therefore, a total of 444 monthly average PWV arrays (37 years \times 12 months) were available for analysis covering the study period, with each array consisting of 44 columns and 72 lines.

6.2.2 Comparison PWV from ERA with PWV derived from radiosonde and MODIS

Figure 6.2 and Table 6.2 summarize the comparison results. Examining Figure 6.2, it is evident that unlike SP and KL, BK and DN span a wider range of PWV as it experiences both a dry season during winter months (November to February) and a wet season during the southwest monsoon which encompasses June to October (Janjai et al., 2013). By contrast, both KL and SP experience wet conditions throughout the year, resulting in a lower coefficient of variance (R^2) compared to BK. Mean bias error (MBE) comparisons between ERA-Interim and MODIS ($\text{PWV}_{\text{ERA}} - \text{PWV}_{\text{MODIS}}$) range between 0.014 cm for BK to 0.370 cm for DN. ERA-Interim shows a tendency

to underestimate slightly when compared to IGRA, with MBE ($PWV_{ERA} - PWV_{IGRA}$) ranging between -0.296 cm (DN) to -0.025 cm (BK). Root mean square error (RMSE) between PWV from ERA-Interim and IGRA are high and of the same order of magnitude as that between PWV from ERA-Interim and MODIS. Coefficients of variance are higher for ERA-Interim/IGRA compared to ERA-Interim/MODIS.

Table 6.2 Comparison of ERA-Interim vs IGRA and ERA-Interim vs MODIS

Station	ERA vs IGRA				ERA vs MODIS			
	R ²	MBE (cm)	RMSE (cm)	N	R ²	MBE (cm)	RMSE (cm)	N
Bangkok (BK)	0.95	-0.025	0.244	70	0.91	0.014	0.283	84
Singapore (SP)	0.82	-0.068	0.169	84	0.35	0.170	0.339	83
Kuala Lumpur (KL)	0.74	-0.144	0.242	71	0.16	0.293	0.463	83
Danang (DN)	0.98	-0.296	0.359	83	0.75	0.370	0.571	84

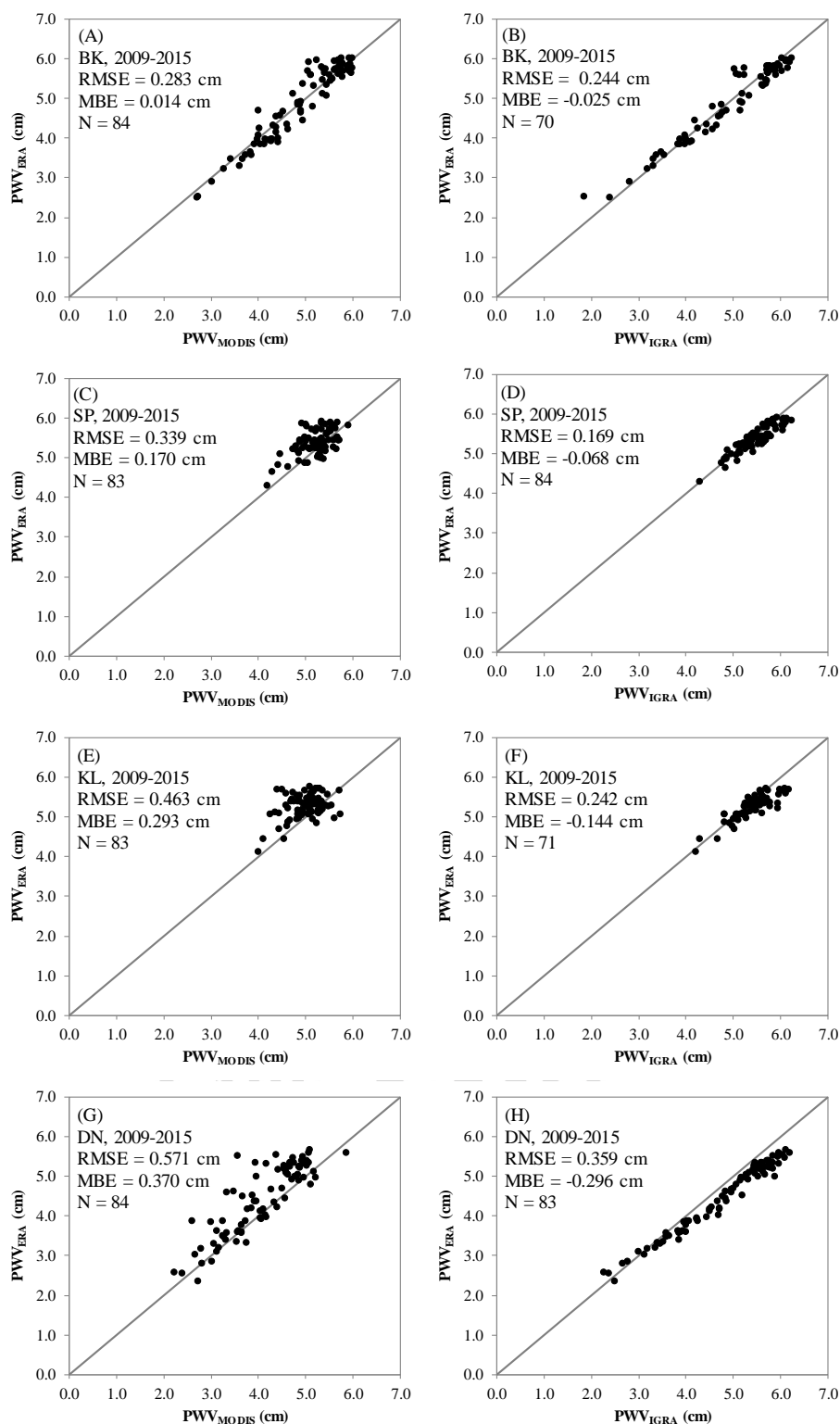


Figure 6.2 Monthly comparisons of PWV from ERA-Interim (PWV_{ERA}) vs PWV from MODIS (PWV_{MODIS}) radiosonde and from IGRA (PWV_{IGRA}).

Uncertainties expressed in Figure 6.2 and Table 6.2 result from uncertainties inherent in each method. For MOD08_M3 and MYD08_M3, there are approximately 10% and are attributed to various factors such as changes in surface spectral reflectance, errors in sensor calibration, and incorrect pixel registration between channels (Kaufman and Gao, 1992; Gao and Kaufman, 2003; Li et al., 2003). Additionally, haze effects may introduce up to a 10% uncertainty. As discussed, the methodology employed in re-analysis data is different and incorporates measured PWV estimates within its calculation (Berrisford et al., 2011). An approximate estimate of the error involved in the comparison may be obtained by estimating the ratio of RMSE to the mean PWV. This calculation gives 5.8%, 6.5%, 9.3%, and 14.0% for BK, SP, KL and DN, respectively. These figures average to 8.9% which is close to the overall published uncertainty of 10%. Therefore, it is likely that the uncertainty seen in Figures 6.2(A), 6.2(C), 6.2(E) and 6.2(G) is largely driven by the established MODIS uncertainties.

Uncertainties in radiosonde on a global scale have been related to the type of humidity sensors, which in western countries use capacitance sensors as opposed to goldbeater's skin humidity sensor used in the former Soviet Union and China (Soden and Lanzante, 1996). This study also showed that upper troposphere humidity appears to be underestimated by capacitance sensors when compared with TOVS data. These observations are in agreement with results in Ethiopia by Mengistu Tsidu et al. (2014) who reported a mean bias of -3.17 mm (radiosonde – ERA-Interim) with concurrent measurements of these two quantities. Other errors relate to the horizontal drift of the radiosonde (Li et al., 2003) and to the type of radiosonde which may or may not include radiation corrections (Li et al., 2003; Namaoui et al., 2017). RMSE in Figures 6.2(B), 6.2(D), 6.2(F) and 6.2(H) average to 0.264 cm, which is close to the average figure of 0.429 cm in Figures 6.2(A), 6.2(C), 6.2(E) and 6.2(G). However, the coefficient of variance is higher in the former group, perhaps reflecting the dependence of ERA-Interim in the radiosonde data and additional errors in the MODIS calculations.

6.3 Results

6.3.1 Seasonal and yearly average PWV

The contours of monthly average PWV obtained from the ERA data set (1981 – 2017) are displayed in Figure 6.3. It is important to note that the significance of the estimates are around ± 0.5 cm but a finer contour interval has been used for display purposes (0.2 cm and 0.3 cm).

Figure 6.3(A) presents monthly average PWV for the winter season. This figure shows a marked gradient with latitude, with high values in tropical areas (~ 5 cm) to lower values in the northern highland regions (~ 2.5 cm).

The summer season is characterized by an increase in PWV in the northern regions but relatively little change in the south. The gradual decrease in PWV with latitude observed in the map for winter is disrupted by a marked increase in PWV inland, especially in the east and southeast of the country (Figure 6.3(B)).

Gradients are very weak in the rainy season, as shown in Figure 6.3(C). The contour pattern does not show a consistent change in the country as most values are from 4.8 to 5.5 cm. However, there is a pronounced lowering of PWV with latitude in the north of Thailand. For yearly average in Figure 6.3(D), the map still shows a pattern of decreasing PWV with latitude, extending from 5.0 cm in the south to 3.5 cm in the north.



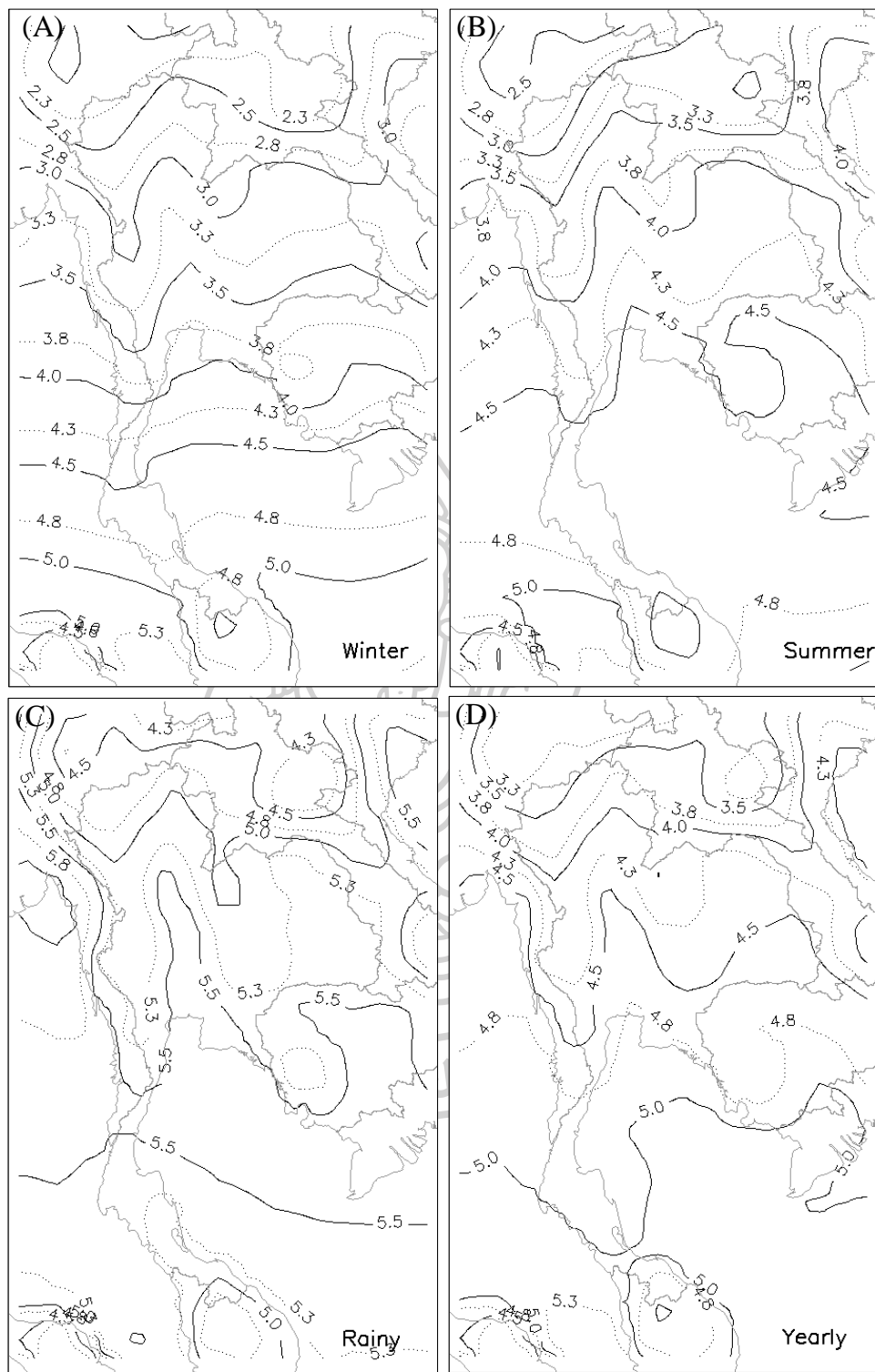


Figure 6.3 The monthly average PWV for (A) winter, (B) summer, (C) rainy and (D) yearly average PWV.

6.3.2 Long-term yearly trends

The long-term trends of PWV are examined for each season using the following procedure. Firstly, each PWV seasonal map was sectorised into square grids (0.25° latitude \times 0.25° longitude). A second step used robust analysis for detection of outliers which can potentially distort the trend (Rosseeuw and Leroy, 2005; Heritier and Cantoni, 2009; Muhlbauer et al., 2009). The Least Trimmed Square (LTS) estimator technique involves applying all possible combination of slopes and intercepts, obtaining squared residuals for each regression set, ordering the squared residuals according to magnitude, and summing the n^{th} lowest squared residuals, where n is a median value. The slope/intercept combination giving the lowest sum will be the required slope and intercept (Muhlbauer et al., 2009). The regression pair is then used to estimate the residuals. Any residuals larger than 2.5 standard deviations are eliminated from the analysis (Rosseeuw and Leroy, 2005). Approximately 12% in rainy season and 1% in summer season of the data sequence failed the residual test and was eliminated.

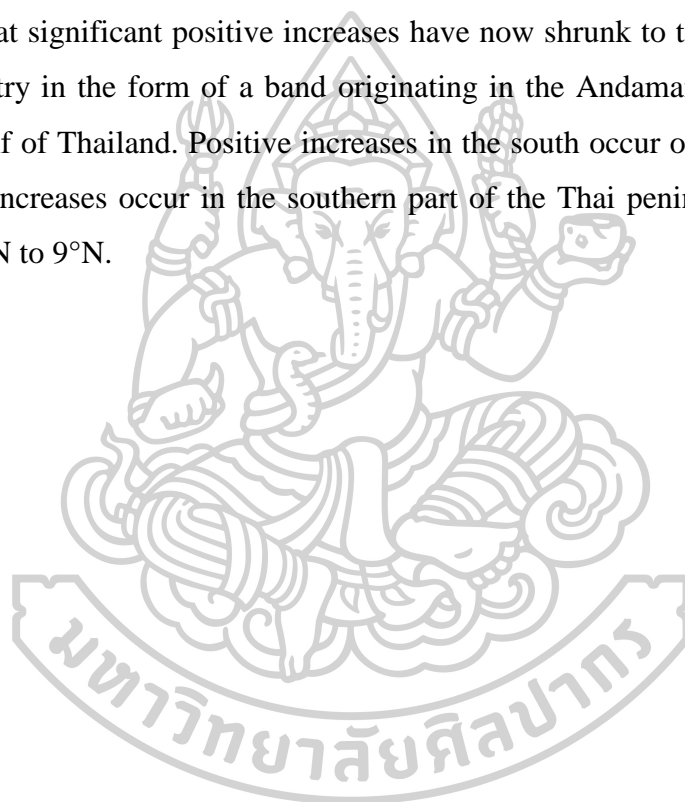
The data in each grid that passed the residual test was plotted against time from 1981 to 2017 and a linear least square regression was used to fit the plot of each grid. Lastly, the slopes of the regression for all grids were presented as contours to reveal the temporal trend of PWV and the results are shown in Figure 6.4. Significance levels in Figure 6.4 are shown as dark and light shades representing the 1% and 5% significance level of the trends appearing purely due to chance, respectively.

The winter pattern (Figure 6.4(A)) features a strong north/south gradient in PWV increases, from a maximum of 0.015 cm yr^{-1} over Malaysia (Figure 6.1) to around 0.01 cm yr^{-1} in the Bangkok region. However, the trends are not statistically significant for north of around 14°N .

No trends throughout the country are obtained in the summer season with the exception of a narrow region along the northeast showing decreases of 0.005 cm yr^{-1} (Figure 6.4(B)). Positive increases of 0.01 cm yr^{-1} are estimated in the extreme south of the study area, over Malaysia. Small significant increases of 0.005 cm yr^{-1} and larger are estimated over Myanmar, in the northwest while central Laos experiences decreases of 0.005 cm yr^{-1} .

The pattern for the rainy season is dominated by an east/west positive increase extending from latitude 10°N to the northern boundaries (20°N) and beyond (Figure 6.4(C)). Trends increase in magnitude and in significance in a westward direction, reaching values of approximately 0.005 cm yr^{-1} along the Thailand/Myanmar border. No significant trends are observed over south of 10°N , although positive increases are observed over Malaysia.

The yearly pattern clearly reflects the two dominant processes occurring in the rainy and winter seasons (Figure 6.4(D)). The most outstanding feature in Figure 6.4(D) is that significant positive increases have now shrunk to the southwestern part of the country in the form of a band originating in the Andaman Sea and extending into the Gulf of Thailand. Positive increases in the south occur over Malaysia, but no significant increases occur in the southern part of the Thai peninsula, approximately between 6°N to 9°N .



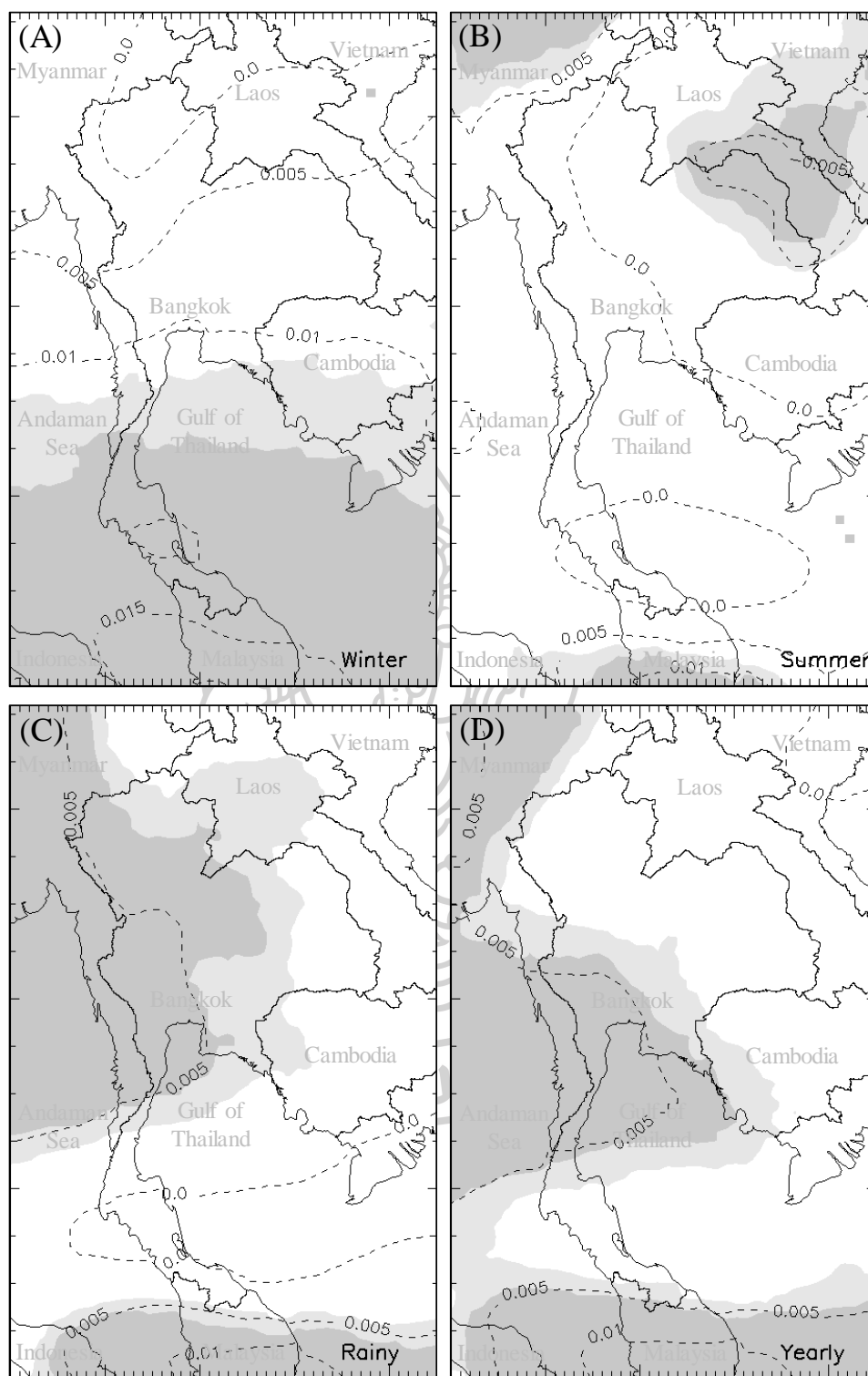


Figure 6.4 Temporal trends of PWV for (A) winter, (B) summer, (C) rainy and (D) yearly average. The values at the contours indicate the values of the trends. Dark and light shades represent that the trends were statistically significant at 99% and 95% confidence levels, respectively.

6.3.3 PWV changes and its relationship to changes in air temperature

In this section, we investigated how yearly average changes in PWV relate to air temperature with focus on Bangkok, a location with significant and positive increases over 0.005 cm yr^{-1} (Figure 6.4(D)). It is convenient in the analysis to relate PWV to its causal factors using simple meteorological variables acquired at the surface. Various studies (Reitan, 1963; Bolsenga, 1965; Smith, 1966) used dew point temperature (T_D) as a predictor of PWV. These can take the form:

$$\ln(\text{PWV}) = \alpha_0 + \alpha_1 T_D \quad (6.1)$$

where T_D is screen-level dew point temperature and α_0 and α_1 are regression constants that depend on geographic location and time of year (Reitan, 1963; Gueymard, 1994; Okulov et al., 2002). Using physical arguments, Reitan (1963) developed an exponential relationship between vapour density and height of the form:

$$\rho(Z) = \rho_0 \exp(-\beta Z) \quad (6.2)$$

where $\rho(Z)$ and ρ_0 is absolute humidity at height Z and surface, respectively and β is a rate of change in $\rho(Z)$ with height expressed in km^{-1} . Integration of $\rho(Z)$ from $Z=0$ to height Z can provide an exponential expression for precipitable water vapour (Okulov et al., 2002):

$$\text{PWV} = \frac{\rho_0}{\beta} (1 - e^{-\beta Z}) \quad (6.3)$$

Assuming Z approaches infinity, it is possible to equate PWV to the product of surface absolute humidity and a “characteristic height H ” ($=1/\beta$) delimiting a layer where absolute humidity is constant and equal to ρ_0 (Leckner, 1978). Although H is

not the real height Z where $\rho(Z)$ goes to zero, it is a convenient way to visualize the physical processes (Okulov et al., 2002). Therefore, Equation (6.3) reduces to:

$$\text{PWV} = \frac{\rho_0}{\beta} = \rho_0 H \quad (6.4)$$

Typically, β has been measured at varying between 0.40 to 0.60 km^{-1} , implying that H varies between 2.5 km to 1.7 km. A plot of monthly average β for the period 1981 to 2017 (Figure 6.5) reveals a well-defined seasonal change and the low standard deviation. A decrease during the monsoon summer months very likely relate to well mixed layers characterized by free convection in the upper layers (Stull, 2000).

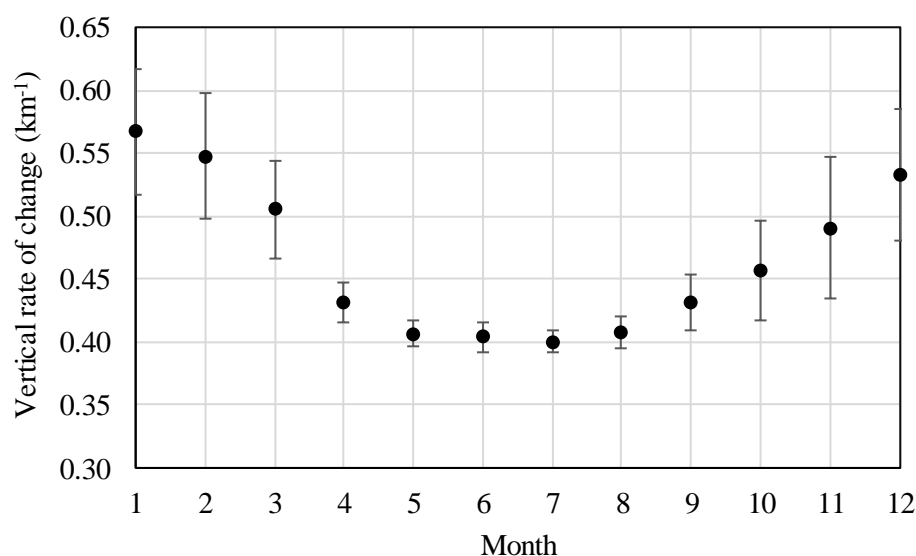


Figure 6.5 Monthly average rate of change β (km^{-1}). Each monthly statistic is the average of 37 yearly observations.

It is possible to use the seasonal pattern in β to predict PWV for all 444 months of the study period. The simple relationship for any year i and month j is as follows:

$$\text{PWV}_{ij} = \frac{\rho_{ij}}{\beta_j} = \rho_{ij} H_j \quad (6.5)$$

where ρ_{ij} is surface water vapour density for year i ($i=1,2,\dots,37$) and month j ($j=1,2,\dots,12$), and β_j, H_j are rate of change and mixing height at month j . Figure 6.6(A) shows the satisfactory performance of Equation (6.5) when tested against monthly PWV from ERA-Interim. However, it is important to note that H_j and β_j are based on measured long-term monthly data and their value rests on their ability to predict PWV for individual months with a satisfactory level of performance.

On a yearly basis, Equation (6.5) can be described as

$$\begin{aligned} \text{PWV}_{ij} &= \frac{1}{12} \sum_{j=1}^{j=12} \rho_{ij} / \beta_j = \sum_{j=1}^{j=12} \rho_{ij} H_j \\ &= \bar{\rho}_i \bar{H}_i + \langle \rho' H' \rangle \end{aligned} \quad (6.6)$$

where the overbars denote averages and the term in brackets is a covariance in ρ and H . Examination of the data revealed that the covariance term is small, between 0.8% to 1.6% of the product of averages and therefore can be neglected for purpose of this analysis. Therefore, the yearly average PWV reduces to the product of two yearly averages: ρ and H (Figure 6.6(B)). Notice the lower coefficient of variance and RMSE in Figure 6.6(B) compared to Figure 6.6(A), a result of temporal averaging (lower RMSE) and smaller data span (lower RMSE).

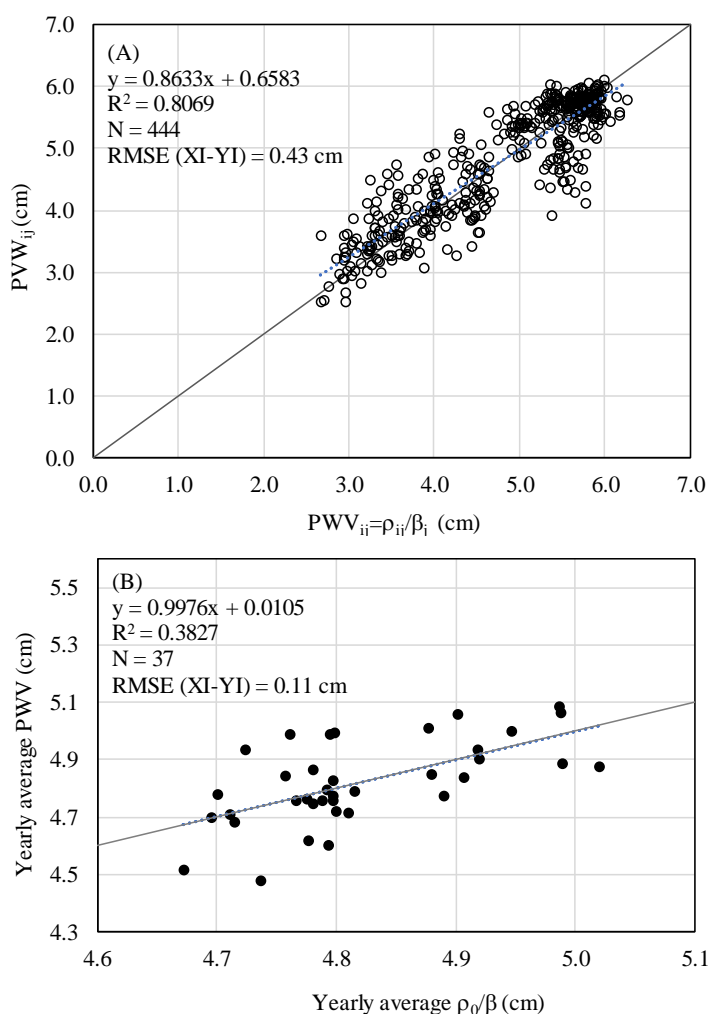


Figure 6.6 (A) Performance of a simple model for PWV (using surface vapour density divided by rate of change β vs ERA-Interim PWV). Each data point represents year i and month j . (B) As in Figure 6.6(A) but with averages calculated for each of the 37 years.

Examining yearly estimates of H over the period of record ($\bar{H}_i = PWV_i / \bar{\rho}_i$, $i=1,2,\dots,37$) reveal no significant trend with time at the 95% confidence limit. The distribution in yearly H follows a normal curve as obtained by chi square analysis (Young, 1962), with an average value of 2.12 km (H_0) and standard deviation of 0.056 km. The water vapour density in Equation (6.5) may be expanded as:

$$PWV = \rho_0 H_0 = (\rho_D \varepsilon / P_0) * RH_0 * e_s(T_0) * H_0 \quad (6.7)$$

where ρ_D are surface air density, ε is a ratio of gas constant of dry air to that of water vapour, P_0 is surface pressure, RH_0 is relative humidity at the surface and e_s is the saturation vapour pressure which is a function of screen level air temperature T_0 (Stull, 2000). The performance of Equation (6.7) as a predictive relationship is modest since only 36% of the yearly variance is explained, very likely a result of the small but significant yearly changes in H_0 and the lower data span as discussed in the paragraph above. Nevertheless, it is a convenient tool for examining the dominant terms influencing yearly changes in PWV, as explained below. Using error analysis, a change in PWV over the 37 years may be written as (Young, 1962):

$$\begin{aligned} \delta PWV &= (\partial PWV / \partial e_s) \delta e_s + (\partial PWV / \partial RH) \delta RH \\ &= [(\rho_D \varepsilon / P_0) * RH_0 * H_0] \delta e_s \\ &\quad + [(\rho_D \varepsilon / P_0) * e_s(T_0) * H_0] \delta RH_0 \end{aligned} \quad (6.8)$$

which is dependent on changes in the variables e_s and RH_0 over the period of record (Figure 6.7 and Table 6.3). Saturation vapour pressure increased over the period of study (2.18 mb), increasing PWV by 0.269 cm. It is counteracted by a weak decrease in relative humidity (-0.015), causing PWV to drop by 0.093 cm. The net effect is an increase of 0.176 cm over the 37-year period, as opposed to 0.196 cm obtained directly from the slope in Figure 6.7(A). However, there is overlap in these estimates of PWV which vary considerably given the wide range at the $\pm 95\%$ value of the slopes (Table 6.3).

By using the non-parametric Mann-Kendall test (Matar et al., 2011), the results can be summarized as follows. The increase of PWV in Bangkok is largely driven by increasing saturation vapour pressure as a result of increasing air temperatures, with RH remaining constant or decreasing slightly. The simple model used (Equation (6.8)) showed no yearly trend in H although there is interannual variability. Over the 37 years of record, PWV sensitivity is $4.2\% K^{-1}$, considerably

smaller than the global temperature dependence of $7\text{-}9\% \text{ K}^{-1}$ reported in the literature (Takahashi, 2016; Trenberth et al., 2005; Schneider et al., 2010; Wentz and Schabel, 2000).

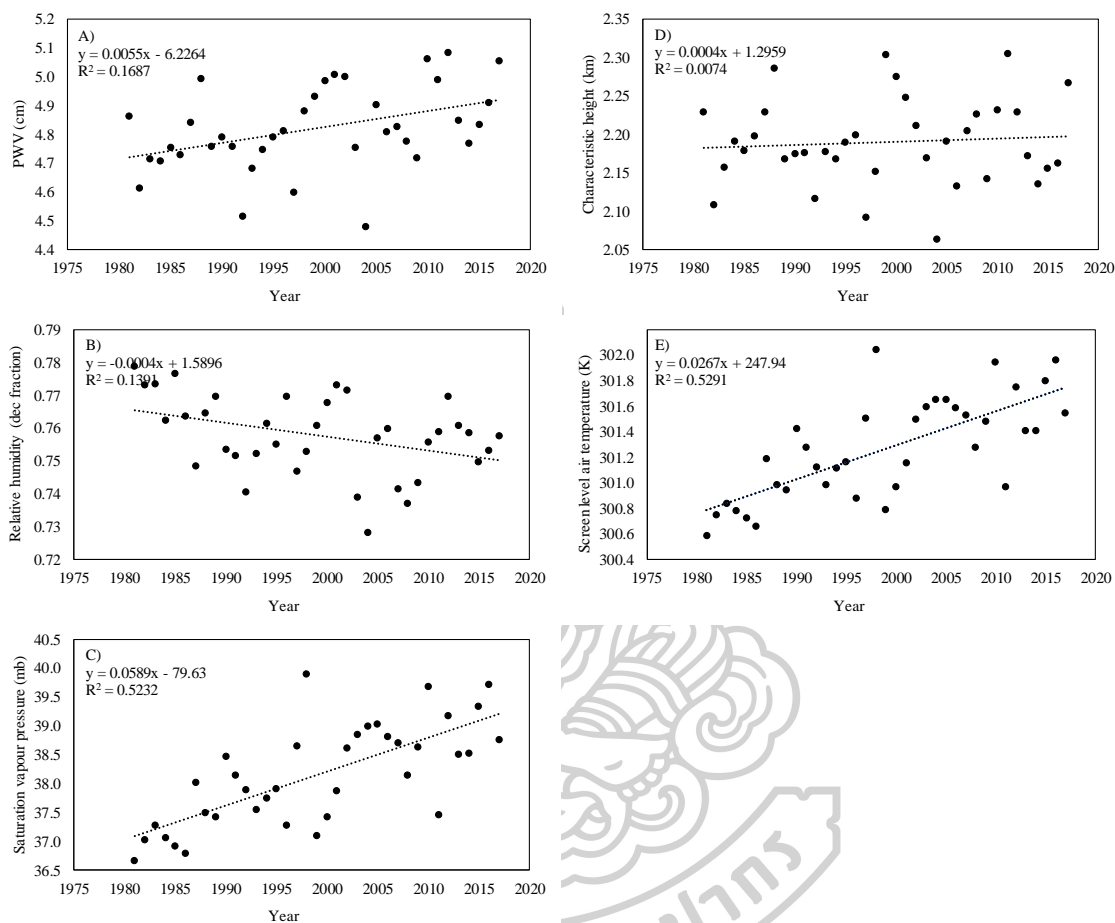


Figure 6.7 Change in yearly average surface data for Bangkok (13.67°N; 100.61°E) as determined from ERA-Interim re-analysis: A) Precipitable water vapour (PWV); B) Relative humidity; C) Saturation vapour pressure; D) Characteristic height and E) screen-level air temperature.

Table 6. 3 Statistics describing change in Preipitable water (PWV), as obtained from direct measurements of PWV (third column), change in saturation vapour pressure (e_s) (fourth column), and change in relative humidity (RH) (fifth column). The last three rows describe the combined effect of e_s and RH in estimating PWV. Notice the overlap between measured and combines estimates (in bold).

		PWV	e_s	RH
Average	1981-2017	4.82 cm	38.15 mb	0.758
Slope	95% min	0.00132 cm yr ⁻¹	0.0396mb yr ⁻¹	-0.00077 yr ⁻¹
	95% max	0.00973 cm yr ⁻¹	0.07822 mb yr ⁻¹	-0.00006 yr ⁻¹
	l.s. fit	0.00553 cm yr ⁻¹	0.05892 mb yr ⁻¹	-0.00042 yr ⁻¹
Change in PWV (37 years)	95% min	0.049 cm (ERA)	0.178 cm	-0.013 cm
	95% max	0.360 cm (ERA)	0.348 cm	-0.174 cm
	l.s. fit	0.196 cm (ERA)	0.269 cm	-0.093 cm
	Combined (e_s +RH) abs min		0.004 cm	
	Combined (e_s +RH) abs max		0.161 cm	
	Combined (e_s +RH) l.s.		0.176 cm	

6.3.4 PWV trends and relevant teleconnections

Dominant teleconnections influencing tropical weather patterns include the West Pacific High Pressure Index (WP, Choi and Moon, 2012; Xue-zhao and Dao-yi, 2002; Qu et al., 2013), the Southern Oscillation Index (SOI, Irwin and Davis, 1999) and the Indian Ocean Dipole Mode Index (IOD, Yang et al., 2015). We have used the WP index, defined as a difference in the 500 mb geopotential height anomaly between two locations in the western Pacific (60°N; 155°E; 30°N; 155°E) (Wallace and Gutzler, 1981; Linkin and Nigam, 2008; Huang et al., 2018). The SOI is defined as the monthly pressure difference between Tahiti and Darwin; while the IOD is a sea surface temperature anomaly difference between the western equatorial Indian Ocean and the Southeastern Equatorial Indian Ocean.

Of these three indices, the WP has undergone a significant westward and southward displacement (Li et al., 2011; Vishnu et al., 2016) and should be expected to possibly exert a long-term influence on PWV for our region. The latter two indices are quasi-stationary (NOAA, www.esrl.noaa.gov), possibly influencing PWV on an interannual scale, but not controlling the long-term behavior.

To investigate the correlation between PWV and particular index, the PWV seasonal map was divided into 0.25 by 0.25 degree square grids and the average value of PWV in each grid was plotted against a particular index. The correlation coefficient (R) of each plot was determined and the value of R was displays as contour maps (Figure 6.8).

Figures 6.8(A), 6.8(B), 6.8(C) and 6.8(D) present patterns of significant correlation between PWV and a particular index. Figure 6.8(A) show negative correlations between PWV and WP during the rainy season. The 95% confidence interval is marked in grey. Note that the grey region encompasses a large part of the positive and significant increases in PWV seen in Figure 6.4(A). It appears that a long-term negative trend in WP (increasing southward displacement of western Pacific Subtropical High pressure) is related to positive increases in PWV during the rainy season.

Indices operating at the interannual scale also influence the PWV trends. SOI has significant correlations with PWV in all seasons except at the yearly scale. Positive correlations are featured between SOI and PWV trends in the rainy season (Figure 6.8(B)), indicating that La Nina years would relate to higher PWV levels in central Thailand and vice-versa. Conversely, in summer a La Nina year would produce lower PWV and vice-versa (Figure 6.8(C)). Finally, the winter season exhibits positive and significant correlation with SOI in eastern Thailand (Figure 6.8(D)).

These interannual indices influence PWV but do not affect the long-term trend. For example, although SOI has a significant and negative correlation on PWV rates in summer (Figure 6.8(C)), SOI does not have a long term trend and therefore will not affect PWV over decadal scales. This may be substantiated by Figure 6.4(B) which shows no significant trend in southern Thailand despite the positive trend in Figure 6.4(A).

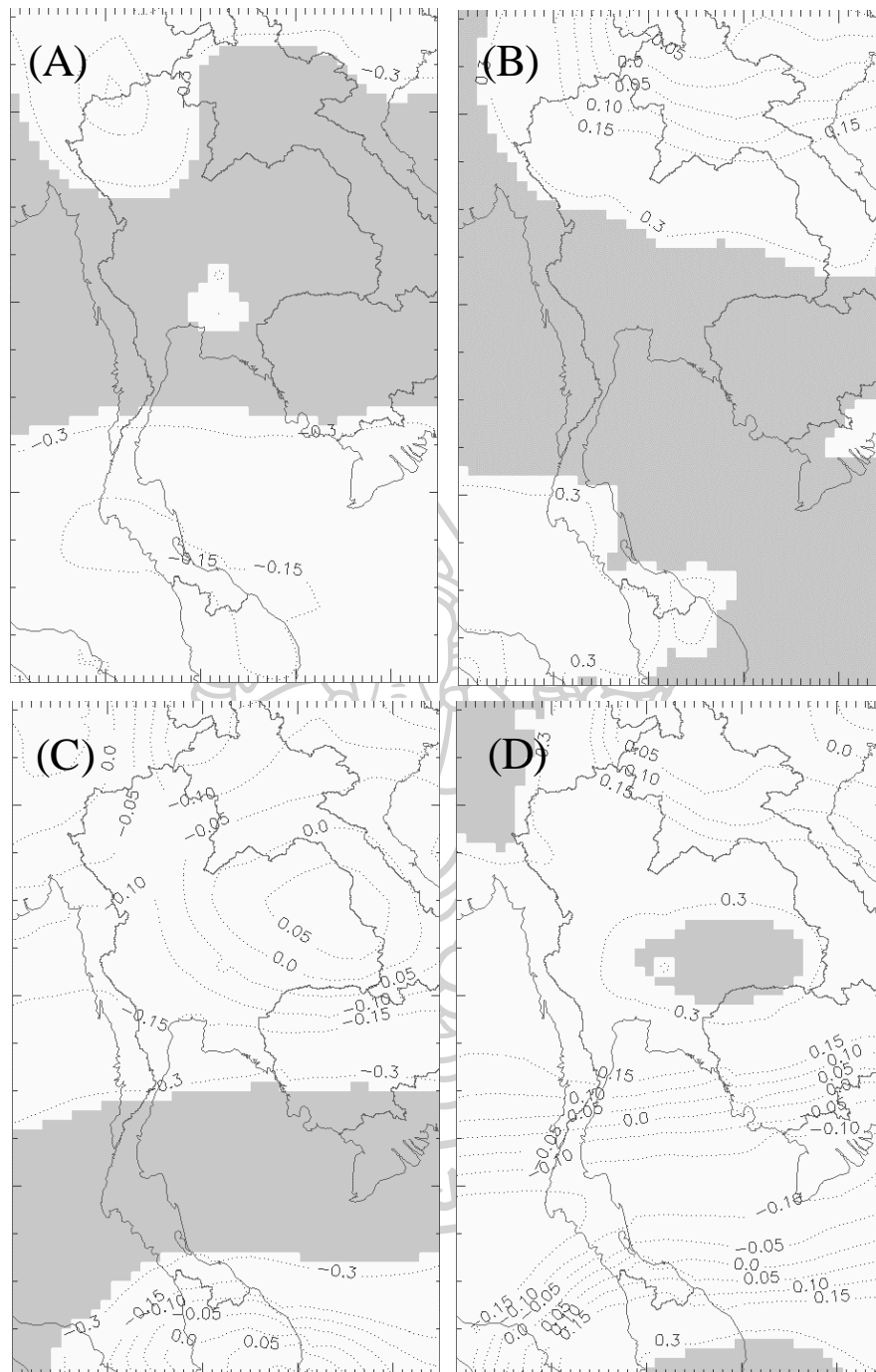


Figure 6.8 The patterns of significant correlation between PWV and particular index (A) PWV and WP in rainy season, (B) PWV and SOI in rainy season, (C) PWV and SOI in summer season, and (D) PWV and SOI in winter season. The 95% confidence interval is marked in gray.

6.4 Discussion and Conclusion

This study has examined spatial and temporal changes in PWV over the Thailand region. It was our intention to provide long-term figures that would encompass the last few decades which have experienced pronounced global changes. Our choice of data sets for the long-term study excluded recent satellite and surface-based radiometric data, and we concentrated on re-analysis data from ECMWF regional scale model, e.g., ERA-Interim model data. Nevertheless, we used PWV estimated from the IGRA radiosonde and MODIS at various stations for comparison and validation purposes. The radiosonde IGRA data set has a thorough quality control as well as a station instrumental history, and this feature is important as temporal trends in precipitable water vapour using radiosonde data may be affected by either a change in radiosonde instrument model number, or a change in radiosonde instrument. In their study, Mattar et al. (2011) showed that changes in the radiosonde instrument related to an abrupt change in yearly trends, for example, in Munich Germany after 1990. These problems argue for independent data sets that may be used for validation, which may be partly accomplished by re-analysis data.

Comparison of monthly average PWV from ERA-Interim with PWV derived from radiosonde at the four surface stations gave MBE ranged from -0.296 to -0.025 cm. Other studies have reported negative MBE, but lower in absolute value for example -0.26 cm in Barcelona, Spain (Campmany et al., 2010), -0.12 cm in Izana, Spain (Schneider et al., 2010), and at various global locations giving values between -0.09 and 0.04 cm (Pérez-Ramírez et al., 2014). The RMSE between PWV from ERA and PWV from radiosonde is in the same order of magnitude as that of between PWV from ERA and MODIS.

The PWV from ERA data exhibits strong N/S gradients in winter and summer, in contrast to the rainy season which exhibits a maximum south of Bangkok and in the Andaman sea. The N/S trend also appears in the yearly figure, but is slightly more irregular.

The outstanding feature in the PWV seasonal trends is a distinct zone of increasing PWV during the rainy season which is statistically significant at the 95% confidence level or higher (Figure 6.4(C)). The only other statistically significant trend occurred during the winter season in the southern half of the country (Figure

6.4(A)). The PWV increasing trend during the rainy season was shown to correlate well with the WP index. Studies document a westward and southward shift of the western Pacific subtropical high pressure in recent years, which induce a stronger flow in the western equatorial Pacific and increased storminess over the South China Sea and SE Asia in general (Li et al., 2011; Simmonds et al., 1999; Vishnu et al., 2016).

No statistically significant relationship was obtained between the increase in wintertime PWV over southern Thailand and the indices of WP, SOI and IOD. Its relationship to external influences or other indices are unclear at present. However, our further study shows that the increase may be caused by the Siberian high (Cohen et al., 2001). The vertically integrated northward mass flux ($\text{kg}\cdot\text{m}^{-1}\cdot\text{s}^{-1}$) from the ERA-Interim re-analysis data at latitude 5°N - 45°N and longitude 100°E during the winter season of 1981-2017 were examined. The result shows that the mass flux over the southern part of Thailand (5°N - 10°N) moving northward has been increasing while the mass flux over the region of Siberian high (35°N - 45°N) moving southward has been decreased. However, the trends are just above the 5% probability threshold and therefore must be listed as non-significant. These processes could make the basis of a future study.



Chapter 7

Investigation of water vapour in the upper atmosphere

7.1 Introduction

The upper atmosphere refers to the atmosphere that is higher than the boundary layer to the upper troposphere and lower stratosphere. Water vapour in the upper atmosphere originates mostly from deep convection that penetrates the cold tropopause region, forming ice clouds by freeze-drying and cold trap mechanisms (Jensen and Pfister, 2004; Read et al., 2008; Schiller et al., 2009). Variability of water vapour in the upper troposphere and lower stratosphere region can exert significant impact on the climate system as it interacts strongly with the infrared radiation (Forster et al., 2002). It impacts radiative processes including stratospheric temperature (potentially even impacting surface temperatures). In addition, water vapour in the upper atmosphere plays an important role in the weather and climate of the Earth-atmosphere system through their potential contribution in heterogeneous chemistry at this low temperature regime and also in the formation of liquid and ice clouds (Oltmans et al., 2000).

As the importance of the water vapour in the upper atmosphere, in this study, we aim to investigate the water vapour in this layer. In the process, measurements of relative humidity and air temperature from radiosonde allow to estimate water vapour mixing ratios in the vertical column from the ground to the lower of stratosphere. The details of the research are as follows.

7.2 Measurement and Data

For the investigation of the water vapour in the upper atmosphere, in this study, the data from radiosonde launched in 2017 at the Thai Meteorological Department (TMD) in Bangkok (13.67°N, 100.60°E) as shown in Figure 7.1 were used. The details of the work are described as follows.



Figure 7.1 Location of the upper air weather station of the Thai Meteorological Department (TMD), Bang Na, Bangkok in Thailand.

To measure the amount of water vapour at various altitudes, in this work, the radiosondes (iMet-1) (Figure 7.2) tied to a parachute and balloon were released into the atmosphere.



Figure 7.2 Internet iMet-1 radiosonde with temperature and humidity sensors.

Each radiosonde includes sensors for measuring air temperature (T_i), relative humidity (RH_i) and air pressure (P_i) (i is the order of the data ($i = 1, 2, \dots, n$)). The relative humidity, air temperature and air pressure measured at each height will be sent back to the ground receiver using radio waves at the frequency of 403 MHz. Then the received signal is processed and recorded with a computer as shown in Figure 7.3.

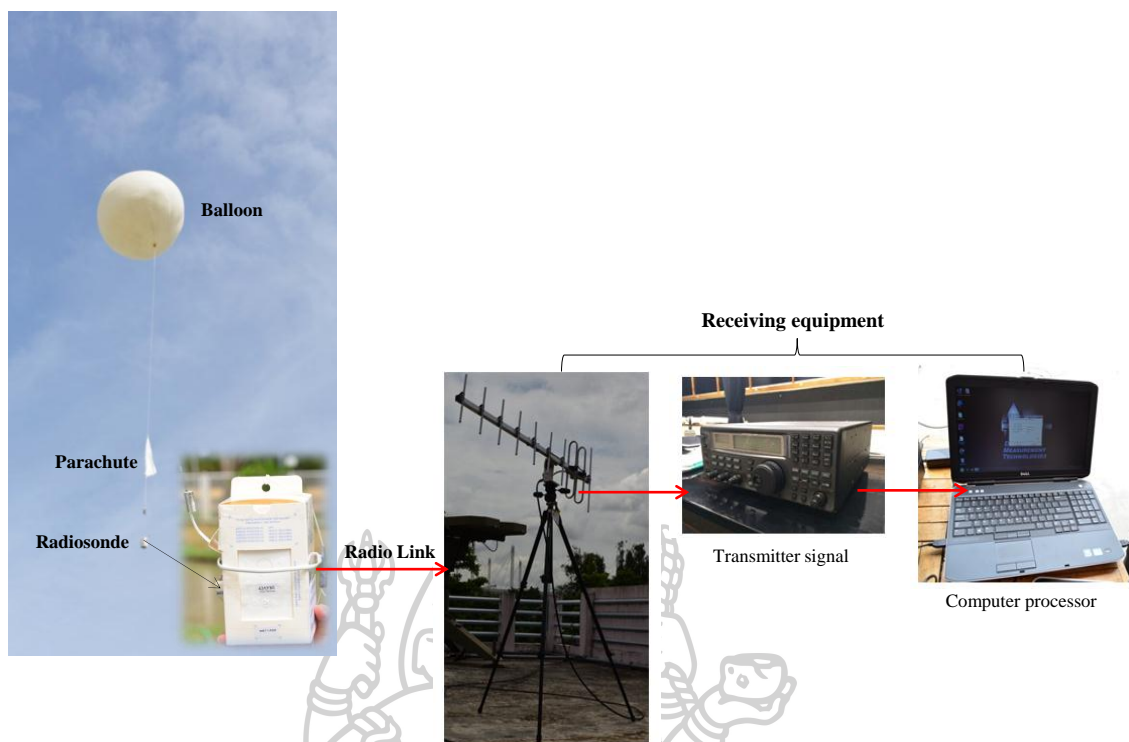


Figure 7.3 The system of the upper air monitoring.

For the preparation of the measurement, Helium (He) was filled in a 1,600 g balloon. The amount of helium used can be calculated from the required ascent rate, radiosonde weight and balloon weight. From the calculation, in this case, the helium of about 2,000 g must be filled so that the balloon can lift a weight of 2 kg. Then a parachute, hoist, and radiosonde were installed with the balloon, and then the balloon was released to the atmosphere. The process of releasing a balloon to measure the amount of water vapour in the atmosphere is shown in the following image (Figure 7.4 - 7.11).



Figure 7.4 Attaching a balloon to a helium pipe.



Figure 7.5 Filling helium in a balloon.



Figure 7.6 The balloon lifts Pendulum weight of 2 kg.



Figure 7.7 Parachute preparation.



Figure 7.8 Preparing to release a balloon.



Figure 7.9 Balloon and radiosonde released into the atmosphere.



Figure 7.10 Antenna adjustment receive radio signals from the radiosonde.



Figure 7.11 Ground receiver.

In this research, we conducted measurement of water vapour in the atmosphere from February to December 2017, a total of the 9 times, details are shown in Table 7.1.

Table 7.1 Summary of the radiosonde observations at the Thai Meteorological Department station, Bang Na, Bangkok in 2017.

Date	Time	Burst height	Instrument (iMet-1) Radiosonde
24 February 2017	13:28 – 15:35 hrs.	39.9 km	s/n 43423R
30 March 2017	9:54 – 11:56 hrs.	37.4 km	s/n 43309R
27 April 2017	9:14 – 11:05 hrs.	34.0 km	s/n 43426R
8 June 2017	9:04 – 10:59 hrs.	37.9 km	s/n 43424R
28 June 2017	13:05 – 15:10 hrs.	39.0 km	s/n 42773R
28 August 2017	7:52 – 10:07 hrs.	40.0 km	s/n 43460R
28 September 2017	6:52 – 9:09 hrs.	38.6 km	s/n 43260R
30 November 2017	7:49 – 9:51 hrs.	39.5 km	s/n 43238R
22 December 2017	7:51 – 9:51 hrs.	38.5 km	s/n 43059R

Figure 7.12-7.20 shows the profiles of air temperature (T_a), relative humidity (RH) in the upper troposphere and lower stratosphere (UTLS) obtained from the radiosonde carried out in 2017. It can be seen that the data received each time has a similar tendency. In general, the air temperature decreases with the height in the troposphere and then increases with height in the stratosphere. For the relative humidity, it varies near the ground and decrease with height. It also shows that the relative humidity is very low in the stratosphere or at an altitude above 15 km. These data were used in our analysis.

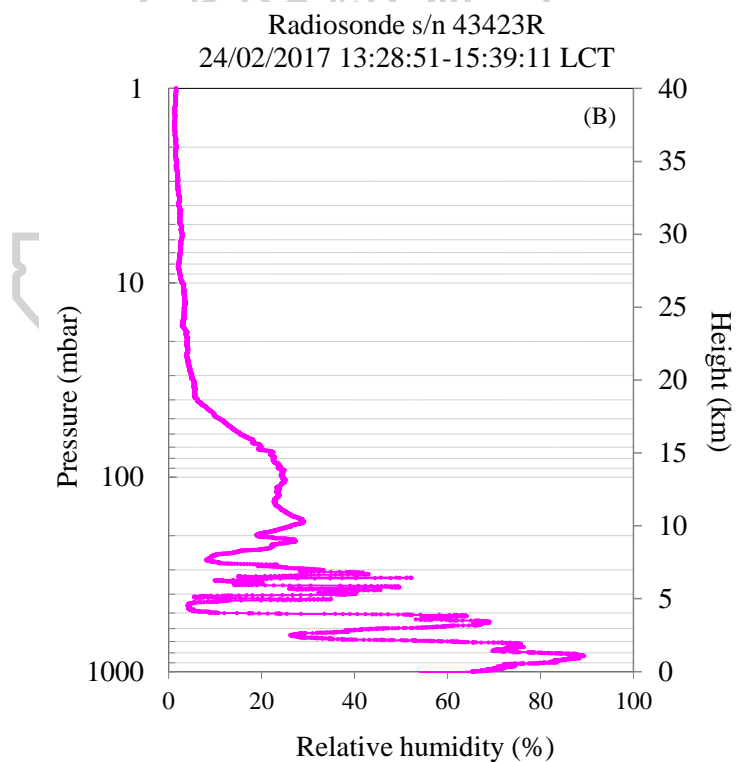
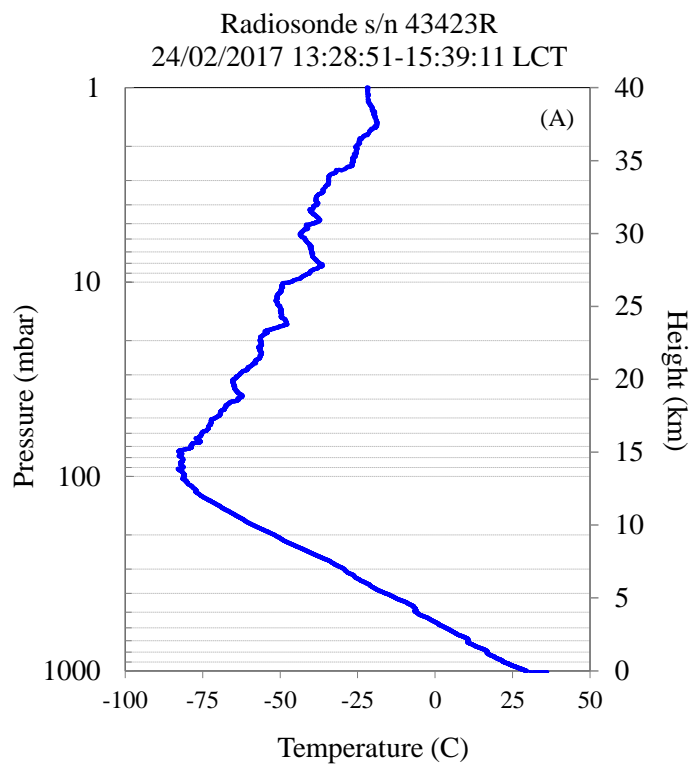


Figure 7.12 Altitude profiles of air temperature; T_a (A) and relative humidity; RH (B) in the upper troposphere and lower stratosphere (UTLS) obtained from radiosonde (i-Met 1) over Bangkok, Thailand on 24 February 2017.

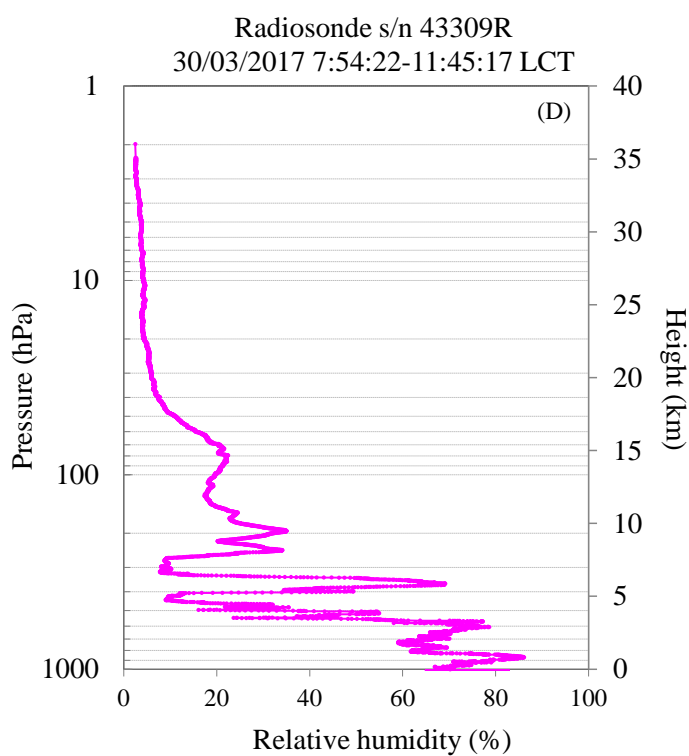
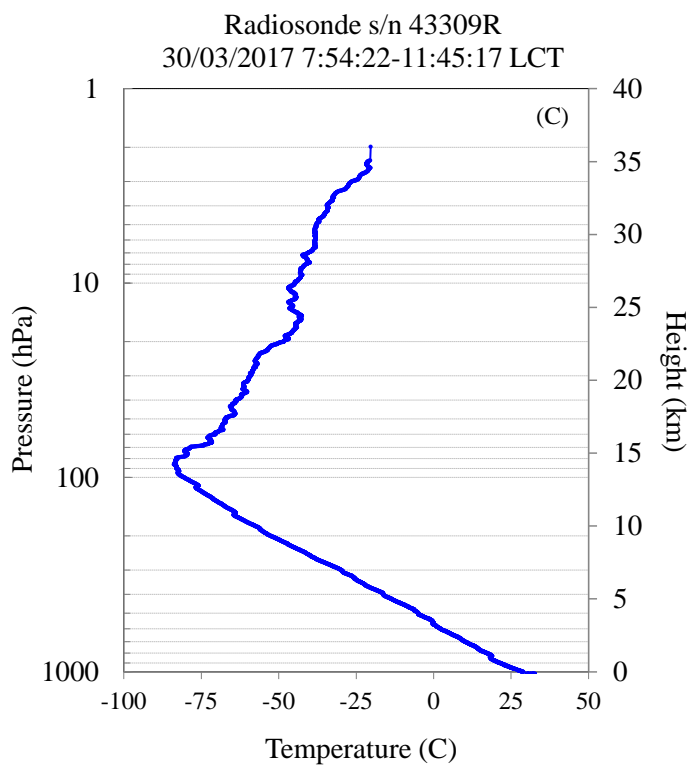


Figure 7.13 Altitude profiles of air temperature; T_a (C) and relative humidity; RH (D) in the upper troposphere and lower stratosphere (UTLS) obtained from radiosonde (i-Met 1) over Bangkok, Thailand on 30 March 2017.

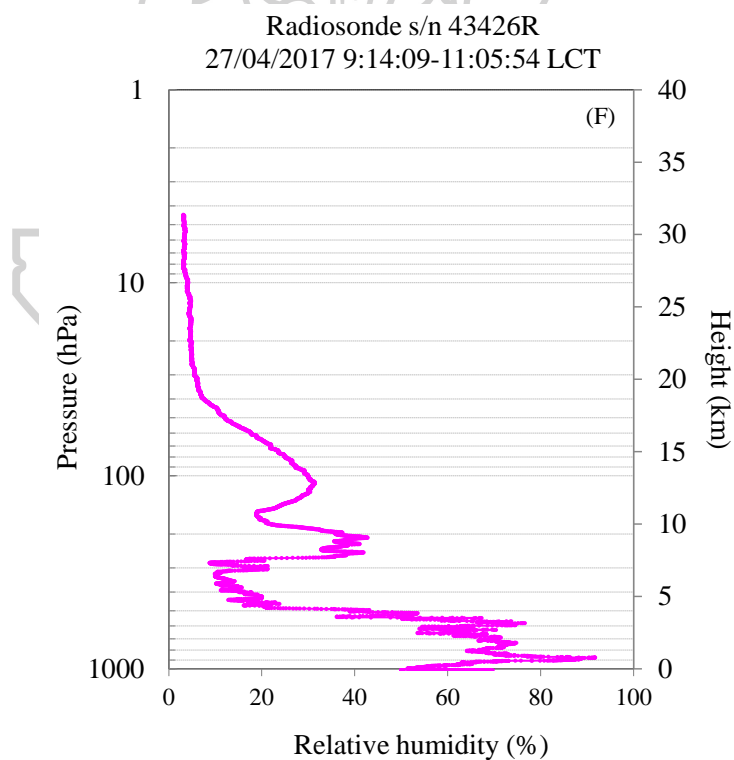
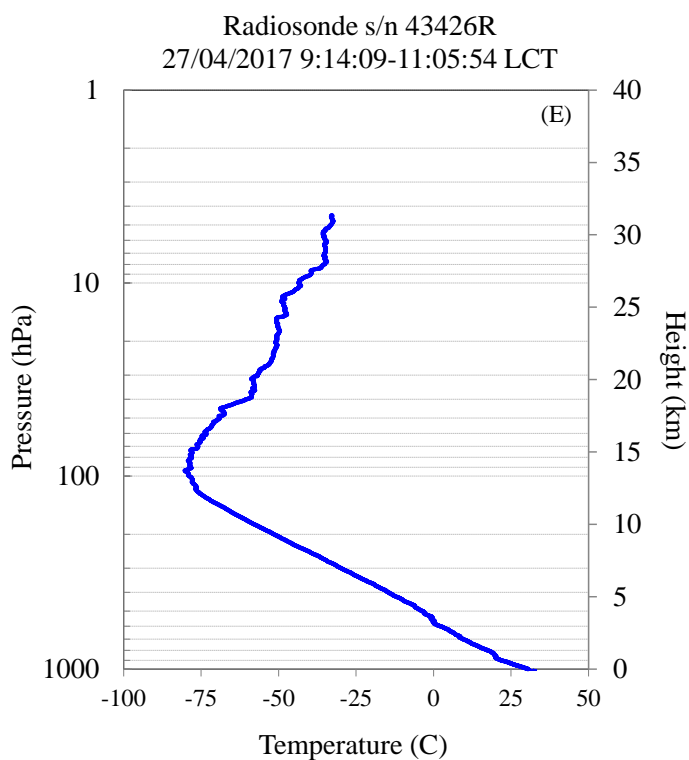


Figure 7.14 Altitude profiles of air temperature; T_a (E) and relative humidity; RH (F) in the upper troposphere and lower stratosphere (UTLS) obtained from radiosonde (i-Met 1) over Bangkok, Thailand on 27 April 2017.

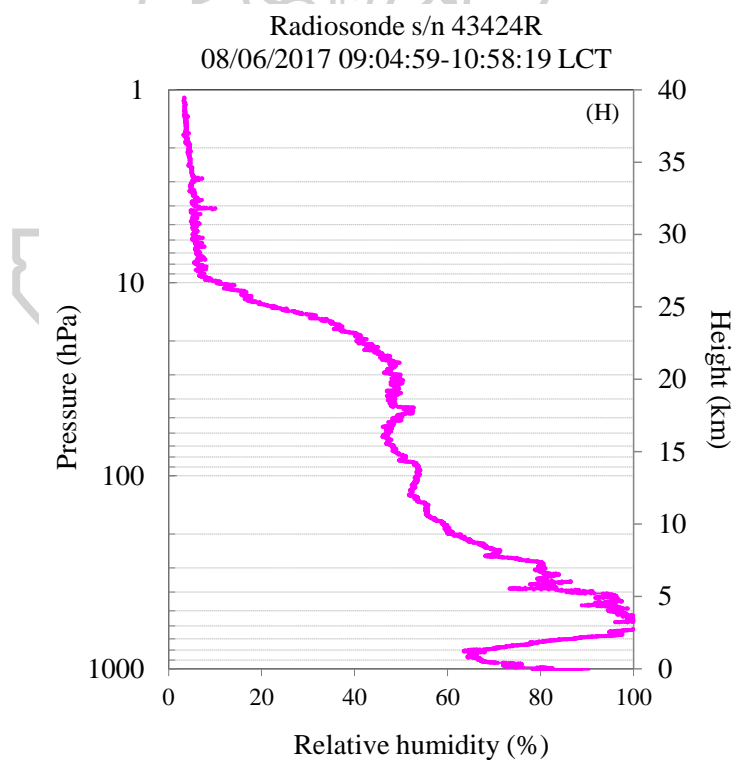
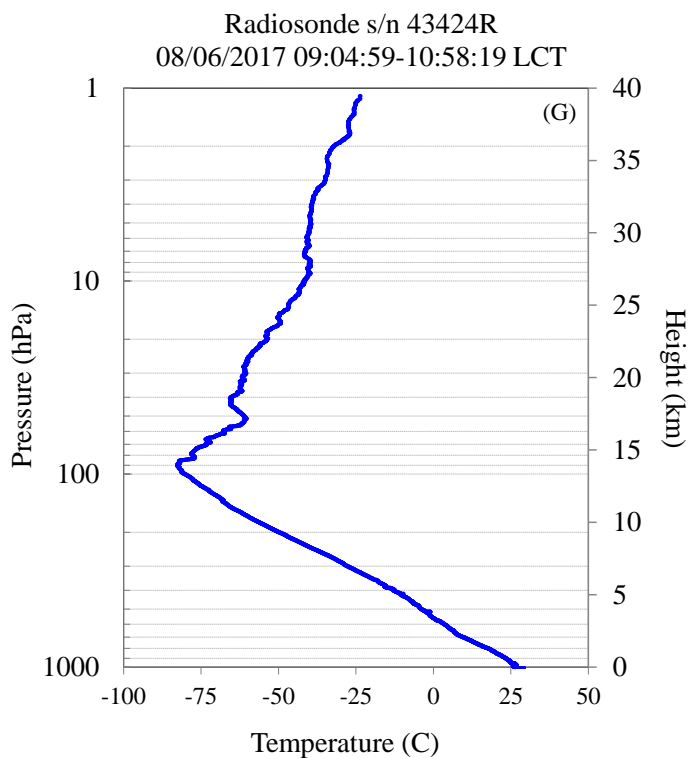


Figure 7.15 Altitude profiles of air temperature; T_a (G) and relative humidity; RH (H) in the upper troposphere and lower stratosphere (UTLS) obtained from radiosonde (i-Met 1) over Bangkok, Thailand on 8 June 2017.

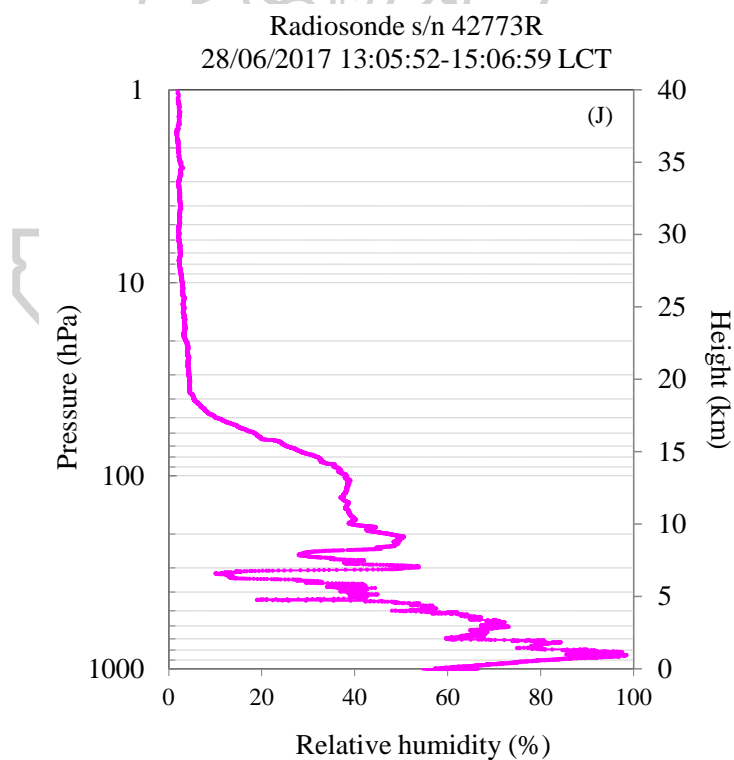
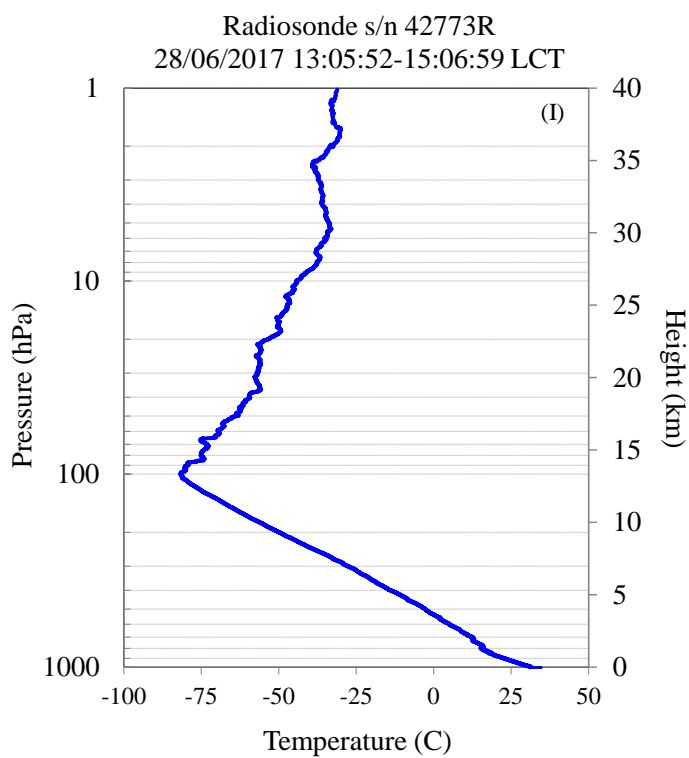


Figure 7.16 Altitude profiles of air temperature; T_a (I) and relative humidity; RH (J) in the upper troposphere and lower stratosphere (UTLS) obtained from radiosonde (i-Met 1) over Bangkok, Thailand on 28 June 2017.

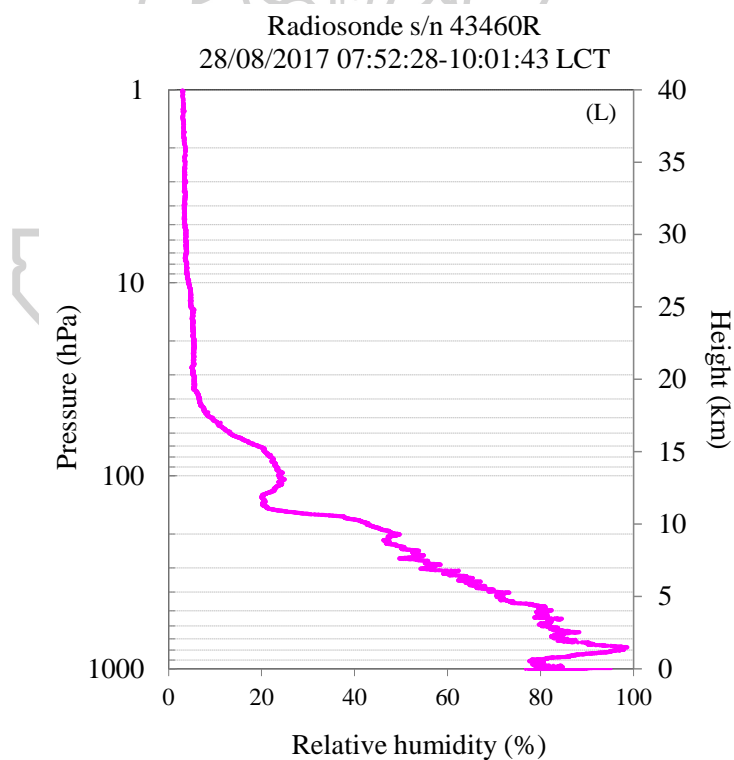
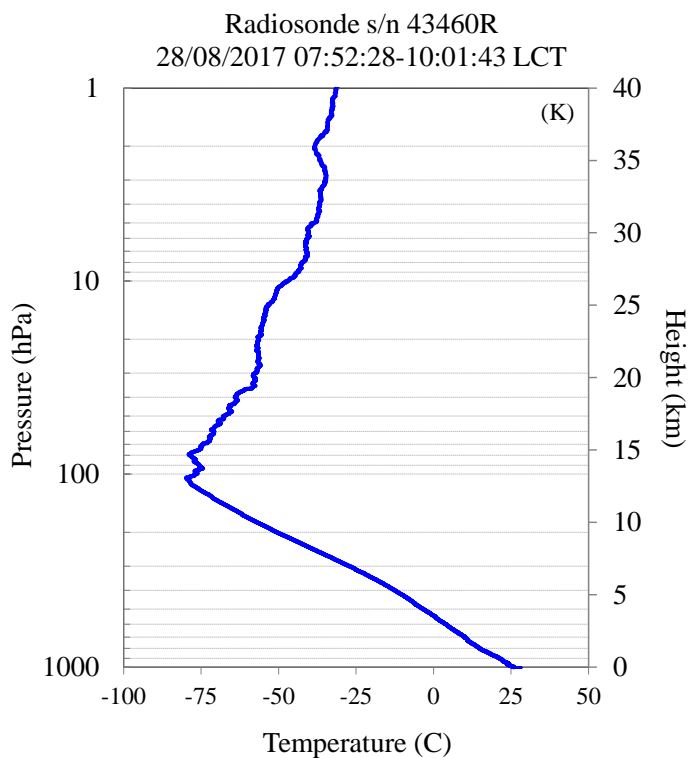


Figure 7.17 Altitude profiles of air temperature; T_a (K) and relative humidity; RH (L) in the upper troposphere and lower stratosphere (UTLS) obtained from radiosonde (i-Met 1) over Bangkok, Thailand on 28 August 2017.

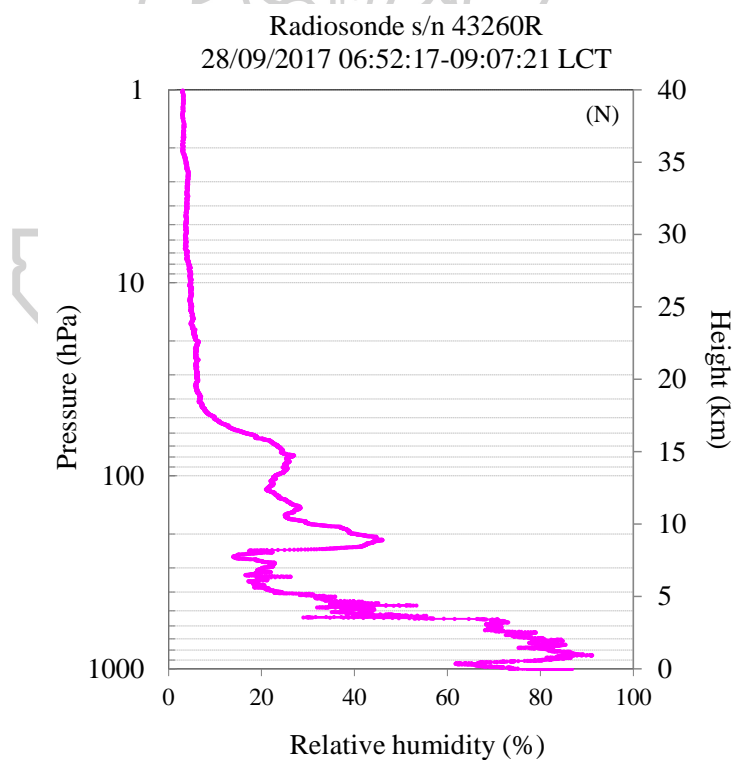
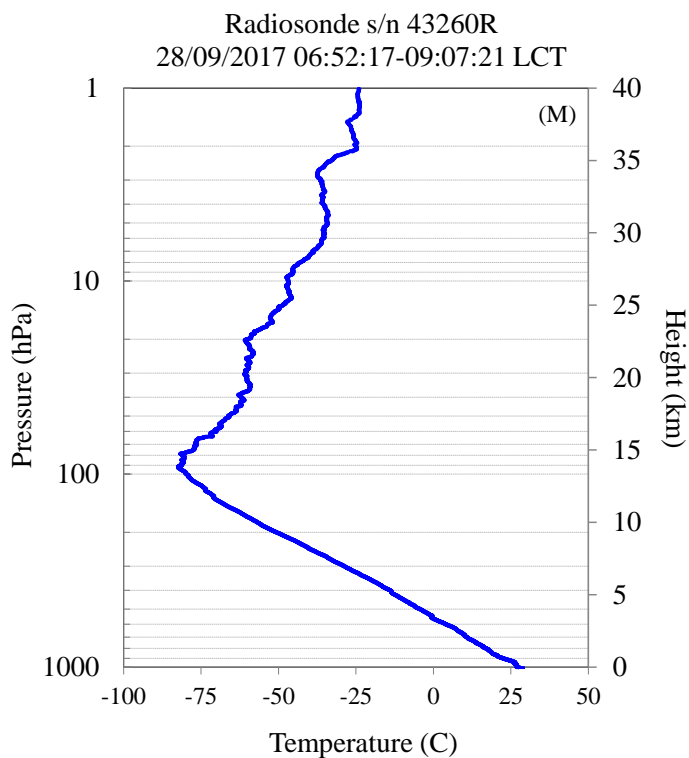


Figure 7.18 Altitude profiles of air temperature; T_a (M) and relative humidity; RH (N) in the upper troposphere and lower stratosphere (UTLS) obtained from radiosonde (i-Met 1) over Bangkok, Thailand on 28 September 2017.

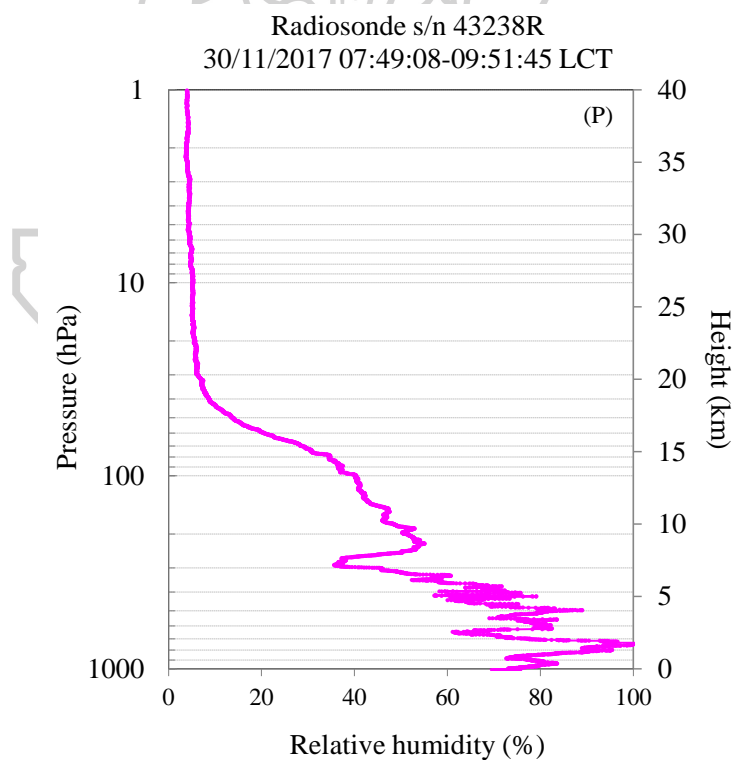
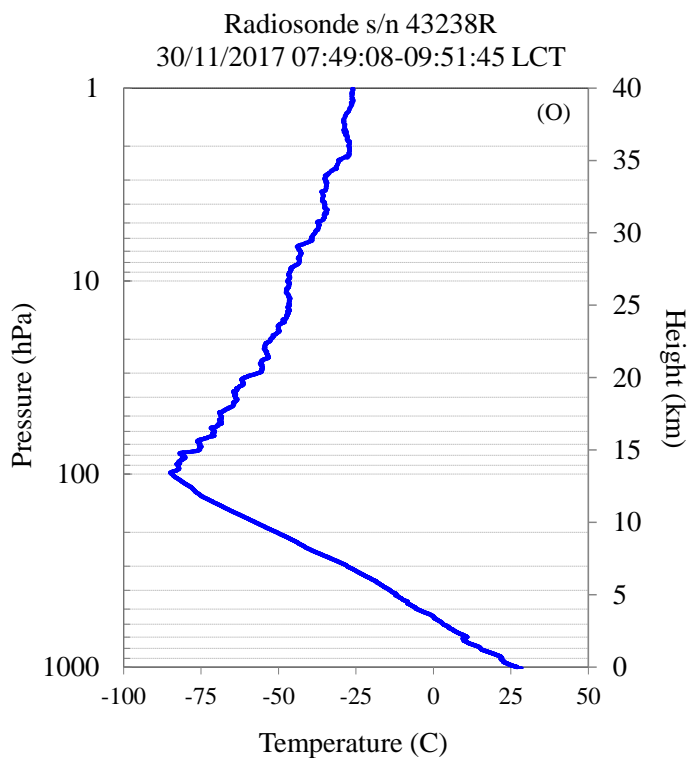


Figure 7.19 Altitude profiles of air temperature; T_a (O) and relative humidity; RH (P) in the upper troposphere and lower stratosphere (UTLS) obtained from radiosonde (i-Met 1) over Bangkok, Thailand on 30 November 2017.

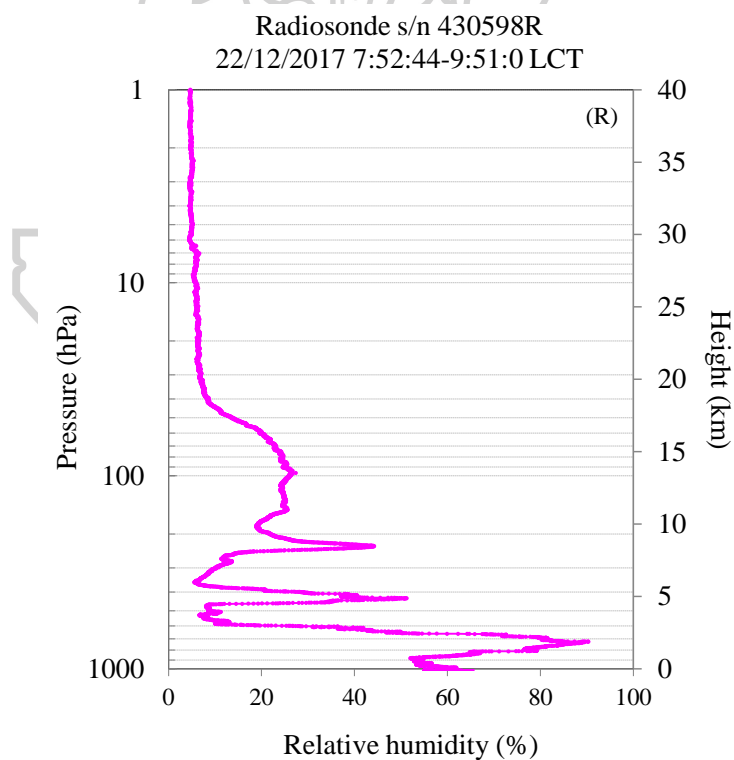
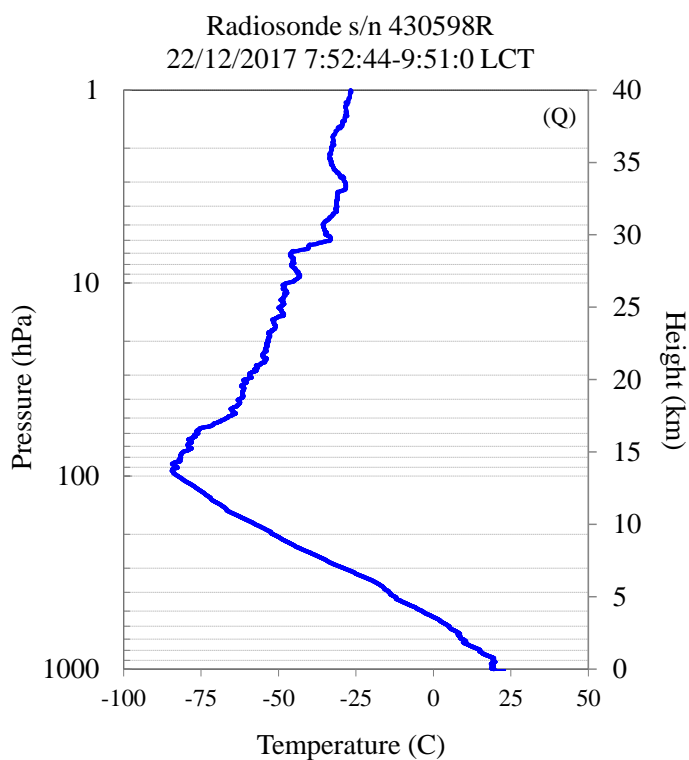


Figure 7.20 Altitude profiles of air temperature; T_a (Q) and relative humidity; RH (R) in the upper troposphere and lower stratosphere (UTLS) obtained from radiosonde (i-Met 1) over Bangkok, Thailand on 22 December 2017.

7.3 Analysis

In analyzing the amount of water vapour in the upper atmosphere (UTLS), air temperature and relative humidity at each atmospheric pressure were used to calculate the amount of water vapour in form of volume mixing ratio at different atmospheric pressure (μ_i), which is in a unit of parts per million by volume (ppmv). The calculation is as follows:

$$\mu_i = \frac{p_{vi}}{p_i} \times 10^6 \quad (7.1)$$

where μ_i is the water vapour mixing ratio at level i [ppmv]. p_i is the pressure of the air at level i [hPa]. p_{vi} is the water vapour pressure [hPa]. For water vapour pressure at various heights, it can be calculated from the relative humidity as the equation:

$$p_{vi} = RH_i \times p_{vsi} \quad (7.2)$$

where RH_i is the relative humidity [-]. p_{vsi} is the saturated water vapour pressure [hPa]. Because the saturated water vapour pressure depends on the temperature of the air, the saturated water vapour pressure can be calculated from the air temperature using the equation (Murray, 1966)

$$p_{vsi} = \begin{cases} 6.106607 \times 10^{(7.5T_i/237.3+T_i)}, & T_i > 0 \\ 6.106607 \times 10^{(9.5T_i/265.5+T_i)}, & T_i < 0 \end{cases} \quad (7.3)$$

where T_i is the air temperature [$^{\circ}\text{C}$]

From then, profiles of the volume mixing ratio of water vapour are shown in Figure 7.21 - 7.29 for each measurement.

The results are shown and show the variation of the volume mixing ratio of water vapour in the year 2017 as shown in Figure 7.30.

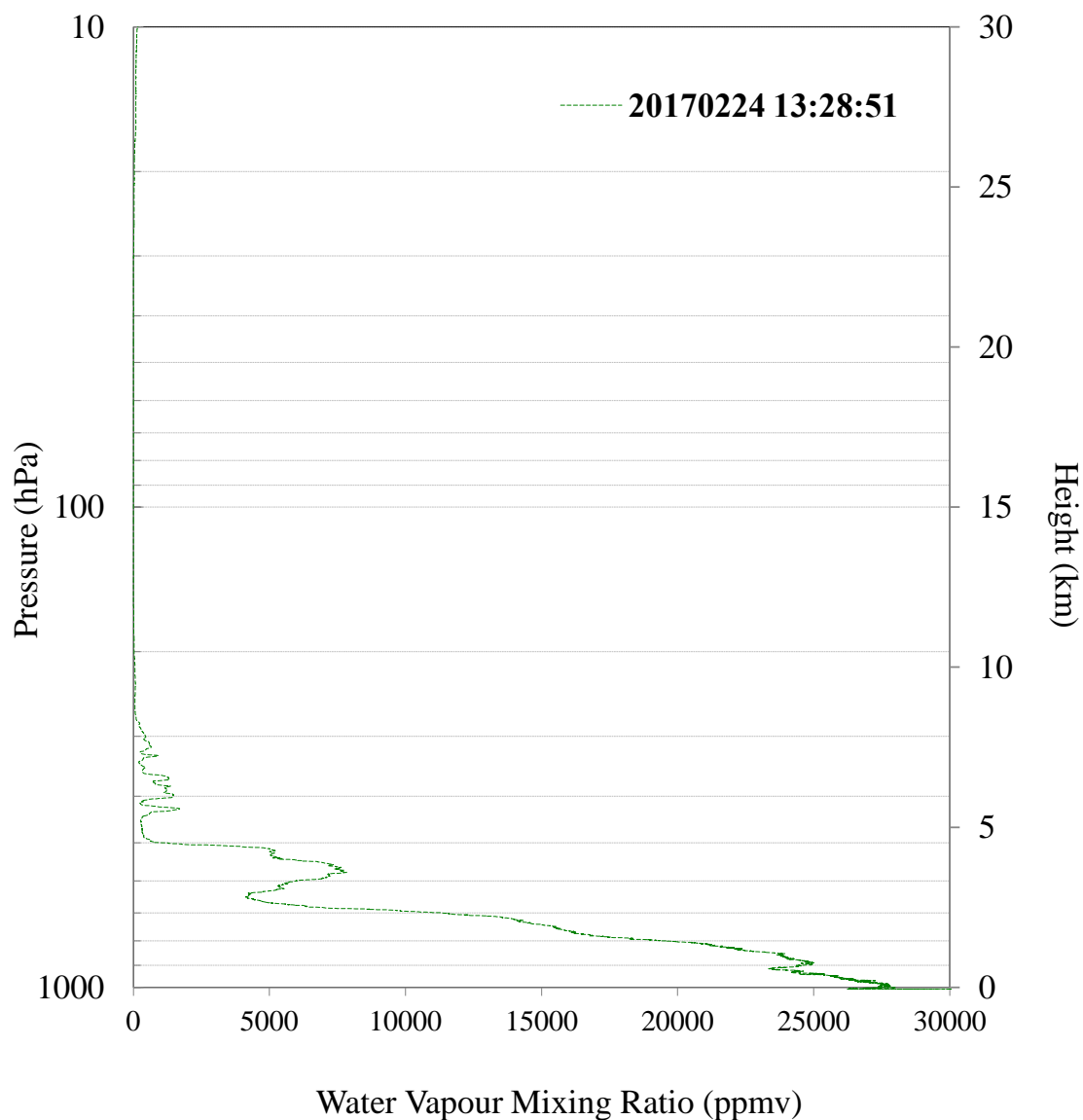


Figure 7.21 Vertical distributions of water vapour mixing ratio obtained from the iMet-1 Radiosonde over Bangkok, Thailand on 24 February 2017 (during controlled descent at 39.9 km).

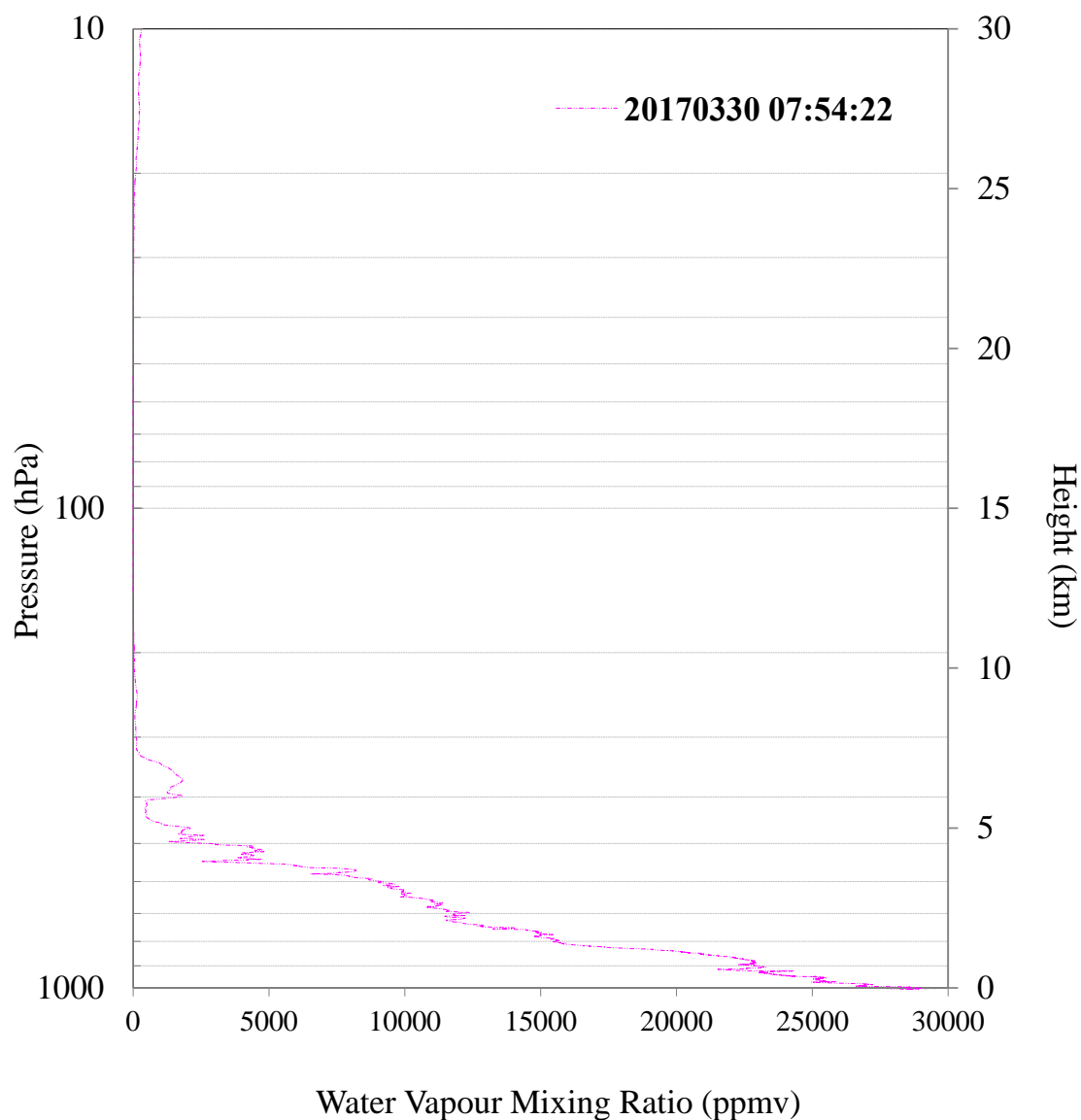


Figure 7.22 Vertical distributions of water vapour mixing ratio obtained from the iMet-1 Radiosonde over Bangkok, Thailand on 30 March 2017 (during controlled descent at 37.4 km).

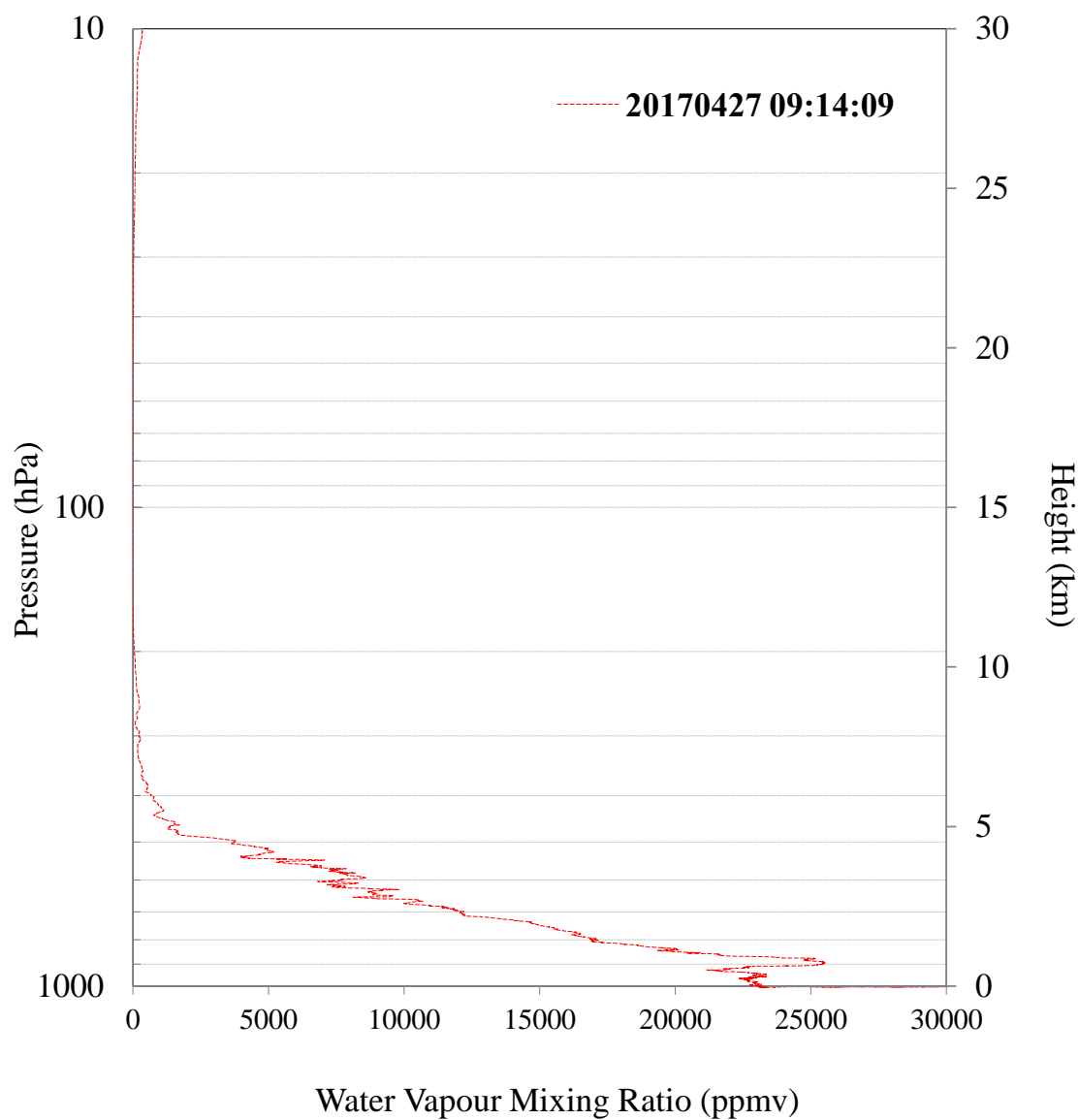


Figure 7.23 Vertical distributions of water vapour mixing ratio obtained from the iMet-1 Radiosonde over Bangkok, Thailand on 27 April 2017 (during controlled descent at 34.0 km).

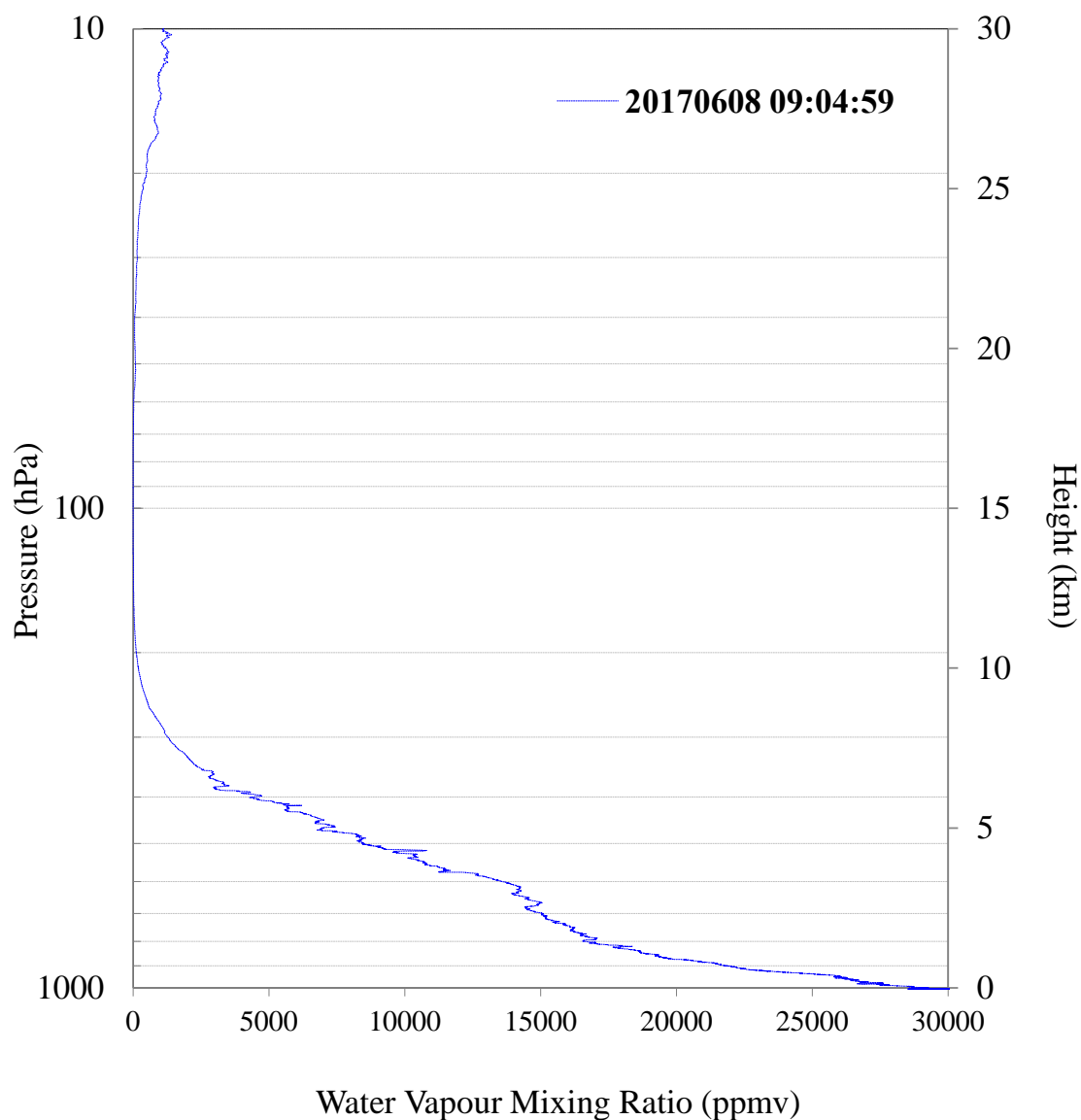


Figure 7.24 Vertical distributions of water vapour mixing ratio obtained from the iMet-1 Radiosonde over Bangkok, Thailand on 8 June 2017 (during controlled descent at 37.9 km).

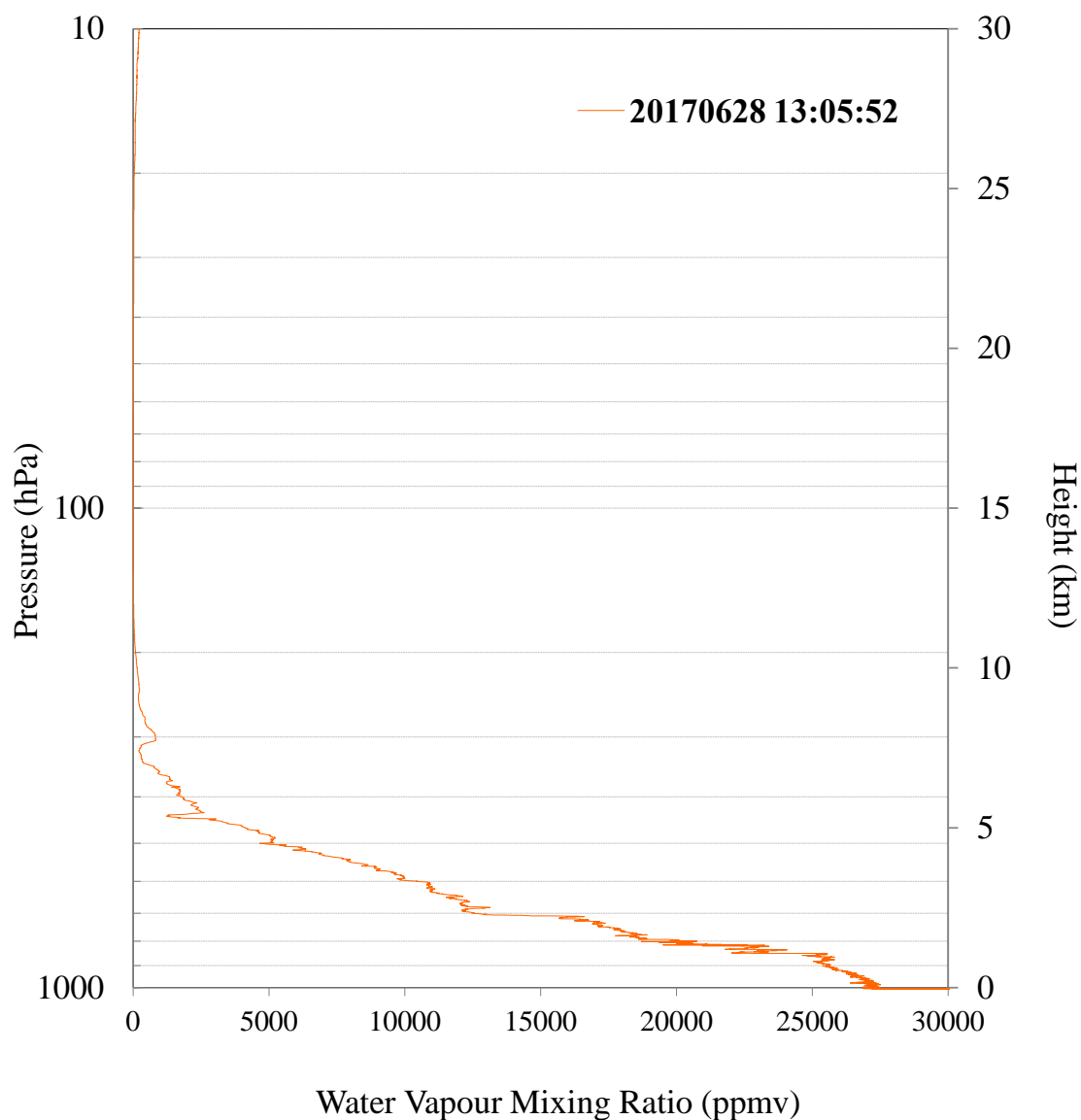


Figure 7.25 Vertical distributions of water vapour mixing ratio obtained from the iMet-1 Radiosonde over Bangkok, Thailand on 28 June 2017 (during controlled descent at 39.0 km).

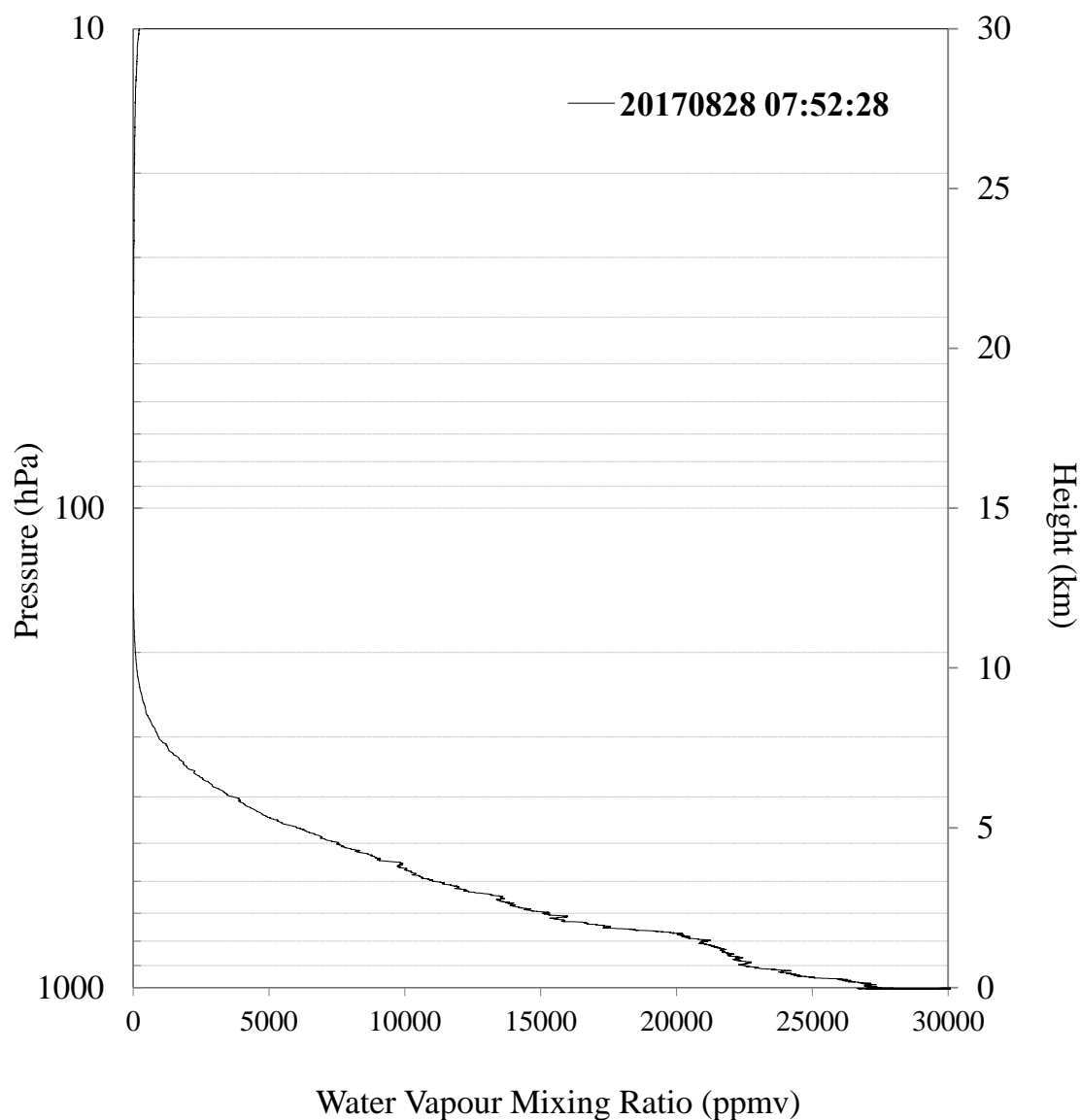


Figure 7.26 Vertical distributions of water vapour mixing ratio obtained from the iMet-1 Radiosonde over Bangkok, Thailand on 28 August 2017 (during controlled descent at 40.0 km).

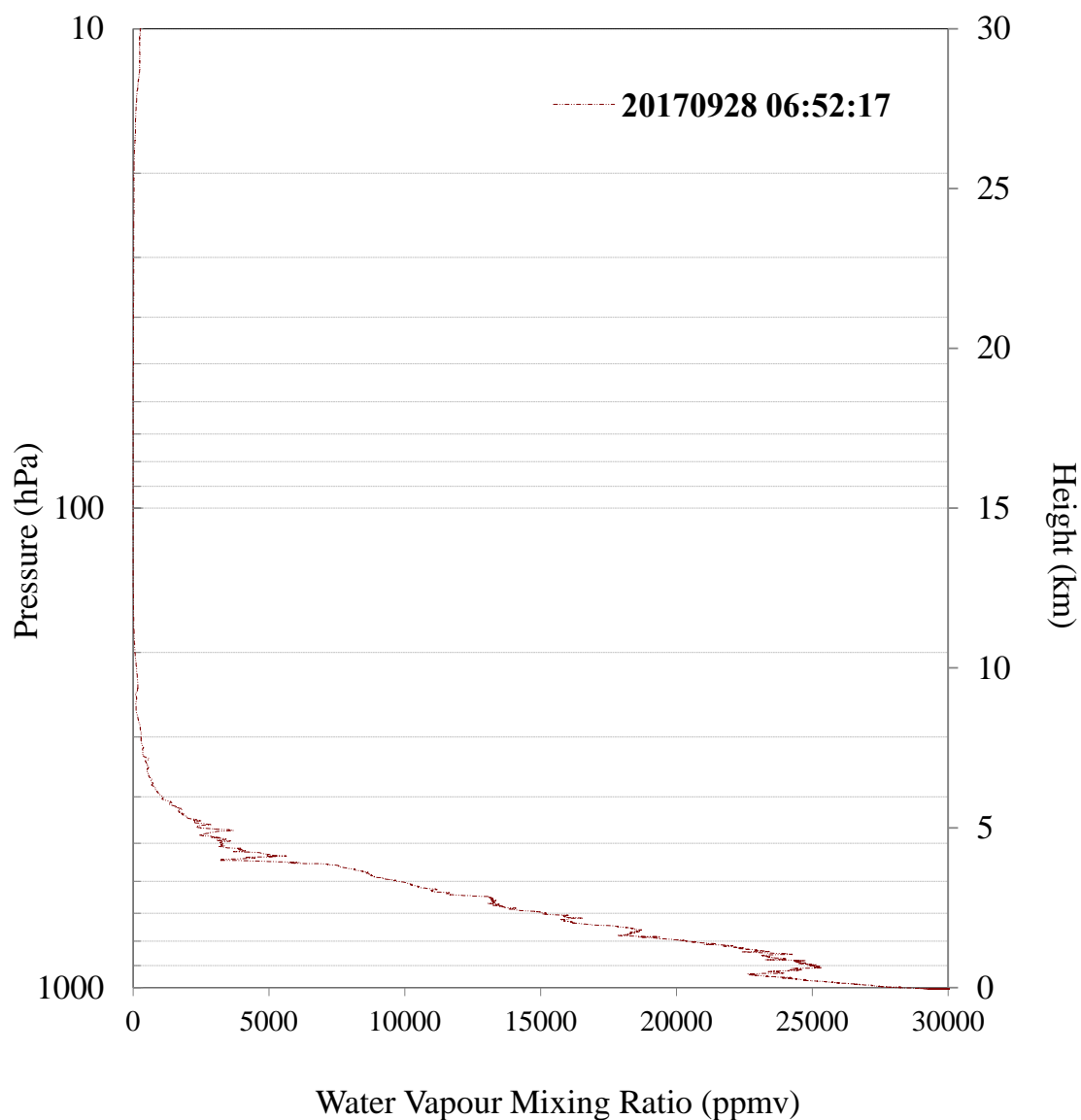


Figure 7.27 Vertical distributions of water vapour mixing ratio obtained from the iMet-1 Radiosonde over Bangkok, Thailand on 28 September 2017 (during controlled descent at 38.6 km).

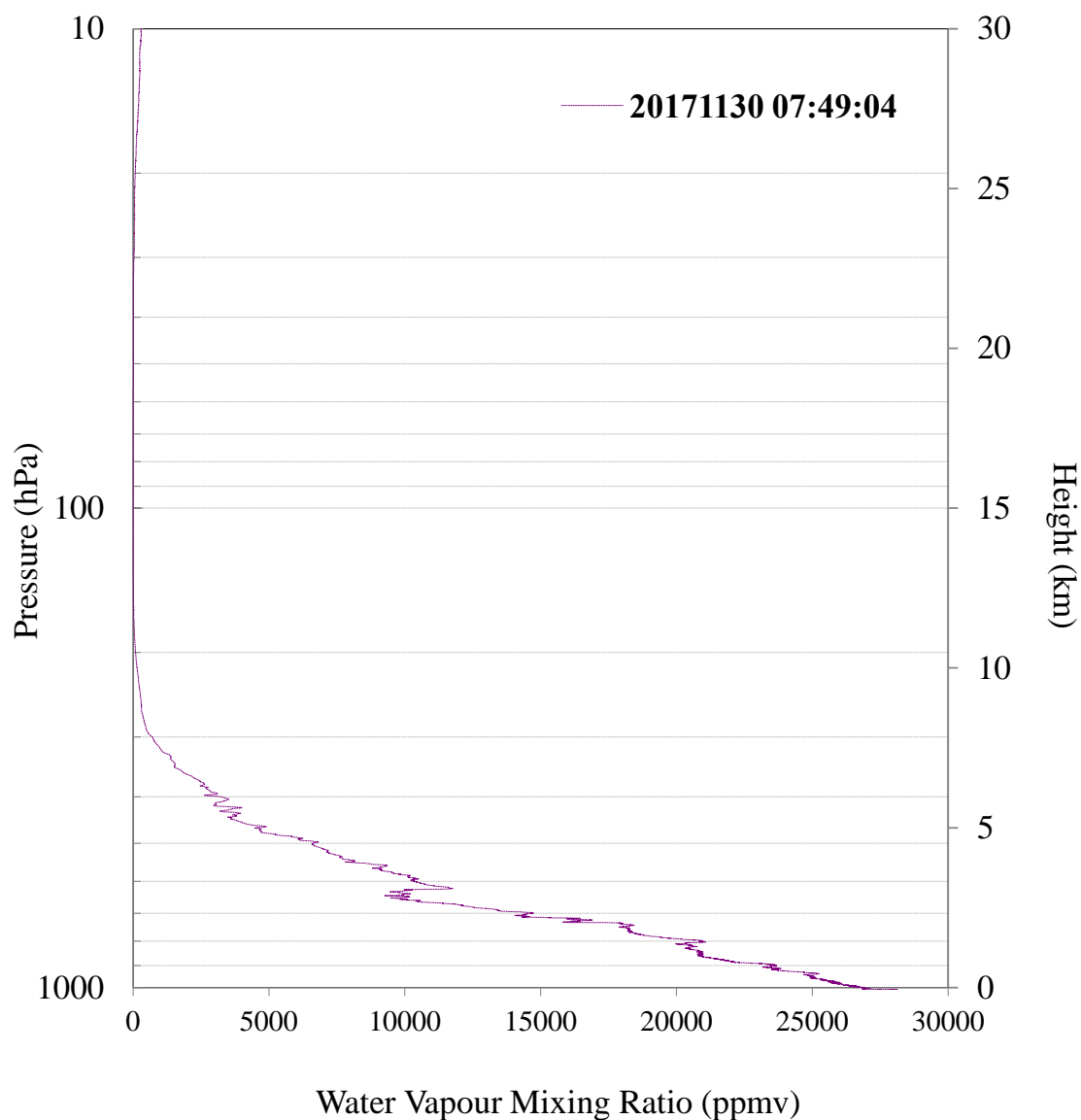


Figure 7.28 Vertical distributions of water vapour mixing ratio obtained from the iMet-1 Radiosonde over Bangkok, Thailand on 30 November 2017 (during controlled descent at 39.5 km).

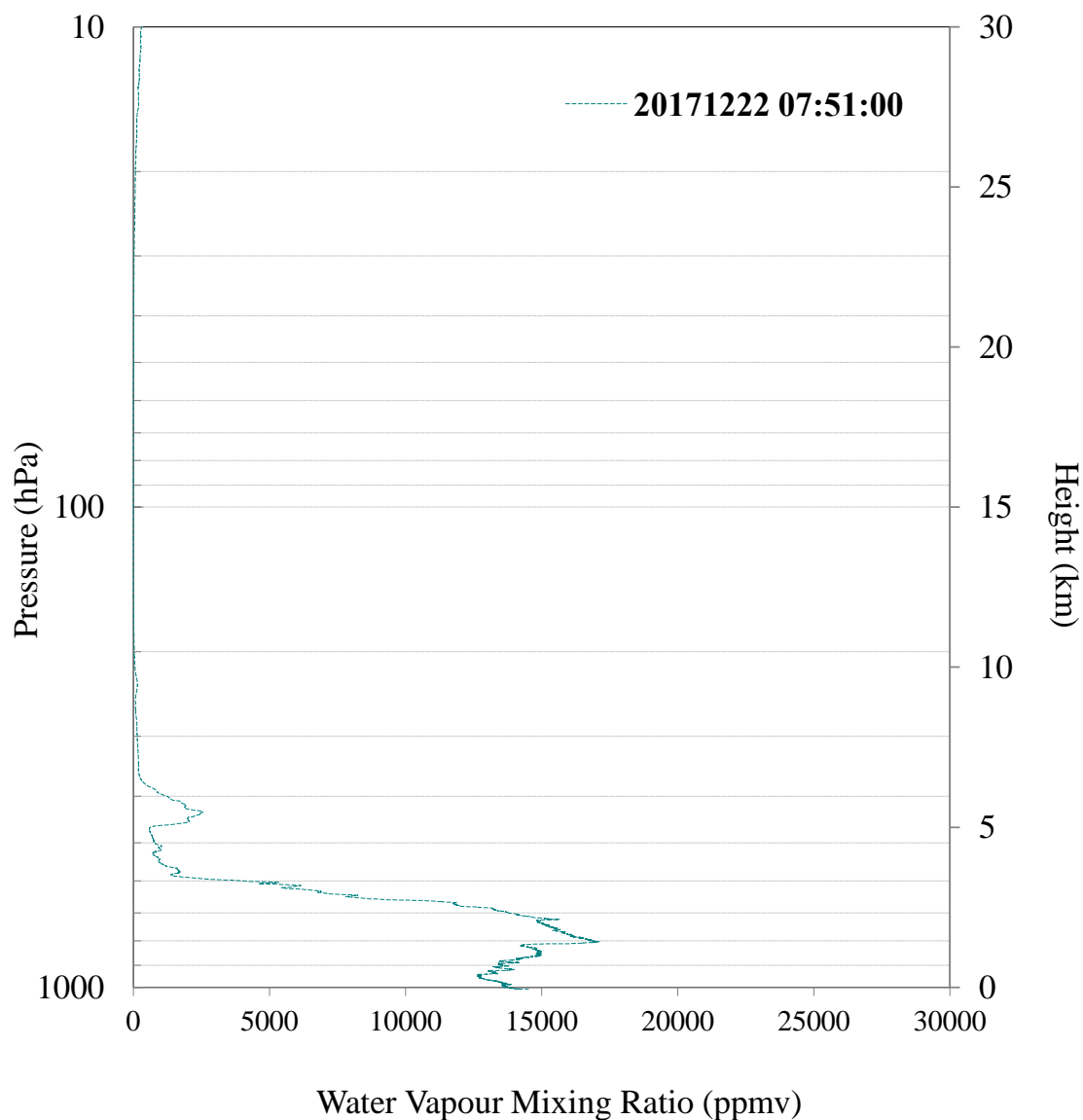


Figure 7.29 Vertical distributions of water vapour mixing ratio obtained from the iMet-1 Radiosonde over Bangkok, Thailand on 22 December 2017 (during controlled descent at 38.5 km).

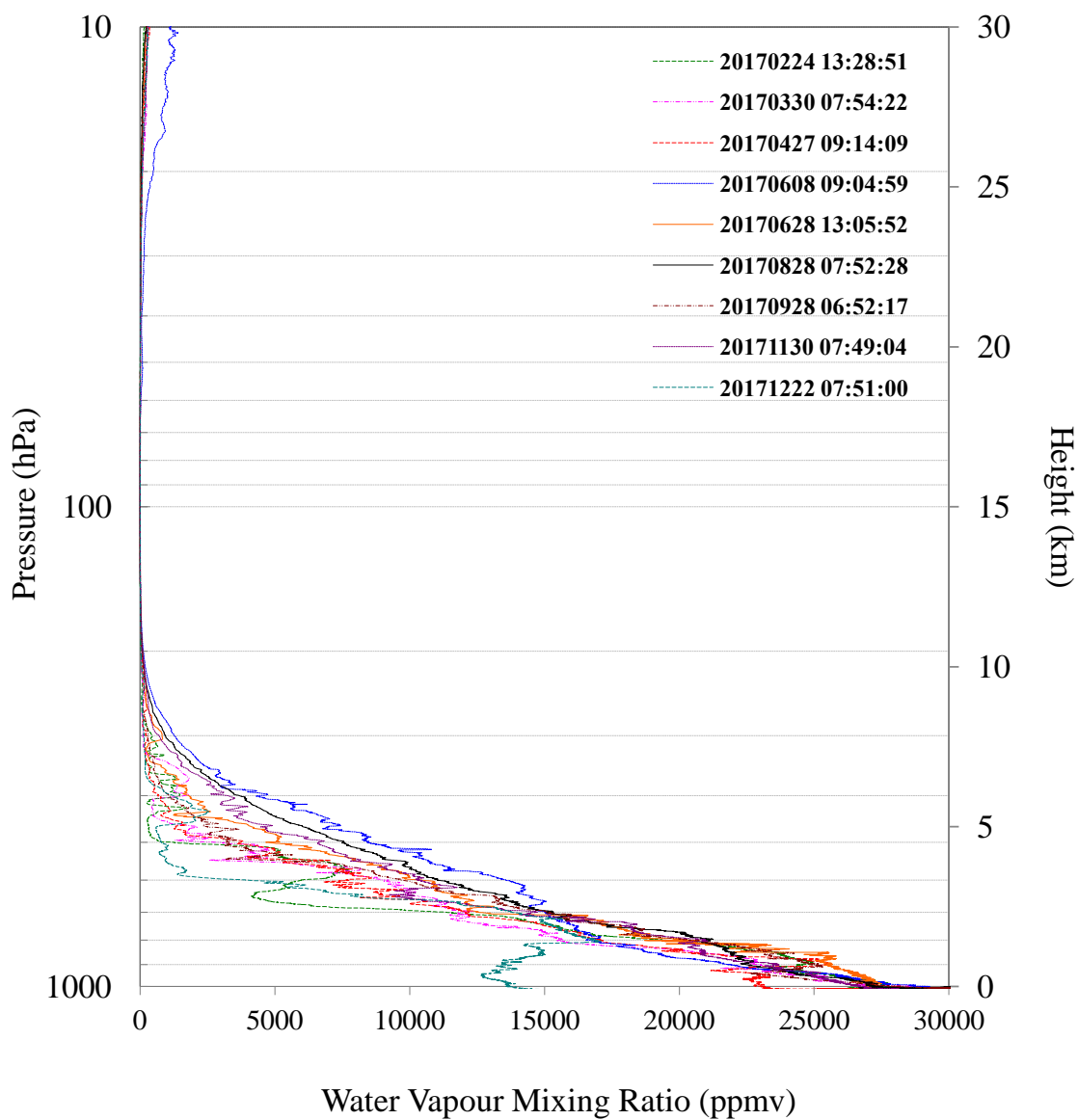
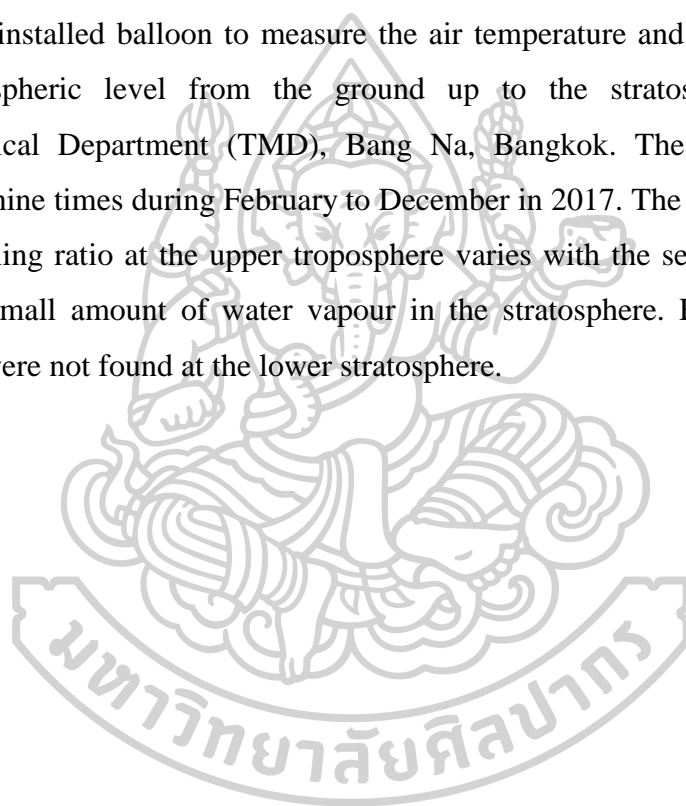


Figure 7.30 Vertical distributions of volume mixing ratio (ppmv) in the UTLS region obtained from the iMet-1 Radiosonde over (13.67°N, 100.60°E) Bangkok, Thailand from February through December in 2017.

From in Figure 7.30, it can be seen that the water vapour in the atmosphere changes with height, with the volume mixing ratio decreasing steadily in the troposphere and the small amount of water vapour is detected in the lower stratosphere. The amount of water vapour in the troposphere has seasonal variations, but there was no systematic variation in the water vapour in the lower stratosphere.

7.4 Conclusion

For studying of the water vapour in the upper atmosphere, we have released a radiosonde installed balloon to measure the air temperature and relative humidity at each atmospheric level from the ground up to the stratosphere at the Thai Meteorological Department (TMD), Bang Na, Bangkok. The measurement were carried out nine times during February to December in 2017. The result shows that the volume mixing ratio at the upper troposphere varies with the seasonal variation and there is a small amount of water vapour in the stratosphere. However, systematic variations were not found at the lower stratosphere.



Chapter 8

Conclusion

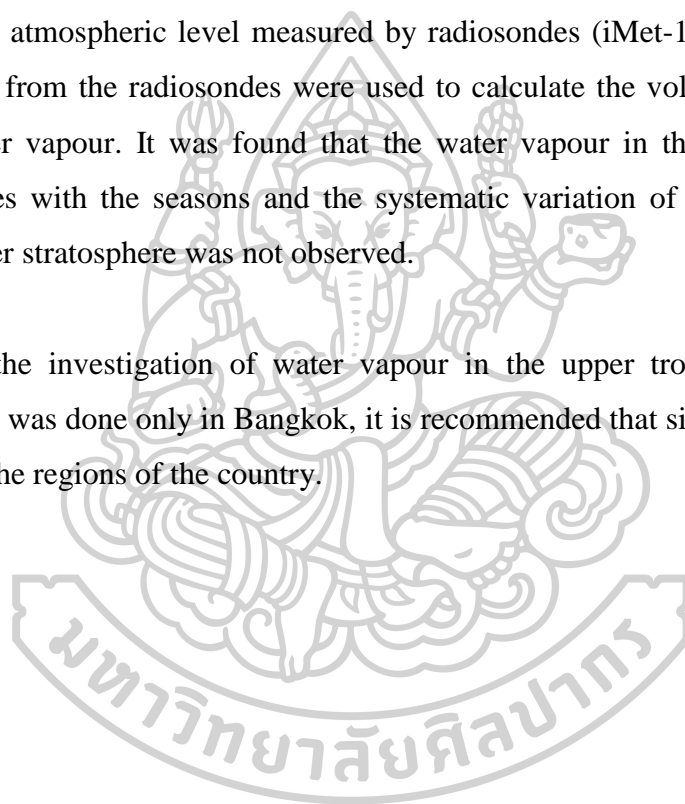
In this study, we have investigated the amount of water vapour in the atmosphere in Thailand. This study comprises five parts that are 1) Development of an empirical model for calculation of precipitable water in the atmosphere using surface meteorological data 2) Estimation of atmospheric PWV in Thailand using an Artificial Neural Network 3) Distribution of PWV over Thailand using MTSAT-1R satellite data 4) Spatial and temporal changes of PWV in Thailand and 5) Investigation of water vapour in the upper atmosphere. This can be summarized as follows:

- 1) The simple empirical model to estimate monthly average PWV proposed in this study based on the surface meteorological data i.e. relative humidity and air temperature. This model performs reasonably when tested against the ground based measurement with the RMSE and MBE of 14.3% and -9.2%, respectively.
- 2) The artificial neural network (ANN) model used to estimate monthly average PWV in this work consist of four input data that are surface ambient air relative humidity, surface ambient air temperature, saturated water vapour pressure and month. The validation result shows that PWV estimated from the ANN agrees well with that obtained from the ground-based measurement with RMSE and MBE of 7.5% and -0.1%, respectively.
- 3) A statistical model related the satellite-derived brightness temperature to PWV was introduced. After the validation, it was found that PWV derived from the model agrees well with that obtained from the measurement with RMSE and MBE of 12.2% and 1.3%, respectively. The model was used to calculate PWV over Thailand and the results were displayed as monthly and maps. The maps reveal that PWV depends strongly on seasonality and geographical region.
- 4) This study has examined spatial and temporal changes in monthly PWV over the Thailand region using the re-analysis data from ERA-Interim model dataset (1981–2017). The PWV from ERA data was used to estimate spatial

patterns of monthly average PWV for the winter, summer and rainy seasons as well as the yearly averages. Statistically significant increases in PWV are found in the rainy season which has been related to the West Pacific index (WP). A second statistically significant increasing trend is found over the southern half of Thailand during the winter season which could be influenced by changes related to the Siberian High pressure.

- 5) The investigation of water vapour in the upper troposphere and lower stratosphere was performed using the temperature and relative humidity at each atmospheric level measured by radiosondes (iMet-1R) in Bangkok. The data from the radiosondes were used to calculate the volume mixing ratio of water vapour. It was found that the water vapour in the upper troposphere varies with the seasons and the systematic variation of the water vapour in lower stratosphere was not observed.

As the investigation of water vapour in the upper troposphere and lower stratosphere was done only in Bangkok, it is recommended that similar investigation be done in the regions of the country.



Appendix 1

Publication

Parts of this thesis have been published international journals and conference proceeding as follows:

- 1.) S. Buntoung, S. Janjai, M. Nunez, S. Pattarapanitchai, P. Nimnuan & **J. Pariyothon** (2020). Spatial and temporal changes of precipitable water vapour (<https://doi.org/10.1080/02723646.2019.1710433>).
- 2.) Sumaman Buntoung, Serm Janjai, **Jindarat Pariyothon**, Manuel Nunez (2020). Distribution of precipitable water vapour over Thailand using MTSAT-1R satellite data. Science, Engineering and Health Studies. (Under review)
- 3.) **Pariyotorn J.**, Buntoung S., Pattarapanitchai S. & Janjai S. (2018). Estimation of Atmospheric Precipitable Water Vapour in Thailand using an Artificial Neural Network. Paper presented at Siam physics congress, 21-23 May 2018, Phitsanulok, Thailand. (Conference Series)

REFERENCES

- Akatsuka, S., Oyoshi, K., & Takeuchi, W. (2010). *Mapping of precipitable water using MTSAT data*. Paper presented at the Proceedings of 31st Asian Conference on Remote Sensing (ACRS), Hanoi, Vietnam.
- Alshawaf, F., Balidakis, K., Dick, G., Heise, S., & Wickert, J. (2017). Estimating trends in atmospheric water vapor and temperature time series over Germany. *Atmospheric Measurement Techniques*, 10(9), 3117.
- Bates, D. M., & Watts, D. G. (1988). *Nonlinear regression analysis and its applications* (Vol. 2): Wiley New York.
- Bengtsson, L., Hagemann, S., & Hodges, K. I. (2004). Can climate trends be calculated from reanalysis data? *Journal of Geophysical Research: Atmospheres*, 109(D11).
- Berrisford, P., Kållberg, P., Kobayashi, S., Dee, D., Uppala, S., Simmons, A., . . . Sato, H. (2011). Atmospheric conservation properties in ERA-Interim, QJ Roy. Meteor. Soc., 137, 1381–1399.
- Bock, O., Keil, C., Richard, E., Flamant, C., & Bouin, M. n. (2005). Validation of precipitable water from ECMWF model analyses with GPS and radiosonde data during the MAP SOP. *Quarterly Journal of the Royal Meteorological Society: A journal of the atmospheric sciences, applied meteorology and physical oceanography*, 131(612), 3013-3036.
- Bolsenga, S. (1965). The relationship between total atmospheric water vapor and surface dew point on a mean daily and hourly basis. *Journal of Applied Meteorology*, 4(3), 430-432.
- Bruegge, C. J., Conel, J. E., Green, R. O., Margolis, J. S., Holm, R. G., & Toon, G. (1992). Water vapor column abundance retrievals during FIFE. *Journal of Geophysical Research: Atmospheres*, 97(D17), 18759-18768.
- Campmany, E., Bech, J., Rodríguez-Marcos, J., Sola, Y., & Lorente, J. (2010). A comparison of total precipitable water measurements from radiosonde and sunphotometers. *Atmospheric research*, 97(3), 385-392.

- Choi, K.-S., & Moon, I.-J. (2012). Influence of the Western Pacific teleconnection pattern on Western North Pacific tropical cyclone activity. *Dynamics of atmospheres and oceans*, 57, 1-16.
- Cimel, (2001). Sunphotometer User Manual Cimel CE 318, V. 4.6, Cimel. 172 rue de Charonne, 75011 Paris, France, 79 pp
- Cohen, J., Saito, K., & Entekhabi, D. (2001). The role of the Siberian high in Northern Hemisphere climate variability. *Geophysical Research Letters*, 28(2), 299-302.
- Cuomo, V., Tramutoli, V., Pergola, N., Pietrapertosa, C., & Romano, F. (1997). In place merging of satellite based atmospheric water vapour measurements. *International Journal of remote sensing*, 18(17), 3649-3668.
- Dai, A. (2011). Drought under global warming: a review. *Wiley Interdisciplinary Reviews: Climate Change*, 2(1), 45-65.
- Dee, D. P., Uppala, S. M., Simmons, A., Berrisford, P., Poli, P., Kobayashi, S., . . . Bauer, d. P. (2011). The ERA- Interim reanalysis: Configuration and performance of the data assimilation system. *Quarterly Journal of the royal meteorological society*, 137(656), 553-597.
- Durre, I., Vose, R. S., & Wuertz, D. B. (2006). Overview of the integrated global radiosonde archive. *Journal of Climate*, 19(1), 53-68.
- Durre, I., Vose, R. S., & Wuertz, D. B. (2008). Robust automated quality assurance of radiosonde temperatures. *Journal of Applied Meteorology and Climatology*, 47(8), 2081-2095.
- Exell, E., & EHB, E. (1978). The water content and turbidity of the atmosphere in thailand, *Solar Energy*, 20, 429-430.
- Feng, S., Hu, Q., & Qian, W. (2004). Quality control of daily meteorological data in China, 1951–2000: a new dataset. *International Journal of Climatology: A Journal of the Royal Meteorological Society*, 24(7), 853-870.
- Gao, B. C., & Kaufman, Y. J. (2003). Water vapor retrievals using Moderate Resolution Imaging Spectroradiometer (MODIS) near- infrared channels. *Journal of Geophysical Research: Atmospheres*, 108(D13).
- Garson, G. D. (1998). *Neural networks: An introductory guide for social scientists*: Sage.

- Gueymard, C. (1994). Analysis of monthly average atmospheric precipitable water and turbidity in Canada and northern United States. *Solar Energy*, 53(1), 57-71.
- Hay, J. E. (1971). Precipitable water over Canada: II distribution. *Atmosphere*, 9(4), 101-111.
- Hecht-Nielsen, R. (1992). Theory of the backpropagation neural network *Neural networks for perception* (pp. 65-93): Elsevier.
- Heritier, S., Cantoni, E., Copt, S., & Victoria-Feser, M.-P. (2009). *Robust methods in biostatistics* (Vol. 825): John Wiley & Sons.
- Holben, B. N., Eck, T. F., Slutsker, I. a., Tanre, D., Buis, J., Setzer, A., . . . Nakajima, T. (1998). AERONET—A federated instrument network and data archive for aerosol characterization. *Remote sensing of environment*, 66(1), 1-16.
- Huang, Y., Wang, B., Li, X., & Wang, H. (2018). Changes in the influence of the western Pacific subtropical high on Asian summer monsoon rainfall in the late 1990s. *Climate Dynamics*, 51(1-2), 443-455.
- Iqbal, M. (2012). *An introduction to solar radiation*: Elsevier.
- Irwin III, R. P., & Davis, R. E. (1999). The relationship between the Southern Oscillation Index and tropical cyclone tracks in the eastern North Pacific. *Geophysical Research Letters*, 26(15), 2251-2254.
- Janjai, S., Masiri, I., Pattarapanitchai, S., & Laksanaboonsong, J. (2011). An Improved Model for the Estimation of Solar Radiation from Satellite Data for Thailand. *Journal of the Institute of Engineering*, 8(3), 130-139.
- Janjai, S., Masiri, I., Pattarapanitchai, S., & Laksanaboonsong, J. (2013). Mapping global solar radiation from long-term satellite data in the tropics using an improved model. *International Journal of Photoenergy*, 2013.
- Janjai, S., Nimnuan, P., Nunez, M., Buntoung, S., & Cao, J. (2015). An assessment of three satellite-based precipitation data sets as applied to the Thailand region. *Physical Geography*, 36(4), 282-304.
- Kämpfer, N. (2012). *Monitoring atmospheric water vapour: ground-based remote sensing and in-situ methods* (Vol. 10): Springer.

- Kaufman, Y. J., & Gao, B.-C. (1992). Remote sensing of water vapor in the near IR from EOS/MODIS. *IEEE Transactions on Geoscience and Remote Sensing*, 30(5), 871-884.
- King, M. D., Kaufman, Y. J., Menzel, W. P., & Tanre, D. (1992). Remote sensing of cloud, aerosol, and water vapor properties from the moderate resolution imaging spectrometer(MODIS). *IEEE Transactions on Geoscience and Remote Sensing*, 30(1), 2-27.
- King, M. D., Menzel, W. P., Kaufman, Y. J., Tanré, D., Gao, B.-C., Platnick, S., . . . Hubanks, P. A. (2003). Cloud and aerosol properties, precipitable water, and profiles of temperature and water vapor from MODIS. *IEEE Transactions on Geoscience and Remote Sensing*, 41(2), 442-458.
- Larsen, N. F., & Stamnes, K. (2005). Use of shadows to retrieve water vapor in hazy atmospheres. *Applied optics*, 44(32), 6986-6994. Retrieved from <https://www.osapublishing.org/ao/abstract.cfm?uri=ao-44-32-6986>
- Leckner, B. (1978). The spectral distribution of solar radiation at the earth's surface—elements of a model. *Solar Energy*, 20(2), 143-150.
- Lee, K.-M., & Park, J.-H. (2007). *Retrieval of total precipitable water from the split-window technique in the East Asian region*. Paper presented at the Proceedings of the EUMETSAT Meteorological Satellite Conference, Amsterdam, The Netherlands.
- Li, X., Wen, Z., & Zhou, W. (2011). Long-term change in summer water vapor transport over South China in recent decades. *Journal of the Meteorological Society of Japan. Ser. II*, 89, 271-282.
- Li, Z., Muller, J. P., & Cross, P. (2003). Comparison of precipitable water vapor derived from radiosonde, GPS, and Moderate- Resolution Imaging Spectroradiometer measurements. *Journal of Geophysical Research: Atmospheres*, 108(D20).
- Linkin, M. E., & Nigam, S. (2008). The North Pacific Oscillation–west Pacific teleconnection pattern: Mature-phase structure and winter impacts. *Journal of Climate*, 21(9), 1979-1997.

- Mattar, C., Sobrino, J. A., Julien, Y., & Morales, L. (2011). Trends in column integrated water vapour over Europe from 1973 to 2003. *International Journal of Climatology*, 31(12), 1749-1757.
- Mengistu Tsidu, G., Blumenstock, T., & Hase, F. (2014). Observations of precipitable water vapour over complex topography of Ethiopia from ground-based GPS, FTIR, radiosonde and ERA-Interim reanalysis. *Atmospheric Measurement Techniques Discussions*, 7(9).
- Mieruch, S., Noël, S., Bovensmann, H., & Burrows, J. (2008). Analysis of global water vapour trends from satellite measurements in the visible spectral range.
- Minschwaner, K., & Dessler, A. E. (2004). Water vapor feedback in the tropical upper troposphere: Model results and observations. *Journal of Climate*, 17(6), 1272-1282.
- Muhlbauer, A., Spichtinger, P., & Lohmann, U. (2009). Application and comparison of robust linear regression methods for trend estimation. *Journal of Applied Meteorology and Climatology*, 48(9), 1961-1970.
- Murray, F. W. (1966). *On the computation of saturation vapor pressure*. Retrieved from
- Namaoui, H., Kahlouche, S., Belbachir, A. H., Van Malderen, R., Brenot, H., & Pottiaux, E. (2017). GPS water vapor and its comparison with radiosonde and ERA-Interim data in Algeria. *Advances in atmospheric sciences*, 34(5), 623-634.
- Nunez, M. (1993). The development of a satellite-based insolation model for the tropical western Pacific Ocean. *International Journal of Climatology*, 13(6), 607-627.
- Okulov, O., Ohvri, H., & Kivi, R. (2002). Atmospheric precipitable water in Estonia, 1990-2001. *Boreal environment research*, 7(3), 291-300.
- Paliwal, M., & Kumar, U. A. (2009). Neural networks and statistical techniques: A review of applications. *Expert systems with applications*, 36(1), 2-17.
- Pasini, A., & Ameli, F. (2003). Radon short range forecasting through time series preprocessing and neural network modeling. *Geophysical Research Letters*, 30(7).

- Pasini, A., Lorè, M., & Ameli, F. (2006). Neural network modelling for the analysis of forcings/temperatures relationships at different scales in the climate system. *Ecological Modelling*, 191(1), 58-67.
- Pérez- Ramírez, D., Whiteman, D. N., Smirnov, A., Lyamani, H., Holben, B. N., Pinker, R., . . . Alados- Arboledas, L. (2014). Evaluation of AERONET precipitable water vapor versus microwave radiometry, GPS, and radiosondes at ARM sites. *Journal of Geophysical Research: Atmospheres*, 119(15), 9596-9613.
- Pierrehumbert, C. (1972). *Precipitable Water Statistics, Australia: Monthly Statistics of Precipitable Water Between Surface and 400 Mb at 2300 GMT, 1958-1969*: Bureau of Meteorology, Department of the Interior.
- Platnick, S., King, M., Meyer, K., Wind, G., Amarasinghe, N., Marchant, B., Ridgway, B. (2015). MODIS cloud optical properties: User guide for the collection 6 level-2 MOD06/MYD06 product and associated level-3 datasets, version 1.0. *NASA Goddard Flight Center (GSFC), Greenbelt, MD, USA*.
- Platnick, S., Hubanks, P., Meyer, K. & King, M. D. (2015). MODIS Atmosphere L3 Monthly Product (08_L3). *NASA MODIS Adaptive Processing System*, Goddard Space Flight Center.
- Qu, W., Wang, J., Gao, S., & Wu, T. (2013). Effect of the strengthened western Pacific subtropical high on summer visibility decrease over eastern China since 1973. *Journal of Geophysical Research: Atmospheres*, 118(13), 7142-7156.
- Randall, D. A., Wood, R. A., Bony, S., Colman, R., Fichefet, T., Fyfe, J., . . . Srinivasan, J. (2007). Climate models and their evaluation *Climate change 2007: The physical science basis. Contribution of Working Group I to the Fourth Assessment Report of the IPCC (FAR)* (pp. 589-662): Cambridge University Press.
- Reagan, J. A., Thome, K., Herman, B., & Gall, R. (1987). *Water vapor measurements in the 0.94 micron absorption band-Calibration, measurements and data applications*. Paper presented at the IGARSS'87-International Geoscience and Remote Sensing Symposium.

- Reitan, C. H. (1960). Distribution of precipitable water vapor over the continental United States. *Bulletin of the American Meteorological Society*, 41(2), 79-87.
- Reitan, C. H. (1963). Surface dew point and water vapor aloft. *Journal of Applied Meteorology*, 2(6), 776-779.
- Renzullo, L. J., Barrett, D. J., Marks, A. S., Hill, M. J., Guerschman, J. P., Mu, Q., & Running, S. W. (2006). Application of multiple constraints model-data assimilation techniques to coupling satellite passive microwave and thermal imagery for estimation of land surface variables and energy fluxes.
- Revuelta, A., Rodriguez, C., Mateos, J., & Garmendia, J. (1985). A model for the estimation of precipitable water. *Tellus B: Chemical and Physical Meteorology*, 37(4-5), 210-215.
- Rienecker, M. M., Suarez, M., Todling, R., Bacmeister, J., Takacs, L., Liu, H., . . . Gelaro, R. (2008). The GEOS-5 Data Assimilation System: Documentation of Versions 5.0. 1, 5.1. 0, and 5.2. 0.
- Rousseeuw, P. J., & Leroy, A. M. (2005). *Robust regression and outlier detection* (Vol. 589): John wiley & sons.
- Şahin, M. (2012). Modelling of air temperature using remote sensing and artificial neural network in Turkey. *Advances in space research*, 50(7), 973-985.
- Şahin, M., Yıldız, B. Y., Şenkal, O., & Peştimalcı, V. (2012). Modelling and remote sensing of land surface temperature in Turkey. *Journal of the Indian Society of Remote Sensing*, 40(3), 399-409.
- Schneider, T., O'Gorman, P. A., & Levine, X. J. (2010). Water vapor and the dynamics of climate changes. *Reviews of Geophysics*, 48(3).
- Simmonds, I., Bi, D., & Hope, P. (1999). Atmospheric water vapor flux and its association with rainfall over china in summer. *Journal of Climate*, 12(5), 1353-1367.
- Simmons, A. (2006). ERA-Interim: New ECMWF reanalysis products from 1989 onwards. *ECMWF newsletter*, 110, 25-36.
- Smith, W. L. (1966). Note on the relationship between total precipitable water and surface dew point. *Journal of Applied Meteorology*, 5(5), 726-727.

- Soden, B. J., & Bretherton, F. P. (1993). Upper tropospheric relative humidity from the GOES 6.7 μm channel: Method and climatology for July 1987. *Journal of Geophysical Research: Atmospheres*, 98(D9), 16669-16688.
- Soden, B. J., & Lanzante, J. R. (1996). An assessment of satellite and radiosonde climatologies of upper-tropospheric water vapor. *Journal of Climate*, 9(6), 1235-1250.
- Sözen, A., Arcaklioğlu, E., & Özalp, M. (2004). Performance analysis of ejector absorption heat pump using ozone safe fluid couple through artificial neural networks. *Energy Conversion and Management*, 45(13-14), 2233-2253.
- Stull, R. (2000). *Meteorology for scientists and engineers*: Brooks/Cole.
- Takahashi, H., Su, H., & Jiang, J. H. (2016). Error analysis of upper tropospheric water vapor in CMIP5 models using “A-Train” satellite observations and reanalysis data. *Climate Dynamics*, 46(9-10), 2787-2803.
- TAKEUCHI, W., NEMOTO, T., KANEKO, T., & YASUOKA, Y. (2008). Development of MTSAT data processing, visualization and distribution system on WWW. *Journal of the Japan society of photogrammetry and remote sensing*, 46(6), 42-48.
- Taylor, F. W. (2005). *Elementary climate physics*: Oxford Univ. Press.
- Trenberth, K. E., Fasullo, J., & Smith, L. (2005). Trends and variability in column-integrated atmospheric water vapor. *Climate Dynamics*, 24(7-8), 741-758.
- Tuinenburg, O., & de Vries, J. (2017). Irrigation patterns resemble ERA- Interim Reanalysis soil moisture additions. *Geophysical Research Letters*, 44(20), 10,341-310,348.
- Vishnu, S., Francis, P., Shenoi, S., & Ramakrishna, S. (2016). On the decreasing trend of the number of monsoon depressions in the Bay of Bengal. *Environmental Research Letters*, 11(1), 014011.
- Wallace, J. M., & Gutzler, D. S. (1981). Teleconnections in the geopotential height field during the Northern Hemisphere winter. *Monthly Weather Review*, 109(4), 784-812.
- Wallace, J. M., & Hobbs, P. V. (2006). *Atmospheric science: an introductory survey* (Vol. 92): Elsevier.

- Wasserman, P. D. (1989). *Neural computing: theory and practice*: Van Nostrand Reinhold Co.
- Wentz, F. J., & Schabel, M. (2000). Precise climate monitoring using complementary satellite data sets. *Nature*, 403(6768), 414-416. Retrieved from <https://www.nature.com/articles/35000184>
- Wolberg, J. (2006). *Data analysis using the method of least squares: extracting the most information from experiments*: Springer Science & Business Media.
- Wong, M. S., Jin, X., Liu, Z., Nichol, J. E., Ye, S., Jiang, P., & Chan, P. W. (2015). Geostationary satellite observation of precipitable water vapor using an empirical orthogonal function (eof) based reconstruction technique over eastern china. *Remote sensing*, 7(5), 5879-5900.
- Xue-zhao, H., & Dao-yi, G. (2002). Interdecadal change in western Pacific subtropical high and climatic effects. *Journal of Geographical Sciences*, 12(2), 202-209.
- Young, H. D., & Statistical Treatment, S. (1962). *of Experimental Data*: McGraw-Hill Book Company, New York.
- Zhang, Q., Ye, J., Zhang, S., & Han, F. (2018). Precipitable water vapor retrieval and analysis by multiple data sources: Ground-based GNSS, radio occultation, radiosonde, microwave satellite, and NWP reanalysis data. *Journal of Sensors*, 2018.

REFERENCES



VITA

NAME Jindarat Pariyothon

DATE OF BIRTH 18 Aug 1991

PLACE OF BIRTH Ratchaburi

INSTITUTIONS ATTENDED 2014, Bachelor of Science (Physics) Silpakorn University, Nakhon Pathom Thailand.
2017, Master of Science (Physics) Silpakorn University, Nakhon Pathom Thailand.

HOME ADDRESS 114/71 Banpakraet Road, Tambon Banpong, Amphur Banpong, Ratchaburi 70110

PUBLICATION 1.) S. Buntoung, S. Janjai, M. Nunez, S. Pattarapanitchai, P. Nimnuan & J. Pariyothon (2020): Spatial and temporal changes of precipitable water vapour in Thailand. Physical Geography, ISSN: 0272-3646.
2.) Sumaman Buntoung, Serm Janjai, Jindarat Pariyothon, Manuel Nunez (2020): Distribution of precipitable water vapour over Thailand using MTSAT-1R satellite data. Science, Engineering and Health Studies.
3.) J Pariyotorn, S Buntoung, S Pattarapanitchai and S Janjai. (2018): Estimation of Atmospheric Precipitable Water Vapour in Thailand using an Artificial Neural Network. Paper presented at Siam physics congress, 21-23 May 2018, Phitsanulok, Thailand.

